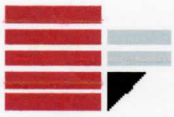

UNIVERSITÀ DELLA CALABRIA

Dottorato di Ricerca in Ingegneria Chimica e dei Materiali
SCUOLA DI DOTTORATO " PITAGORA " IN SCIENZE INGEGNERISTICHE

Tesi

SEGREGATING FLUIDIZATION OF TWO-SOLID BEDS: DEVELOPMENT OF THE APPROACH BASED ON THE FLUIDIZATION VELOCITY INTERVAL

Settore Scientifico Disciplinare ING-IND/25 – Impianti Chimici

Supervisori

Ch.mo Prof. Brunello FORMISANI

Ing. Rossella GIRIMONTE

Il Coordinatore del Corso di Dottorato

Ch.mo Prof. Raffaele MOLINARI

Candidato

Vincenzino VIVACQUA

Ciclo XXIII

A.A. 2009-2010

CONTENTS

Chapter 4

SOLID-SOLID INTERACTIONS AND THE SEGREGATION PATTERN IN THE FLUIDIZATION OF TWO DISSIMILAR SOLIDS

Chapter 5

PHASE EQUILIBRIUM ANALOGY

SOMMARIO

La maggior parte delle operazioni in cui la fluidizzazione ha trovato diffusione, quali la combustione e la gassificazione del carbone, la polimerizzazione catalitica e la granulazione di polveri, letti costituiti da solidi diversi sono processati nella medesima apparecchiatura. L'interazione tra i solidi e il gas di fluidizzazione e l'interazione tra le diverse specie particellari determinano il fenomeno noto come segregazione, ossia l'instaurarsi di un profilo di concentrazione dei componenti lungo l'asse del letto che non è uniforme.

L'efficienza dei processi a letto fluido in cui vengono utilizzati più solidi è fortemente influenzata dalla capacità di governare tali fenomeni ma ad oggi la conoscenza dei meccanismi che regolano il rapporto fra regime di fluidizzazione ed equilibrio di miscelazione-segregazione è ancora oggi del tutto insoddisfacente, persino per i " più semplici" sistemi a due componenti, oggetto di studio di questa tesi.

L'analisi dei lavori che costituiscono lo stato delle conoscenze sul problema ha rivelato la tendenza dominante di analizzare le proprietà di fluidizzazione di una miscela di solidi in analogia a quelle dei letti monodispersi, mutuando da essi il concetto di "velocità minima di fluidizzazione". Benché sia possibile riscrivere le classiche equazioni di previsione della velocità minima di fluidizzazione in forme adatte a tener conto della natura binaria delle miscele, l'approccio che estende ai letti di due solidi il concetto stesso di velocità minima di fluidizzazione è ben lontano dal consentire ulteriori sviluppi dell'analisi teorica. La fluidizzazione di una miscela di due solidi granulari è infatti un processo graduale durante il quale si assiste alla variazione progressiva della distribuzione assiale dei componenti. Appare dunque evidente la necessità di sviluppare un criterio di analisi basato sulla definizione di variabili alternative, che descrivano compiutamente la reale fenomenologia di fluidizzazione delle miscele binarie. Queste variabili possono essere individuate nelle "velocità di inizio -" e "di fine fluidizzazione". Poiché la maggior parte dei fenomeni di segregazione avviene

all'interno di questo intervallo di velocità, l'analisi del comportamento delle miscele binarie attraverso la misura sperimentale di questa coppia di variabili permette di cogliere alcuni aspetti importanti della fenomenologia.

L'approccio basato sull'intervallo di velocità ha infatti consentito di pervenire a una descrizione unificata delle proprietà di fluidizzazione delle miscele di solidi diversi per densità e/o dimensione, attraverso l'elaborazione di un modello fondamentale, basato sulla formulazione di bilanci di forza. Tale modello è in grado di fornire una previsione "ab initio" della velocità di inizio fluidizzazione e consente di conoscere la velocità di fine fluidizzazione attraverso la misura di un singolo parametro fisico indipendente dalla composizione della miscela. La determinazione di tale parametro può essere effettuata con il minimo sforzo sperimentale, essendo sufficiente un singolo esperimento di fluidizzazione per valutarlo.

Il diagramma di velocità è limitato ai suoi estremi dalle velocità minime di fluidizzazione dei singoli solidi e ciò può essere spiegato solo ipotizzando che esista un'interazione tra i due componenti. Attraverso la scrittura di bilanci separati sulle specie particellari costituenti la miscela è possibile pervenire alla quantificazione di tali interazioni, la cui analisi consente di prevedere teoricamente un comportamento "anomalo" che si verifica, in certe condizioni, quando solidi del tutto diversi vengono fluidizzati simultaneamente. Questo comportamento prevede la fluidizzazione di uno dei componenti sul fondo della colonna, mentre l'altro costituisce uno strato superiore fisso.

Questa tesi mette inoltre in risalto il legame esistente tra la velocità di fine fluidizzazione e i profili di concentrazione ottenuti per lenta defluidizzazione di un letto di solidi fino allo stato fisso, mostrando come questi profili possano essere ottenuti dalla conoscenza di questo valore di velocità. Viene infine avanzata l'ipotesi che sia i profili ottenuti per defluidizzazione quanto la velocità di fine fluidizzazione possano essere generati attraverso la massimizzazione di un funzionale, la cui definizione è unica per qualsiasi tipo di miscela binaria.

ABSTRACT

In many industrial processes in which the fluidized bed is employed (gasification of biomass, catalytic polymerization, granulation, etc.), solids of various kinds are simultaneously subjected to fluidization. The gas-solid and solid-solid interaction determines the tendency of system components to segregate or mix up according to a characteristic axial concentration profile. Even with mixtures of only two components, the relationship between fluidization regime and level of segregation is still poorly understood, so that no quantitative theory of segregating fluidization is, to date, available.

This thesis shows how interpretations based on definition of a " minimum fluidization velocity of the mixture" can lead to erroneous conclusions because a single velocity threshold is not capable to properly describe the actual behavior of these systems which undergo a gradual suspension process during which segregation occurs as well. Although it is possible to rewrite the classical equations for predicting the minimum fluidization velocity in forms suitable to take into account the nature of binary mixtures, the approach that extends to beds of two solids the concept of "minimum fluidization velocity" is far from allowing any further developments of the theoretical analysis. An alternative method of investigation is followed which takes into consideration the existence of a finite velocity interval, bounded by the "initial" and "final fluidization velocity" of the mixture, along which the whole process of fluidization has place.

Several series of experiments are presented that provide the initial and final fluidization velocity of the binary mixtures investigated at varying composition. By adapting the classical theory of fluidization to this category of systems and introducing just one parameter to account for their segregation level, the theoretical equations of the two characteristic velocities are derived.

Results relevant to mixtures segregating either by density and/or size difference between components show that a unique theory based on fundamental analysis proves capable to relate the progress of fluidization to the extent of segregation.

Force balances carried out on the individual components of the mixture have shown that solid-solid interaction is at work in the bed. The presence of this interaction provides a theoretical explanation of the fact that the two characteristic velocities are always observed to be included between the single component fluidization velocities. The analysis of this interaction has demonstrated that it is possible to predict theoretically the case of mixtures for which one component achieves the fluidized state at the bottom of the column, while the other solid forms an upper packed layer.

The equation for calculating the final fluidization velocity is then employed to predict the concentration profile obtained by slowly defluidizing the bed down to the fixed state. Eventually, it is assumed that both concentration profiles after defluidization and the final fluidization velocity can be obtained through the maximization of a functional.

INTRODUCTION

One of the features that has fostered the industrial success of the fluid bed technology is its being particularly advantageous to carry out processes that involve contact between a fluid phase, often a gas, and a multisolid charge.

In this category of operations fluidization has been widely employed, as in the case of combustion and gasification of coal, biomass and other solid fuels, catalytic polymerization, incineration of municipal and industrial wastes, granulation of powders, etc. Outside the field of conversion processes, multicomponent solid beds are also subjected to fluidization to achieve the separation of different materials (mining, classification of wastes, etc..) or, conversely, their homogenization (formulation of detergents, preparation of the cement flour, etc...)

Depending on their specific objectives these applications employ mixtures of various types, made up of several materials of different kind. In each of these operations fluidization technology allows operating with relatively simple equipment, low pressure drop, good isothermal conditions and high heat and mass transfer coefficients. Besides these characteristics, however, there is another aspect, almost unavoidable, to be accounted for: due to the fact that solids differing in density, size and shape react differently to the friction exerted by the gas stream in which they are suspended, mixture components tend to accumulate in distinct layers where the presence of a particular species prevails. This

phenomenon is termed "*segregation*" of the solid components, and counteracts to their opposite tendency to mix up.

The importance of segregation as a factor that can strongly affect the efficiency of any fluidized bed process has made this phenomenon a major theme of research. However, despite the efforts made by many groups over the past thirty years and the large number of literature papers dedicated to the subject, the knowledge of the mechanisms that regulate the relationship between the fluidization regime and the mixing-segregation equilibrium is still unsatisfactory, even as what regards systems of two solids, that is the simplest type of multicomponent mixtures. The lack of understanding of the phenomenon is considered a serious obstacle to engineering applications, as it prevents predicting the distribution of the various solids in a fluidized bed equipment at a certain flow regime. That makes impossible to go over the use of empirical solutions on trying to take advantage of the condition of good solid mixing (homogeneity of temperature conditions, uniformity of product quality, easy control of reactions, etc..) or, at the other extreme, of their total stratification (organization of the process in stages, separation of the entry and exit points of materials, etc.).

The need for a better insight into the behavior of multicomponent fluidized beds is strongly felt, with the ultimate aim of predicting and regulating the mixing of the system through an appropriate choice both of the solid properties (average size, size distribution, component concentration), and of some operating parameters (fluidization velocity, bed mass and height). The experimental studies that constitute the state-of-the-art have clearly shown that the tendency toward segregation is essentially due to the difference in density and / or size among particles, two factors acting simultaneously when operating with thoroughly different solids. The ability to predict the equilibrium distribution of the different materials along the axis of the column from the knowledge of particle properties, bed composition and fluidization velocity, remains an objective of fundamental research even for mixtures of only two components, so that these systems are still the favorite subject of the analysis of almost all the papers published so far in the literature. In this frame systematic studies

carried out at the University of Calabria have established the following list of variables that, for various reasons, play an independent role in determining the fluidization properties and the mixing-segregation equilibrium:

- solid densities;
- mean particle sizes;
- shape factors (e.g. sphericities);
- mixture composition;
- bed height;
- column diameter;
- initial arrangement of the bed (well-mixed, segregated, etc.).

The necessity of addressing the influence of each of these parameters on mixture properties makes necessary to organize the experimental investigation by a method that tries to isolate and measure separately the effects of the variation of each factor, keeping constant all the other variables, with the ultimate objective of composing the different effects to achieve in this way a comprehensive interpretation of the phenomena under scrutiny.

Following this method, it is of help to work with spherical particles, to eliminate, as a first step, the effect of the diversity of shape among particles, and to distinguish, through distinct series of experiments, the case of mixtures that undergo segregation by density from that where segregation is caused by differences in size, as usual in almost all the studies carried out to date. Whatever the type of mixture subjected to investigation, solid stratification is always the result of the tendency of one of the two components, usually referred to as "Flotsam" (according to the terminology first introduced by Peter N. Rowe), to migrate

upwards and accumulate in the upper part of the bed, while the other, called "Jetsam", tends to segregate at its bottom.

In beds of two solids differing only in density or in particle diameter, the role of flotsam is played, respectively, by the less dense or smaller particles, but with thoroughly dissimilar materials is not always clear which of the two species will constitute the top layer of the bed; this uncertainty is due to the difficulty of quantifying the extent at which the two main factors of segregation, i.e. density and size differences, affect the dynamics of the system.

The objective of this study is to clarify through the experimental investigation the relationship between properties of the solids and of their mixtures, fluidization regime and mixing-segregation equilibrium.

As it will be discussed in the analysis of the literature that constitutes the state of the knowledge on the topic, it has been tried so far to analyze the fluidization properties of a mixture in analogy to those of monodisperse beds, by adapting the concept of "minimum fluidization velocity" to more complex systems, so as to quantify the intensity of the bubbling regime typical of higher velocities. This choice is also related to the line of interpretation of most scientists, namely that the dynamics of segregation is regulated by the action exerted by bubbles, since they prove capable of gathering particles in their wake. Though widespread, this theory does not seem supported by any conclusive evidence and it is not clear whether the action of bubbles determines the equilibrium of segregation or it is only dynamically superimposed to the migration of particles caused by forces acting in the dense phase of the fluidized bed. In any case, many authors have made substantial efforts to identify a relationship between segregation and bubble flow rate, to correlate the degree of mixing of the bed to the "*excess velocity* $u - u_{mf}$", contemplated by the simple " two-phase theory ". However the implicit assumption that this parameter is able to quantify the

intensity of the bubbling regime, like in the case of single solid systems, turns out to be wrong, because in the fluidization process of two-solid mixtures particle suspension and bubbling are simultaneous, rather than sequential phenomena.

Starting from these considerations, well established by previous research, this work will show how the actual phenomenology of binary fluidization can be captured only by an approach that replaces the concept of minimum fluidization velocity with a new choice of variables. The development of this novel approach, based on observations made for the first time by Chen and Keairns more than thirty years ago and then substantially abandoned, is on its own an objective of this study. The results obtained by this methodology of analysis show that important aspects of the behaviour of mixtures of two solids can be analyzed in fundamental terms, thus minimizing the use of empirical descriptions.

Chapter 1

A LITERATURE SURVEY

In the industrial processes where fluidization has been employed solids different in many factors (size, density, shape, etc.) are usually handled. With the word *segregation* we refer to the tendency of these solids to accumulate in distinct layers, where the presence of a particular species prevails. Fluid-solid and solid-solid interactions determine the segregation pattern and the particle axial distribution in the bed is set up by the equilibrium between competing mechanisms of solids mixing and particle segregation. Thus, by setting the appropriate operating conditions, the fluidized bed reactors can be operated in different modes either to promote particle mixing or to enhance particle segregation. However in spite of the huge number of experimental studies published in the last three decades, even with mixtures of only two components, the relationship between fluidization regime and level of segregation is still poorly understood, so that no quantitative theory of segregating fluidization is, to date, available.

This history of failures is probably related to the dominant approach followed by almost all the authors so far. This line of thought is presented in section 1.1 together with some of its most notable and unsatisfactory products. This approach considers bubbles as the main cause of segregation and makes use of the "two-phase theory", which is valid for monosolid beds. It is based on the concept of the "excess gas flow rate" u-u_{mf} which requires the

definition of the minimum fluidization velocity u_{mf} of the mixture to quantify the bubble flow rate.

In section 1.2 it is shown as many correlations for u_{mf} have been proposed in literature, which are often arbitrary and purely empirical. This large number of expressions is due to the fact that there is uncertainty even in the definition of this variable, which actually depends on many factors like the initial arrangement of the bed and the rapidity of the defluidizing procedure. However starting from a fixed bed whose state of mixing is known, it is shown as the classical equations used in monocomponent fluidization can be rewritten to take into account the binary nature of the bed.

1.1 PREVIOUS WORKS ON PARTICLE SEGREGATION

1.1.1 MIXING AND SEGREGATION MECHANISMS INVOLVING BUBBLES

In 1962 Rowe and Partridge[1] made a photographic study of the movement of solids produced by the rise of a single bubble. As the bubble forms and rises, it gathers a wake of particles and then draws up a spout of solids behind it as shown in Figure 1.1. The wake grows by the addition of particles and then becomes so large that it sheds a fragment of itself, usually in the form of a complete ring.

The same mechanism was seen to be important in binary gas segregating fluidized beds by Rowe et al.[2] in a pioneering work in 1972, where mixtures of two different kind of near-spherical particles were examined using pairs that differed in size, density or in both ways. Different combinations were studied by identifying the particles differing in density with the words (*L)ight* and *(H)eavy*, those of different size with *(S)mall* and *(B)ig*, those that fluidized at lower velocity (lower u_{mf}) with *(F)luid* as opposed to *(P)acked*. However it should be noted that particles must differ in at least two properties since only two are independent.

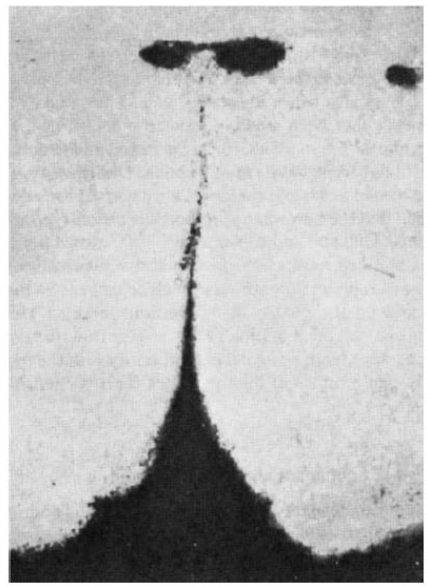

Figure 1.1: Photograph of the solid displacement caused by a single bubble[1].

In all there are six possible combinations which are shown in Table 1.1. This simple and concise terminology is still in common use. The terms *jetsam* and *flotsam*, widely accepted for the component that settles to the bottom and the component that floats to the top, respectively, was also first suggested in this paper.

By fluidizing the mixture from some initial arrangement in either a two-dimensional or a usual cylindrical bed and by following the way in which segregation occurred, three distinctly different mechanisms were found to be important in causing the relative movement of particles in the bed, all associated with bubbles. The lifting of particles in the wake of a rising gas bubble was found to be, at the same time, the primary particle mixing and segregation mechanism (Figure 1.2a).

Table 1.1: Combinations of solids in binary mixtures.	
HBP/LSF	(Heavy, Big, Packed / Light, Small, Fluid)
HSP/LBF	(Heavy, Small, Packed / Light, Big, Fluid)
HSF/LBP	(Heavy, Small, Fluid / Light, Big, Packed)
BP/SF	(equal density)
HP/LF	(equal size)
HS/LB	(equal u_{mf})

Bubbles formed near the bottom of the bed gather solids in their wakes and exchange their content in the upper region by wake shedding (Figure 1.2b); in this way segregated material that has settled to the bottom may be mixed again. This mechanism was seen as the only means by which flotsam particles find their way to the top of the bed.

The jetsam component can migrate down to the bottom of the bed according to two distinct mechanisms: the larger and denser particles descend by falling through bubbles, while the smaller, denser particles percolate downward interstitially (Figure 1.2c). The second mechanism, however, was found to be not an important one, occurring only with jetsam particles sufficiently small, and is restricted only to the regions recently disturbed by a passing bubble.

When the bed is mainly jetsam with a little flotsam tending to float on the surface, an additional mixing mechanism is present. Bubbles arrive at the surface carrying a wake of jetsam which is deposited as a “splash” on top of the bed. This covers and buries flotsam on the surface, which is slowly carried downwards until passing bubbles give it an opportunity to be lifted to the surface again (Figure 1.3).

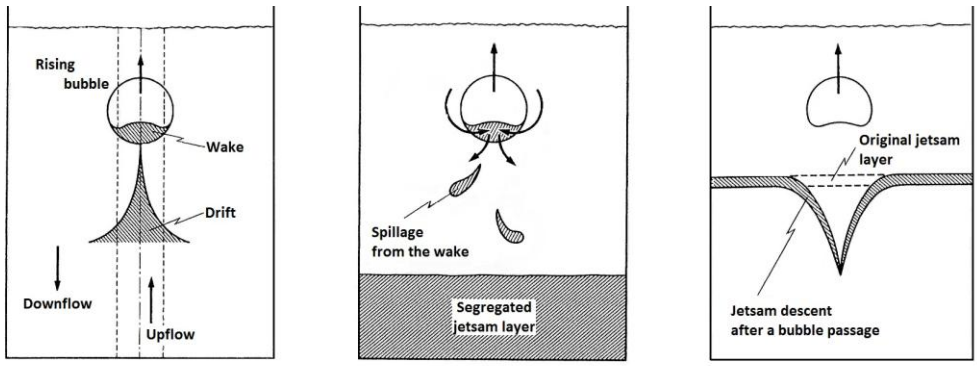

Figure 1.2: Segregation and mixing mechanisms due to bubbles: a) circulation caused by a bubble; b) exchange due to wake shedding; c) descent of jetsam induced by a bubble passage.[3]

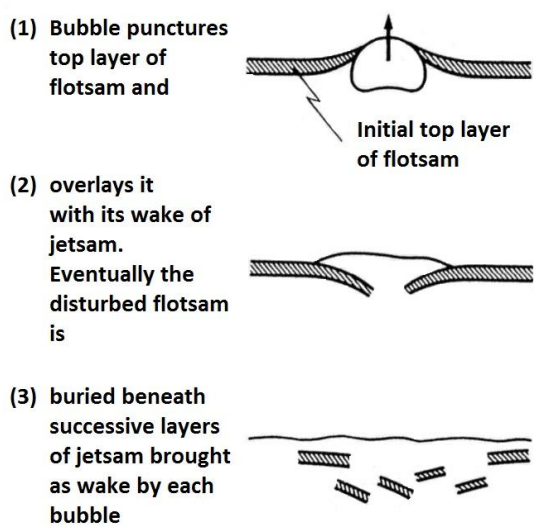

Figure 1.3: Jetsam-rich mixing mechanism.[3]

1.1.2 MATHEMATICAL MODELS AND EMPIRICAL CORRELATIONS

After the work of Rowe et al. a single theory has been prevailing in the scientific community. The presence of an upward flow of bubbles, typical of the gas fluidization regime, has been considered as the main cause of segregation and, at the same time, mixing of the two solids. Following this interpretation, their distribution along the bed height at a given operating condition (average composition of the mixture, fluidizing velocity, etc..) is due to the prevalence of one of the effects over the other. From these observations many mathematical models have been developed to predict the internal homogeneity of the binary system through the quantification of the various effects associated with the passage of bubbles.

A fundamental model for the calculation of segregation patterns was first proposed by Gibilaro and Rowe[5] (the GR model). The bed was assumed to consist of two phases, a wake phase (bubbles) and a bulk phase, among which interchange of solids occurs. Four model parameters were defined to represent the competitive mixing and segregation rate mechanisms: circulation rate *w*, exchange rate *q* between the phases, segregation rate *k* and axial dispersion rate D_p in the bulk phase. The material balance equations describing the movement of jetsam are:

$$\frac{D_p}{H}\frac{d^2x_{j,B}}{dZ^2}+\left(w+k-2k\cdot x_{j,B}\right)\frac{dx_{j,B}}{dZ}+qH\left(x_{j,W}-x_{j,B}\right)=0 \qquad (1.1.1)$$

$$w\frac{dx_{j,W}}{dZ}-qH\left(x_{j,B}-x_{j,W}\right)=0 \qquad (1.1.2)$$

After integration of the previous equations the average volumetric jetsam fraction at the dimensionless height *Z* is (see Figure 1.4):

$$x_j=a_W x_{j,W}+\left(1-a_W\right)x_{J,B} \qquad (1.1.3)$$

In order to make the previous equations deterministic the parameters must be linked to the characteristics of the bed material and the conditions of fluidization. Neglecting axial dispersion (there is no physical reason that justifies the inclusion of a pseudo dispersion mixing mechanism), this was accomplished by using bubble flow models, experimental correlations and the two-phase theory, which in its simplest form states that:

$$Q_B / A = u - u_{mf} \tag{1.1.4}$$

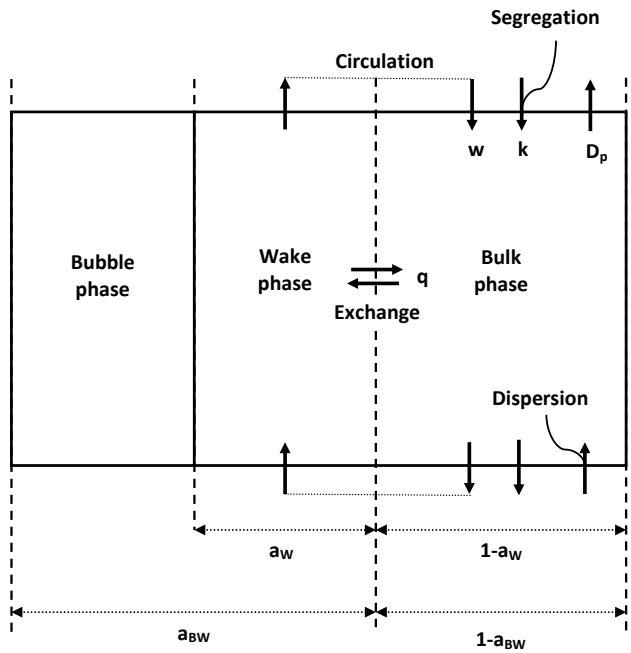

Figure 1.4: Gibilaro and Rowe's model of solid mixing and segregation.[5]

where Q_B is the volumetric bubble flow rate, u is the superficial velocity and u_{mf} is the minimum fluidization velocity. The final result is the set of the following relationships (rewritten here after some rearrangements):

$$q/w = \frac{3}{2}\frac{u_{mf}}{\varepsilon_{mf} d_B u_B} \qquad k/w \approx \frac{1}{2}\left(\frac{\rho_j}{\rho_f}\frac{d_j}{d_f}\right)^{0.3} \qquad a_W = \frac{f_W}{1-f_W}\frac{\left(u-u_{mf}\right)/u_B}{1-\left(u-u_{mf}\right)/u_B}$$

From inspection of the above expressions, it appears that, for a given system and at a given gas velocity, the equilibrium particle concentration profile depends both on bubble parameters (wake fraction, i.e. wake volume/bubble volume, bubble diameter and velocity) and emulsion properties (minimum fluidization velocity and voidage). It should be noted that the actual relationships between these parameters and the operating conditions are quite uncertain and the model provides a qualitative agreement with the segregation pattern only in typical cases and if appropriate values for the parameters are chosen. The uncertainty is related not only to the estimation of bubble parameters, which are difficult to predict even for a monocomponent bed, but also to the evaluation of the minimum fluidization velocity and the interparticle voidage for a mixture. For binary mixtures u_{mf} is a function of the relative proportions of the two components and varies from point to point within the bed, depending on the local composition. After the first attempt of Gibilaro and Rowe other similar models have been proposed (Burgess et al.[6], Yoshida et al[7]). These models all divide the bed into the wake (or bubble) phase and the bulk (or emulsion) phase, but the assumptions made for the particle exchange between the two phases distinguishes each individual model. However, they are all restricted to systems of binary mixtures and of limited accuracy. Since the mechanistic models did not produce further substantial developments, the efforts began to be directed toward empirism.

Thus, even if it is not quite clear whether the action of bubbles determines the segregation equilibrium or is just superimposed to it, many authors have looked for a relationship between segregation and bubble flow rate and several empirical equations have been proposed to relate the degree of mixing of the bed components to the excess gas velocity $u-u_{mf}$. Purely empirical but quantitative analysis of segregation has been conducted by Nienow et al.[8], who reported that during fluidization the upper part of the bed attains a fairly

uniform composition, whereas the component that tends to sink forms a concentrated bottom layer. However this is approximately true only when the flotsam component is the more abundant species. The segregation patterns for practical binary systems are shown in Figure 1.5 for flotsam-rich systems and in Figure 1.6 for jetsam-rich mixtures.

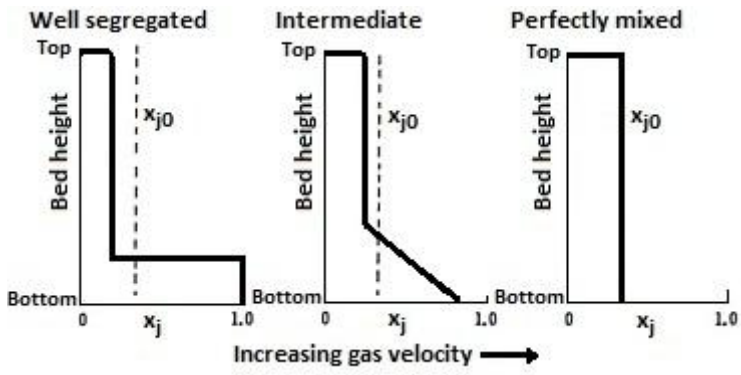

Figure 1.5: Practical states of equilibrium for flotsam-rich systems.

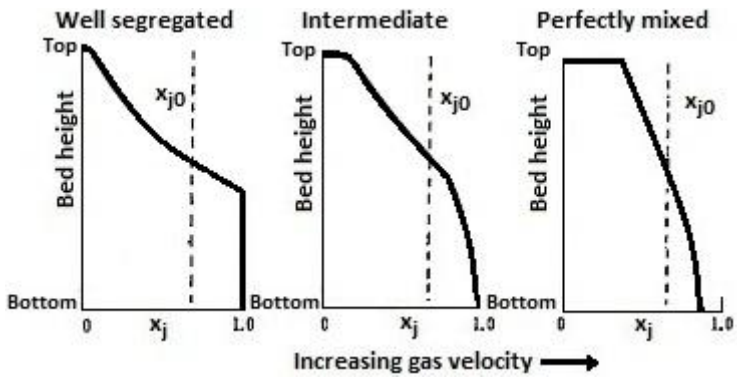

Figure 1.6: Practical states of equilibrium for jetsam-rich systems.

For flotsam-rich systems, containing less than about 50% by volume of jetsam, they introduced a mixing index *M*, which varies between 0 and 1, to measure the degree of homogeneity of the axial distribution of the species in the solid mixture (Figure 1.7):

$$M = \frac{x_j^{sup}}{x_{j0}} \tag{1.1.6}$$

Looking once again at bubbles as the main cause of segregation and mixing, the authors assumed that their flow starts at the incipient fluidization velocity of the flotsam component (that with lower u_{mf}) and the values of M are therefore related to the excess gas velocity $u-u_{mf,f}$. They showed that the mixing index could be correlated by a logistic equation:

$$M = \frac{1}{1+e^{-F}} \tag{1.1.7}$$

where:

$$F = \left(\frac{u-u_{T0}}{u-u_{mf,f}}\right)\exp\left(\frac{u}{u_{T0}}\right) \tag{1.1.8}$$

is a function of the "take-over velocity" u_{TO}, a parameter set equal to the value of u at M=0.5, where $dM/d\left(u-u_{mf,f}\right)$ is a maximum. It is conceptually the velocity below and above which predominate, respectively, segregation and mixing.

In the lack of experimental data u_{T0} could be estimated by the following empirical equation:

$$\frac{u_{T0}}{u_{mf,f}} = \left(\frac{u_{mf,j}}{u_{mf,f}}\right)^{0.5} + 0.9\left(\rho_R - 1\right)^{1.1} d_R^{0.7} - 2.2\overline{x_j}^{0.5}\left(H^*\right)^{1.4} \tag{1.1.9}$$

where:

$$\rho_R = \rho_j / \rho_f \qquad d_R = \left(\phi_J d_j\right)/\left(\phi_f d_f\right) \qquad H^* = 1-\exp\left(-H/D\right)$$

Modified versions of Eq. (1.1.8), meant to extend its validity to two-size and jetsam-rich mixtures and to improve its accuracy, were proposed by Rice and Brainovich[9], Peeler and

Huan[10] and Leaper et al.[11] but their usability is complicated by the presence of parameters of difficult determination.

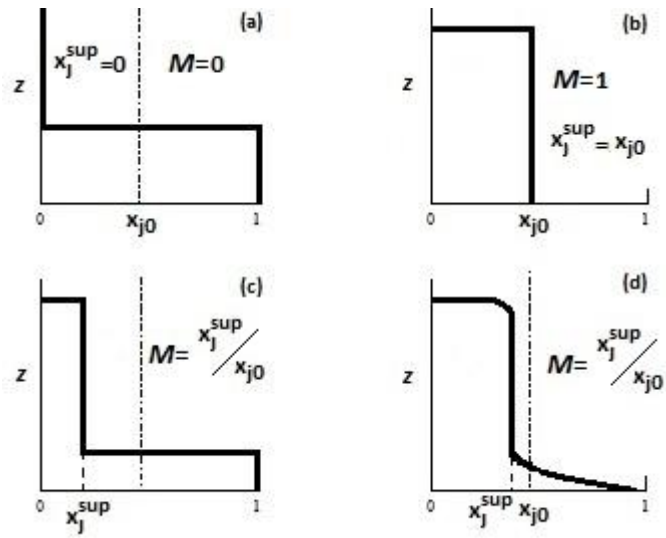

Figure 1.5: Axial concentration distribution and values of *M* :(a) total segregation, (b) perfect mixing, (c) low velocity distribution, (d) high velocity distribution.

The predictive effectiveness of these relationships was tested by Wu and Baeyens[12] who pointed out the limited capacity of all of them to fit experimental data and accordingly proposed a new, supposedly more accurate relationship that makes use of the "minimum fluidization velocity of the mixture" u_{mf} and of the excess gas velocity $u-u_{mf}$, two variables whose definition is taken from the theory of monosolid fluidization. However it is unlikely that giving for granted the similarity of behaviour between monosolid and binary systems can effectively capture the aspects of the mixture behaviour that are essential to identify the independent variables of the segregating fluidization problem. With regard to that, a crucial point is that of addressing the limitations associated to the extension to these systems of the concept of "minimum fluidization velocity".

1.2 THE MEASUREMENT AND DEFINITION OF THE MINIMUM FLUIDIZATION VELOCITY OF A MIXTURE

1.2.1 CORRELATIONS FOR THE MINIMUM FLUIDIZATION VELOCITY OF A MIXTURE

The minimum fluidization velocity of a fluidized bed with a single component bed material, i.e., a bed material with particles of relatively narrow particle size distribution and of similar particle density, is well defined. For mixtures of particles of different size or density, especially for highly segregating system, the definition and determination of the minimum fluidization velocity are not as straightforward. Though the minimum fluidization velocity of a segregating mixture can still be defined conventionally following the procedure suggested for a single component system, that is determining it at the intersection of the two extrapolated linear portion where the whole bed is, first, packed and, second, fluidized, this variable defined in this way loses its physical meaning because the particles in the bed are far from being completely supported by the fluidizing gas at this velocity. For an initially well mixed system the pressure drop versus gas flow rate relationship with increasing gas velocity is generally different from that obtained on subsequently reducing velocity. If the mixture is fluidized at $u>>u_{mf,j}$ and then u is reduced to zero, then depending on the defluidizing procedure and the physical properties of the two components, the settled bed obtained will have one of the three mixing-segregation states indicated by Figure 1.7 (i).

For an ideal system where the particles are of small size difference and of equal density, both the ascending and descending portions of the fluidization curve will coincide, shown as curve (a) in Figure 1.6. In this case a good mixing is obtained at the end of the defluidizing process and the conventional procedure will yield a minimum fluidization velocity, shown as $u_{mf,M}$.

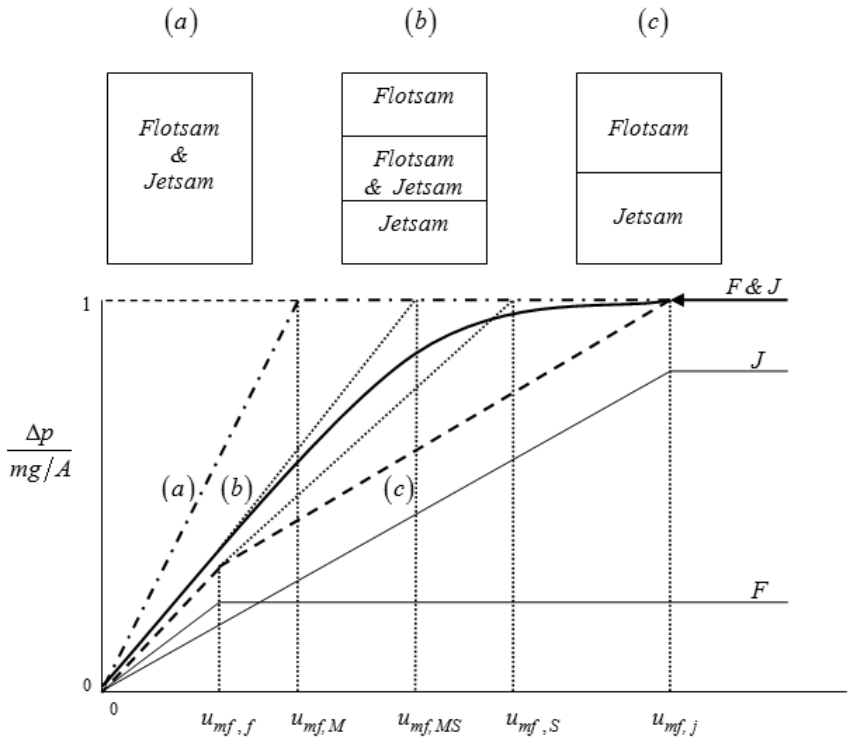

Figure 1.7: Defluidization curve and minimum fluidization velocity of a binary mixture. Final fixed bed: (a) well mixed, (b) partly mixed, (c) totally segregated.

For a highly segregating mixture where the particle separation rate is fast, the fluidization curve follows curve (a) for the ascending portion but descends along curve (c). This is because the mixture separates into two distinct layers of flotsam and jetsam when $u>u_{mf,j}$ and remains completely segregated until all fluidization has ceased (Figure 1.7c). Curve (c) is unique and can be constructed a priori by adding together the contributions from the pure components, as shown in Figure 1.7. The conventional procedure of determining the minimum fluidization velocity will give a velocity $u_{mf,S}$ defined in Chiba et al.[13] as the apparent minimum fluidization velocity.

In the most frequent case the upper part of the bed is flotsam-rich, the lower jetsam-rich and there is a mixed region in the middle (Figure 1.7b). The descending portion of the fluidization curve of any real systems lies between (a) and (c), such as curve (b). Curve (b) will tend towards curve (a) if the species only differ in size and defluidization is rapid, towards curve (c) if defluidization is low and the particles differ in density. Thus the velocity $u_{mf,MS}$ as obtained in Figure 1.7 turns out to depend on the defluidizing procedure.

Despite this variety of situations, it has been attempted to develop equations capable to predict the value of u_{mf} from the properties of the system, adopting the same definition of u_{mf} for monocomponent bed also for a binary mixture. By the experimental determination of the minimum fluidization velocity of different systems, this attempt led to the development of a very large number of correlations whose Table 1.2 shows, in chronological order, a broad overview.

One of the first expression proposed (the first in Table 1.2) due to Otero and Corella[14], calculates u_{mf} as a volume weighted average of the minimum fluidization velocity of the two components. With the advantage of a very simple functional form, this equation provides predictions far from being satisfactory whenever the two solids differ only or also for the particle diameter.

It has been attempted in many studies, to consider the mixture as an "equivalent monodisperse solid", that is characterized by a density and a diameter to be calculated in various ways making the average on the corresponding properties of the individual components. This type of approach is behind the equations in Table 1.2 and include eqns 2, 3, 8 and 11. From their comparison it seems there is no agreement on the type of mean used to define the parameters of the solid and the choice of different authors, nearly always independent from general theoretical considerations, it is often justified with the argument that the average adopted leads to a better agreement between predictions and experimental data.

Table. 1.2: Minimum fluidization velocity of a mixture of two solids: experimental correlations (continues).

N°	*References*	*Correlations and definitions*
1	Otero, A. R., e Corella, J., (1971)[14]	$u_{mf} = u_{mf,f} x_{f0} + u_{mf,j} x_{j0}$
2	Goossens, W. R. A. et al. (1971)[19]	$u_{mf} = \frac{\mu_g}{\rho_g \bar{d}}\left[\left(33.7^2 + 0.0408Ar\right)^{0.5} - 33.7\right]$ $Ar = \frac{\bar{d}^3 \rho_g^2 g\left(\bar{\rho} - \rho_g\right)}{\mu_g^2}$ $\frac{1}{\bar{\rho}} = \frac{w_{f0}}{\rho_f} + \frac{w_{j0}}{\rho_j}$ $\quad$ $\frac{1}{\bar{\rho}\bar{d}} = \frac{w_{f0}}{\rho_f d_f} + \frac{w_{j0}}{\rho_j d_j}$
3	Kumar, A. e Sen Gupta, P., (1974)[20]	$u_{mf} = 0.0054 \frac{\bar{d}^{1.34}\left(\bar{\rho} - \rho_g\right)^{0.78} g^{0.78}}{\mu_g^{0.56} \rho_g^{0.22}}$ $\bar{\rho} = w_{f0}\rho_f + w_{j0}\rho_{j0}$ $\quad$ $\frac{1}{\bar{d}} = \frac{w_{f0}}{d_f} + \frac{w_{j0}}{d_j}$
4	Cheung, L. et al., (1974)[16]	$u_{mf} = u_{mf,f}\left(\frac{u_{mf,j}}{u_{mf,f}}\right)^{w_{j0}^2}$
5	Rowe, P. N. e Nienow, A. W., (1975)[21]	$u_{mf} = u_{mf,f} \frac{\left[\left(\frac{\varepsilon_{mf}}{\varepsilon_{mf,f}}\right)^3 \left(\frac{1-\varepsilon_{mf,f}}{1-\varepsilon_{mf}}\right)^{0.947}\right]^{0.95}}{\left[w_{f0} + \left(\frac{u_{mf,f}}{u_{mf,j}}\right)^{0.54} w_{j0}\right]^{1.85}}$

Table. 1.2: Minimum fluidization velocity of a mixture of two solids: experimental correlations (continues).

N°	*References*	*Correlations and definitions*
6	Chiba, S. (1977)[22]	$u_{mf} = u_{mf,f} \dfrac{\left[x_{f0} + \left(1 - x_{f0}\right)\left(\rho_j / \rho_f\right)\right]^{0.95}}{\left[w_{f0} + \left(\dfrac{u_{mf,f}}{u_{mf,j}} \dfrac{\rho_j}{\rho_f}\right)^{0.54} w_{j0}\right]^{1.85}}$
7	Chiba, S. et al. (1979)[13]	Well mixed bed $u_{mf} = u_{mf,f} \dfrac{\overline{\rho}}{\rho_f}\left(\dfrac{\overline{d}}{d_f}\right)^2$ Segregated bed $u_{mf} = \dfrac{u_{mf,f}}{\left(1 - u_{mf,f}/u_{mf,j}\right) w_{f0} + u_{mf,f}/u_{mf,j}}$ $\dfrac{1}{\overline{\rho}} = \dfrac{w_{f0}}{\rho_f} + \dfrac{w_{j0}}{\rho_j}$ $\quad \overline{d} = \left[f_{N,f} d_f^3 + \left(1 - f_{N,f}\right) d_j^3 \right]^{1/3}$ $f_{N,f} = \left\{ 1 + \left[\left(\dfrac{1}{x_{f0}} \right) - 1 \right] \left(\dfrac{d_f}{d_j} \right)^3 \right\}^{-1}$
8	Thomglimp, V. et al. (1981)[23]	$u_{mf} = \dfrac{\mu_g}{\rho_g \overline{d}} \left[\left(19.9^2 + 0.03196 Ar\right)^{0.5} - 19.9 \right]$ $\dfrac{1}{\overline{\rho}} = \dfrac{w_{f0}}{\rho_f} + \dfrac{w_{j0}}{\rho_j}$ $\quad \dfrac{1}{\overline{d}} = \dfrac{w_{f0}}{d_f} + \dfrac{w_{j0}}{d_j}$

The common feature of these equations is of taking advantage, sometimes in explicit form, of the approximation of Wen and Yu[15], which showed how knowledge of the voidage of the bed and particle shape is not essential (except in very special cases) to give a reasonable

estimate of u_{mf}. This is because for the most commonly used solid, the following correlations are valid:

$$\frac{1-\varepsilon_{mf}}{\phi^2\varepsilon_{mf}^3} \cong 11 \qquad \frac{1}{\phi\varepsilon_{mf}^3} \cong 14 \qquad \text{(1.2.1),(2)}$$

The numerical values expressed by eqns (1.2.1) and (1.2.2) should not vary from mixture to mixture and, in the beds of two spherical solids, this is equivalent to assume that the minimum fluidization voidage ε_{mf} does not depend on the nature (size and density) of particles. As discussed below, this assumption is incorrect and is probably the major cause of inaccuracy of the correlations that use it.

Again with reference to Table 1.2, other equations (4, 5, 6, 7, 9 and 10) calculate the u_{mf} of the mixture as a function of the minimum fluidization velocity of its components. Even on these correlations, none of which has been shown to have good predictive capabilities, it is possible to make a general remark: assuming that in a mixture the u_{mf} of each solid keeps on having some meaning is equivalent to ignore that it is not a material property since it is also function of the voidage condition, which is again implicitly assumed unchanged when the two particles form a mixture. Furthermore the procedure of averaging the values of u_{mf} often corresponds, especially in the viscous regime, to suggesting another particular mean for the physical properties of the two components.

However it should be noted that, over the years, the thoroughly empirical correlation of Cheung et al.[16] (Table 1.2 the number 4) has been the one which leads to predictions of u_{mf} very accurate, even at high pressure, for initially well mixed bed whenever the size ratio d_l / d_f <3 and the difference in density is moderate.

Table. 1.2: Minimum fluidization velocity of a mixture of two solids: experimental correlations (end).

N°	References	Correlations and definitions
9	Obata, E. H. et al. (1982)[24]	$u_{mf} = \sum_i w_{f0,i} / u_{mf,i}$
10	Uchida, S. et al. (1983)[25]	$u_{mf} = u_{mf,j}\left(1 - x_{f0}\right)^m$ $m = 0.17\left[\left(d_j / d_f\right)\left(\rho_f / \rho_j\right)\right]^{0.437}$
11	Noda, K. et al. (1986)[26]	$Ar = A\mathrm{Re}_{mf}^2 + B\mathrm{Re}_{mf}$ $Ar = \frac{\bar{d}^3 \rho_g^2 g\left(\bar{\rho} - \rho_g\right)}{\mu_g^2}$ $\quad Re_{mf} = \frac{\rho_g u_{mf} \bar{d}}{\mu_g}$ $\frac{1}{\bar{\rho}} = \frac{w_{f0}}{\rho_f} + \frac{w_{j0}}{\rho_j}$ $\quad \frac{1}{\overline{\rho d}} = \frac{w_{f0}}{\rho_f d_f} + \frac{w_{j0}}{\rho_j d_j}$ $A = 36.2\left(\frac{d_j}{d_f}\frac{\rho_f}{\rho_j}\right)^{-0.196}$ Well mixed bed $\quad B = 1397\left(\frac{d_j}{d_f}\frac{\rho_f}{\rho_j}\right)^{0.29}$ Partly segregated bed $\quad B = 6433\left(\frac{d_j}{d_f}\frac{\rho_f}{\rho_j}\right)^{-1.86}$
12	Formisani, B. (1991)[18]	$u_{mf} = \frac{\bar{d}^2\left(\rho_s - \rho_g\right) g \varepsilon_{mf}^3}{180\mu\left(1 - \varepsilon_{mf}\right)}$ $\quad \frac{1}{\bar{d}} = \frac{x_{f0}}{d_f} + \frac{x_{j0}}{d_j}$ $\varepsilon_{mf} = \varepsilon_{mf}\left(x_{f0}, d_j / d_f\right)$

1.2.2 A THEORETICAL EQUATION FOR THE U_{MF} OF A MIXTURE

At number 12 of Table 1.1 appears the form in which the equation of Carman-Kozeny (or the Ergun's one with coarse or very dense particles), must be rewritten to take into account the binary nature of the mixture. This research is the result of a study carried out years ago at the University of Calabria and started from a study by Yu and Standish[17] who showed that the homogeneous packing of a binary bed is strongly influenced by both the component size ratio and the volumetric composition. Starting from these considerations Formisani[18] showed that, in two-size mixtures, the voidage can assume values significantly lower than those typical of the monocomponent bed. Neglecting such an effect leads to the systematic underestimation of the interstitial gas velocity and hence of the friction exerted on the particles. The typical variation of the voidage conditions for a homogeneous bed is shown in Figure 1.8, for two mixtures of glass ballotini (GB) with size ratio equals to 2.9 and 4.1 respectively (mean Sauter diameters are in μm), revealing as the interparticle voidage is strongly dependent on composition, displaying often a minimum near x_f=0.4, as well as on the particle diameter ratio d_j/d_f, decreasing considerably when the difference in size increases.

Introducing the experimental value of $\varepsilon_{mf,m}$ in the Carman-Kozeny equation and using a mean particle diameter that returns the surface to volume ratio of the whole mixture, i.e. the Sauter mean diameter:

$$\frac{1}{d_{av}} = \frac{x_{f0}}{d_f} + \frac{1-x_{f0}}{d_j} \tag{1.2.3}$$

the following equation is obtained:

$$u_{mf} = \frac{d_{av}^2\left(\rho_s - \rho_g\right)g\varepsilon_{mf,m}^3}{180\mu\left(1-\varepsilon_{mf,m}\right)} \tag{1.2.4}$$

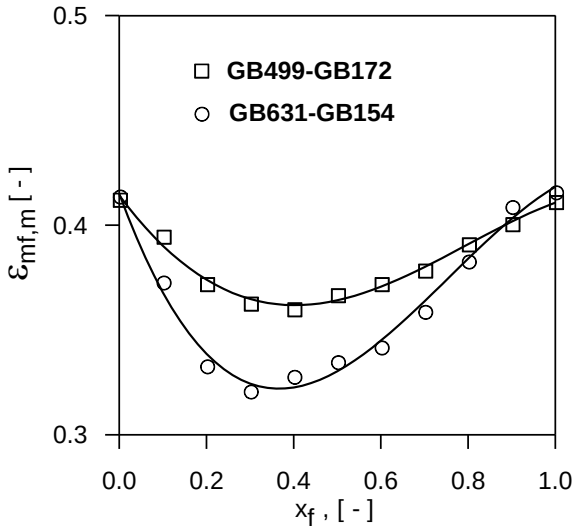

Fig.1.8: Typical voidage variation of well-mixed beds with flotsam composition. Beds of glass ballotini GB of different size (μm).

The predictions of eqn (1.2.4) show a good agreement with experimental data and are very close to those provided by the empirical relationship of Cheung et al., which has already been reported as very reliable.

For a binary system whose components differ only in density, assuming identity of voidage of the individual components and their mixtures, it is easy to verify that the correlations 2, 6 (approximately) and 7 of Table 1.1 simplify to the expression proposed by Otero and Corella:

$$u_{mf} = u_{mf,f}\, x_{f0} + u_{mf,j}\left(1 - x_{f0}\right) \tag{1.2.5}$$

This in turn is equivalent to the equation of Carman-Kozeny rewritten as follows:

$$\frac{180\mu_g u_{mf}}{d^2}\frac{\left(1-\varepsilon_{mf}\right)^2}{\varepsilon_{mf}^3} = \left[\left(\rho_f - \rho_g\right)x_{f0} + \left(\rho_j - \rho_g\right)\left(1 - x_{f0}\right)\right]\left(1-\varepsilon_{mf}\right)g \tag{1.2.6}$$

The velocity calculated by eqn (1.2.6) does not depend on the initial arrangement of the bed and this shows an important limitation of the concept of the minimum fluidization velocity for this category of systems. Thus, u_{mf} is not capable to distinguish the diversity of behavior of two beds with respect to their segregation tendency, since it assumes the same value both for a well-mixed system and a completely segregated one. Furthermore eqn (1.2.6) is valid only if the voidage ε_{mf} that appears in it is assumed to be constant: this is a good assumption whenever particles do not differ in size.

When the solids are initially arranged in the fixed bed as two segregated layers, with the fine component on top, u_{mf} can be evaluated by equation number 7 in Table 1.1 for a segregated bed. It is obtained by modeling the pressure drop in each layer by means of the original Carman-Kozeny equation for a monocomponent bed. Equation 7 is in fact equivalent to the expression:

$$180\mu_g u_{mf}\left[\frac{\left(1-\varepsilon_{mf,f}\right)}{\varepsilon_{mf,f}^3}\frac{x_{f0}}{d_f^2}+\frac{\left(1-\varepsilon_{mf,j}\right)}{\varepsilon_{mf,j}^3}\frac{x_{j0}}{d_j^2}\right]=\left(\rho_s-\rho_g\right)g \qquad (1.2.7)$$

By rearranging eqn (1.2.7), it is possible to show that u_{mf} in this case is the harmonic mean of the single solid minimum fluidization velocities:

$$u_{mf}=\left(\frac{x_{f0}}{u_{mf,f}}+\frac{1-x_{f0}}{u_{mf,j}}\right)^{-1} \qquad (1.2.8)$$

However tthis result is valid only for a size segregating bed.

For an arbitrary initial distribution the most general form to write the equation for u_{mf}, given by Formisani et al.[27], is:

$$180\mu_g u_{mf}\int_0^H \frac{(1-\varepsilon_{mf})^2}{d_{av}^2\varepsilon_{mf}^3}dz = g\int_0^H (\rho_{av}-\rho_g)(1-\varepsilon_{mf})dz = \frac{(m_j+m_f)g}{A} \quad (1.2.9)$$

where ρ_{av} is defined as:

$$\rho_{av} = \rho_f x_f + \rho_j(1-x_f) \quad (1.2.10)$$

For the particular case of a well-mixed bed Eqn (1.2.9) becomes:

$$180\mu_g u_{mf}\frac{(1-\varepsilon_{mf,m})}{d_{av}^2\varepsilon_{mf,m}^3} = (\rho_{av}-\rho_g)g \quad (1.2.11)$$

This same equation can successfully be used for predicting, as well as the minimum fluidization velocity, the axial pressure profile in the packed bed, bearing in mind that any change of x_f along the vertical axis implies a consequent variation both in local voidage and in particle diameter:

$$\Delta p = 180\mu_g u\int_0^H \frac{(1-\varepsilon_{mf})^2}{d_{av}^2\varepsilon_{mf}^3}dz \quad (1.2.12)$$

Thus any intermediate initial state of mixing gives rise to a peculiar Δp versus u curve, so that it can be said that in experiments conducted at increasing gas flow rate any binary system of given average composition x_{f0} exhibits as many values of its minimum fluidization as it has packed bed composition profiles. This implies that evaluating u_{mf} for a initially well mixed or completely segregated bed may have no sense. However Formisani et al.[27] showed that when gradually defluidized from a condition of full fluidization, any mixture gives place to a fixed bed having a repeatable and characteristic axial composition profile, and such a

defluidization pattern defines the only repeatable u_{mf} of the mixture. When, in fact, the determination of u_{mf} is made at decreasing gas flow rate starting from the fully fluidized regime, as generally advised also for monodisperse beds, any mixture gradually reverts to the fixed state along a repeatable pressure drop path which is characteristic of its average composition x_{f0}. Once that the mixture has reached its state of repose, any subsequent fluidization/defluidization cycle follows this pressure drop locus, so that its u_{mf} remains, since then on, unvaried. However understanding the mechanism through which defluidization spontaneously gives rise to equilibrium mixing profiles is not easy, and a better description would be welcome. The rather complex nature of the composition profiles obtained by defluidization can hardly be encompassed, as ordinarily done in the most of literature, in a unique mixing index referred to the whole bed mass or be predicted by the available mechanistic models which fails in providing the equilibrium particle distribution when a defluidized region is present. Anyway, once that the x_f versus z curve in the packed bed has been determined experimentally, it is possible to predict the value of the minimum fluidization velocity it repetitively corresponds to.

However eqn (1.2.9) requires knowledge of the variation of voidage with composition, but the difficulty of dealing with this additional variable can be easily overcome. In fact, when experimental data are lacking, voidage can be estimated by one of the correlations available in literature, among which the equation of Yu et al.[28] is the most used:

$$\left(\frac{V_0 - x_b V_b}{V_s}\right)^2 + 2G\left(\frac{V_0 - x_b V_b}{V_s}\right)\left(\frac{V_0 - x_b - x_s V_s}{V_b - 1}\right) + \left(\frac{V_0 - x_b - x_s V_s}{V_b - 1}\right)^2 = 1 \qquad (1.2.13)$$

where the V_i are specific volumes:

$$V_0 = \frac{1}{1-\varepsilon_0} \qquad V_b = \frac{1}{1-\varepsilon_b} \qquad V_s = \frac{1}{1-\varepsilon_s}$$

and with ε_0 being the porosity of the mixture, ε_b and ε_S the voidage of the bigger and smaller components alone. For Geldart B particles is then possible to assume $\varepsilon_0 \approx \varepsilon_{mf,m}$. The empirical constant *G* is independent on the composition of the mixtures but depends on the size ratio of the particles. The authors gave the following values for *G*:

$$\frac{1}{G} = 1.355\left(\frac{d_S}{d_B}\right)^{1.566} \qquad \text{for} \qquad d_S/d_B \leq 0.824$$

$$\frac{1}{G} = 1 \qquad \text{for} \qquad d_S/d_B \geq 0.824$$

Even if it possible to estimate voidage through correlations available in literature, in order to eliminate any source of error that can interfere with the analysis of other aspects of the dynamics of segregating fluidization, in this work the voidage has been measured experimentally since it is very easy to determine it at laboratory scale.

In this chapter it has been pointed out that the interpretation of the fluidization behavior of segregating binary mixtures of solids can hardly be achieved on a merely empirical ground. On the contrary, some of its essential features can successfully be subjected to a theoretical analysis that accounts for the peculiar nature of the two-component system. In this regard the recognition of the dependence of bed voidage and particle average diameter on mixture composition is the essential condition for getting over current empirical approaches to segregating fluidization and for restoring the predictive ability of theoretical equations. To this purpose, Carman-Kozeny equation should be rewritten in a differential form suitable for the peculiar characteristics of two-component systems, taking into account the axial variability of bed voidage and of particle average diameter.

The value of the minimum fluidization velocity of a binary mixture of solids is thus strongly influenced by the internal composition profile of its bed and, since segregation phenomena

accompanies the transition to the fluidized state, it appears evident as a single velocity threshold is not capable to properly describe the actual behavior of these systems.

In order to overcome this difficulty, a clearer and more rigorous approach is introduced in the next chapter: it is based on the definition of the “fluidization velocity interval” of the mixture.

Chapter 2

THE FLUIDIZATION VELOCITY INTERVAL

Though it is possible to rewrite the classical equations for predicting the minimum fluidization velocity in forms suitable to take into account the binary nature of mixtures, i.e. introducing the variability of the voidage with composition and the initial distribution of the two solids in the fixed bed, the approach that extends to beds of two solids the concept of "minimum fluidization velocity" is far from allowing any further developments of the theoretical analysis. In section 2.1 it is shown as binary fluidization is never an instantaneous process, i.e. it does not occur at a unique velocity threshold. An approach more closer to the actual phenomenology of the process is presented in section 2.2: it is based on the definition of the "*initial*" and "*final fluidization velocity*".

In section 2.3 the early works whose authors have acknowledged the gradual nature of the phenomenon, often in the light of the analogy with thermodynamics, are briefly presented. However, this approach was then substantially abandoned even if, as shown is section 2.3, the definition of the fluidization velocity interval allows easy identifying the independent variables which affect the fluidization properties of a mixture.

2.1 BINARY FLUIDIZATION PHENOMENOLOGY

It has been observed that the fluidization of a mixture of two granular solids is a gradual process during which changes in the axial distribution components occur. The mechanism by which a homogeneous mixture of two solids achieves fluidization is more complex than that of a monosolid system in that it develops along an extended velocity interval and is accompanied by segregation and remixing of system components.

By progressively increasing the velocity of the gas flowing across the fixed bed a point is reached at which the flotsam particles located in the upper region of the bed are first fluidized and gather up in a thin bubbling layer while the jetsam ones, previously mixed with them, form a static layer underneath (Figure 2.1-a). While it fixes the value of "*initial fluidization velocity* u_{if}" , this event coincides with the appearance of a fluidization front which gradually shifts downwards in response to any further increase of the gas flow rate. Subsequently, as much as u exceeds u_{if} a larger part of the system is involved in the suspension process and the two layers grow in thickness (Figure 2.1 b) while, under them, the height of the region not yet reached by the fluidization front, i.e. the residual portion of the original mixture, decreases. Along with the increase of the gas velocity over u_{if}, the intensity of the bubbly flow through the flotsam layer grows and, consequently, the interface between the two layers becomes less and less distinct. Eventually, the whole mixture is suspended into the upflowing gas at the "*final fluidization velocity* u_{ff}"; varying with the specific nature of the mixture as well as with its composition, the state of complete fluidization corresponds to a higher degree of component mixing (Figure 2.1-c) even if a top layer of practically pure flotsam is always observed.

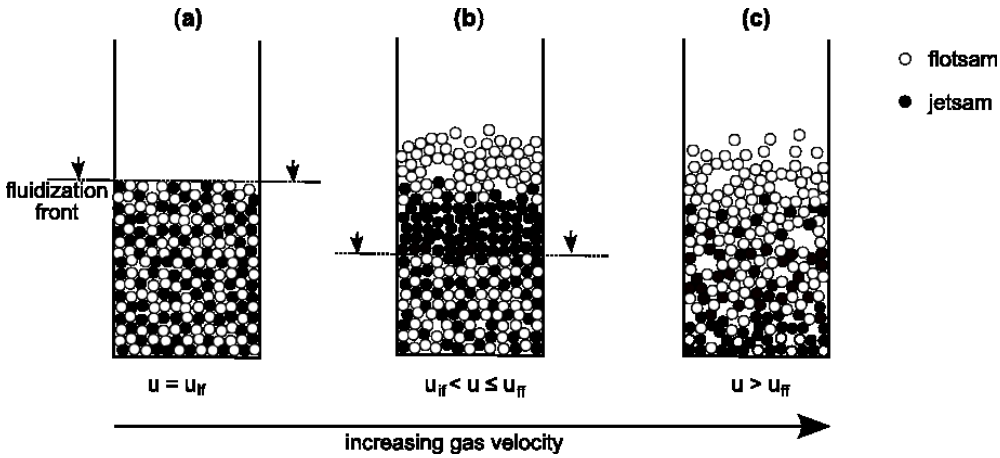

Figure 2.1: Segregation mechanism in the fluidization process of two-solid beds.

In two-size mixtures the tendency of the system to restore the mixed state begins to prevail below the final fluidization velocity, which usually coincides with the threshold at which the system is again practically mixed, except in a region immediately above the gas distributor, whose extension is however of limited extension, in which there is invariably a certain prevalence of the jetsam component. In two-density mixtures, segregation phenomena are more accentuated and in some cases the almost total stratification of the system is observed at the final fluidization velocity.

2.2 A CLEARER APPROACH

Going by what prevails in the literature, devising predictive equations for u_{mf} should be considered a key result for a deeper analysis of binary fluidization, because, when addressing the mechanism of solids segregation, most authors have agreed that it is driven by bubbles flowing through the bed.

However from the example of Figure 2.2, which illustrates the behavior of a size-segregating bed but has a general validity, it is clear that at u_{mf}, defined as for a single component system, the upper portion of the bed is fluidized and the bottom is fixed, indicated by the fact that the gas pressure drop is less than the weight of the bed per unit section.

Even clearer is the case of segregated mixtures whose jetsam component initially forms the top layer. As early reported by Rowe et al.[2] and analyzed also elsewhere[29] the distinctive feature of the process by which a segregated binary mixture with the coarser component initially on top achieves the fluidized state fluidization is that of having an abrupt start, marked by strong system instability.

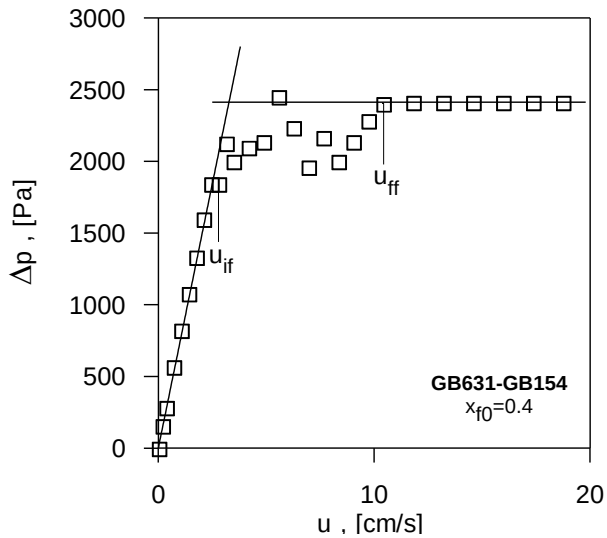

Figure 2.2: Pressure drop diagram of a two-component mixture.

The phenomenology of fluidization observed is summarized in Figure 2.3, where the succession of states encountered at increasing gas flow rate is outlined together with the diagram of the total pressure drop Δp in function of the fluidizing gas velocity u. At low flow rates, the binary bed is at rest in its stratified arrangement (a) while the pressure drop across it steadily grows until, with the increase of fluidization velocity, a critical threshold is

reached at which a horizontal crack develops within the fine component mass (b) (or, sometimes at the distributor level) causing the instantaneous diminution of Δp. This event occurs after the incipient velocity of the finer solid has been exceeded, since the coarse component that forms the upper layer of the bed acts as an obstacle to its mobilization. Subsequently, the particulate mass downstream the crack is lifted bodily as a plug (c) and during its rise the fine particles gradually fall down (d) onto the underlying bubbling bed, while Δp gradually decreases. Eventually, the plug of coarse particles suddenly collapses, so that these mix up with the rest of the bed (e) while the pressure drop stabilizes at its final value. The analysis of the Δp versus u curve of Figure 2.3 clearly indicates that the coarse-on-fine segregated arrangement of the mixture is characterized by a peculiar fluidization pattern, very different from that encountered with binary beds that move from any other initial state of mixing.

The main feature of this pattern, namely the instability through which the particle system abandons its packed state, apparently originates from the fact that the gas pressure drop across the bed grows over the level of the buoyant weight per unit section which normally marks the onset of the fluidization equilibrium. Past a critical value, that gives rise to an unbalanced force which is responsible for the sudden lift of the solid plug. The pressure drop curve provides the evidence that, much more evidently than for the case of well-mixed binary beds, trying to extend the concept of “minimum fluidization velocity” to a stratified mixture is misleading. When the conventional definition of u_{mf} is applied, the intersection between the fixed bed curve with the horizontal line of the fluidized regime invariably identifies a velocity at which the particle assembly is far from being even partially suspended in the upflowing gas.

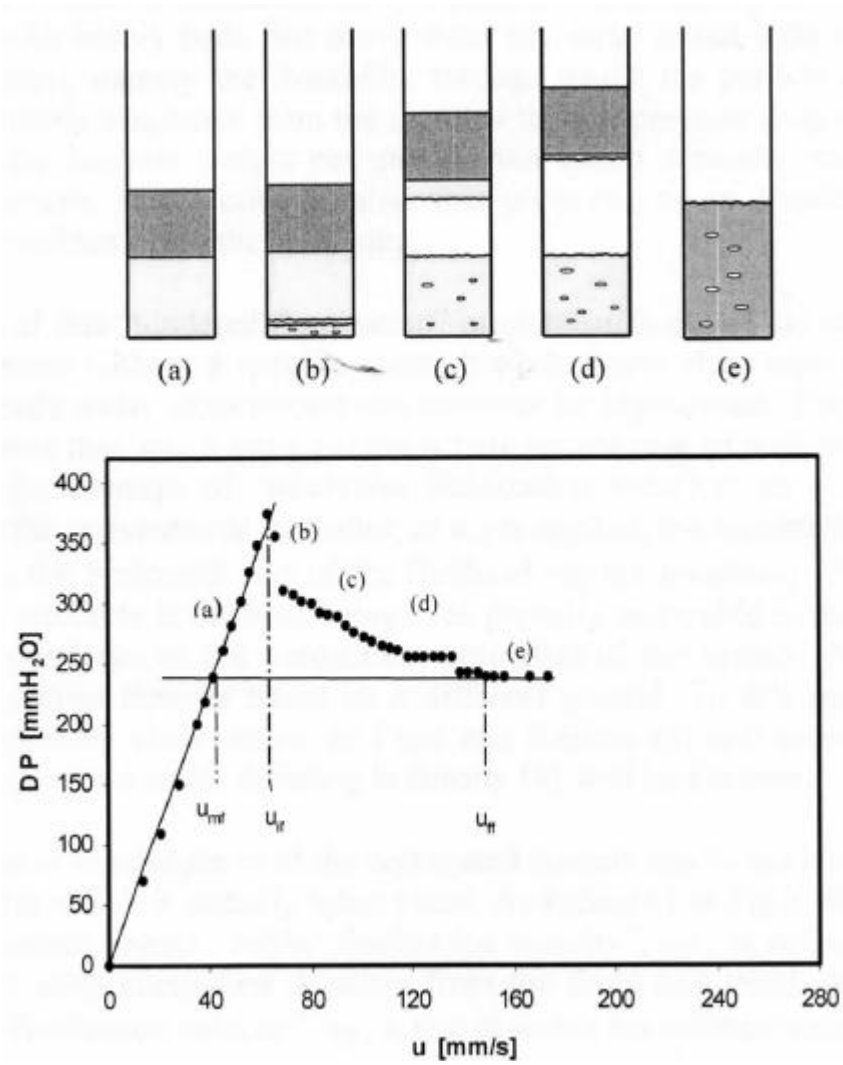

Figure 2.3: Pressure drop diagram at varying superficial velocity for a segregated mixture with the coarser component initially on top

It is thus evident that quantifying the intensity of bubbling by the excess gas velocity u-$u_{mf,}$ as it is usually done with monocomponent beds, assumes that both u_{mf} and u-u_{mf} keep their physical meaning even when applied to two-component systems. In the light of Figures 2.2

and 2.3 this implicit assumption turns out to be wrong and it is therefore needed the development of an analysis based on the definition of new variables addressing the real phenomenology of binary fluidization systems. They are the

- "*initial fluidization velocity*", u_{if} , at which the total pressure drop starts to deviate from the curve typical of the fixed state; and
- the "*final fluidization velocity*", u_{ff} , at which the ultimate value of Δp is first attained.

Thus, these two limits identify the velocity range within which the entire particle collective undergoes suspension into the gaseous stream and respectively constitute the lower and upper boundary of the velocity interval along which any two-solid bed is crossed, from top to bottom, by the fluidization front. Based on this, it is u_{ff} , rather than u_{mf}, that has to be viewed as the velocity at which the entire mixture attains the fluidized condition.

2.3 EARLY STUDIES ON THE FLUIDIZATION VELOCITY INTERVAL

As it is reported by Gelperin and Einstein[30], Kondukov and Sosna (1965) and Gelperin et al. (1967) were the first to study the transition of a packed bed to the fluidized state both for binary and ternary systems. As for the two-solid beds, they provided diagrams where the initial (or beginning) fluidization velocity, u_{if} and the final (or total) fluidization velocity, u_{ff} were plotted as a function of the volumetric concentration of the flotsam component. They gave to these plots the meaning of " phase diagram", making the consideration that a fluidized system goes through phase transformations with changes in fluidizing velocity just like those experienced by a liquid during changes in temperature. According to this authors, the packed-fluidized-dilute phase states in a fluidized system correspond to the solid-liquid-gas phases in a liquid, with the minimum fluidization and the terminal velocities being the

equivalent of the melting and boiling temperatures respectively. As it was shown by Kondukov and Sosna, the analogy between a fluidized bed and a liquid is caused by a similar thermodynamic relationship between the external effect and the corresponding conjugate potential, independently on the physical state of the systems (solid, liquid, gaseous, heterogeneous, etc.). For the solid-liquid-gas system with thermal deformation types of energy exchange, the conjugate parameters are temperature and entropy, pressure and volume. For a heterogeneous system consisting of solid particles and fluidizing fluid in which only momentum is exchanged, the conjugate quantities are velocity of the fluidizing fluid and momentum. Because of thermodynamic generality, phase transitions in a fluidized bed and in similar systems can also be considered by analogy with liquid on the basis of the general propositions of phase transition theory. Thus the *phase rule* can be applied to the solid-particles/fluidizing-fluid system consisting of *N* components and ϕ phases and the following expression for the variance of the system is valid:

$$f = N - \phi + 1 \tag{2.3.1}$$

If the system is monodisperse (*N*=1) then one of the phases (fixed bed, fluidized bed or entrained material) may exist over a certain range of velocity (*f*=1 because ϕ=1), or two phases my co-exist at some fixed velocity (*f*=0 because ϕ=0). This means that in a monodisperse system, fluidization or entrainment occur at definite velocities, but all three phases cannot exist together. A binary system (*N*=2) is monovariant if two phases exist (*f*=1 because ϕ=2), i.e. transition from the stationary state to the fluidized one (or from fluidized to entrained) should take place over a certain velocity range. This system may be invariant if the minimum fluidization velocity of large or heavy particles is the same as that of entrainment of fine or light particles. In polidisperse systems three phases may co-exist over a certain range of fluidizing fluid velocity.

Despite certain differences, among which compressibility and anisotropy of fluidized systems, and the imperfections of the analogy between a liquid and a fluidized bed,

interpretation of properties of the latter in the light of the analogy can be useful. It may be expected that development of statistical method of studying fluidized systems, arising out of their statistical similarity with liquids, will reveal new aspects of the analogy and lead to a stricter theoretical justification.

Afterwards other authors[31-34] produced equilibrium diagrams for binary mixtures. A typical example dating back to those years is presented in Figure 2.4, from Chen and Keairns[31], who studied particle segregation for particles of different size and density in gas fluidized beds. They observed that for a mixture fluidized at low velocity, particles separated sharply into two uniform concentration layers, the upper stratum being fluidized and the lower packed . They constructed phase diagrams from which the equilibrium concentration of components in both layers could be determined and that could be used to select the operating velocities for achieving the desired separation. They also noted, in all systems investigated by them, that particle segregation in a fluidized bed of low velocity was rapid and reached the steady state in less than 30 seconds. In a following study on acrylic-dolomite systems Yang and Keairns[32] confirmed that the process of particle separation was generally accomplished very fast. In the same paper it is also shown that the diagram of the initial and final fluidization velocities is different from a phase diagram in that at u_{ff} the bed may be far from being perfectly mixed.

Thus they proposed a diagram where a new upper boundary is reported as shown in Figure 2.5. This boundary is actually the locus of the minimum gas velocities capable of completely mixing the whole bed. On this boundary, which has a maximum, it is possible to determine the equilibrium concentrations of the two layers in which the bed is assumed to be divided, but in this case both layers are in the fluidized state. However this equilibrium locus at velocities above the minimum fluidization velocity of the jetsam is difficult to determine, because there are definite concentration gradients in both layers. Furthermore equations suggested by Nienow et al.[8] for binary mixtures, at mixing index of 0.95, were used to calculate this locus unsuccessfully.

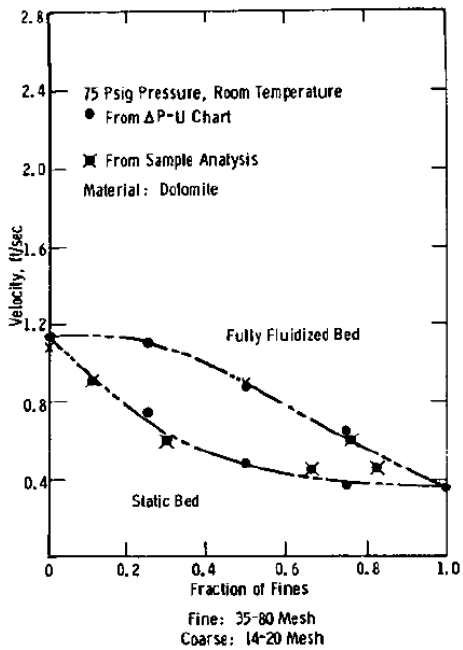

Figure 2.4: Typical phase equilibrium diagram for mixture of two solids of same density.[31]

In Figure 2.5 it is also plotted the equation proposed by Cheung et al.[16] for calculating the minimum fluidization velocity, whose agreement with experimental data is fair, together with the initial and final fluidization velocities calculated from the correlations suggested by Vaid and Sen Gupta[33]. By processing 183 data relevant to mixtures up to five components, in both gas and liquid fluidized beds, these authors proposed the only two equations for calculating u_{if} and u_{ff} for a mixture as follows:

$$52\,\mathrm{Re}_{if}^2 + 1883\,\mathrm{Re}_{if} - Ar \tag{2.3.1}$$

$$18.3\,\mathrm{Re}_{ff}^2 + 877\,\mathrm{Re}_{ff} - Ar \tag{2.3.2}$$

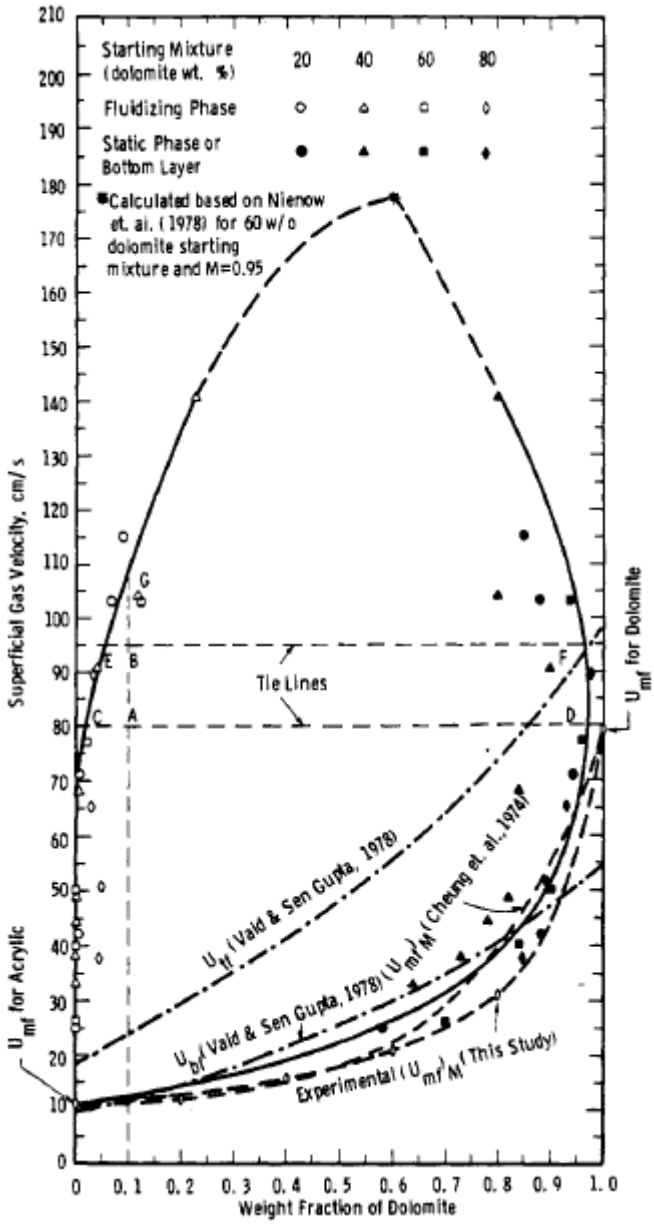

Figure 2.5: Experimental Equilibrium phase diagram of the dolomite-acrylic system.[32]

with

$$Re_{if} = \frac{\rho_g d_{av} u_{if}}{\mu_g} \qquad Re_{ff} = \frac{\rho_g d_{av} u_{ff}}{\mu_g} \qquad Ar = \frac{d_{av}^3 \rho_g \left(\rho_{av} - \rho_g\right)}{\mu_g^2}$$

$$\rho_{av} = \sum_i x_i \rho_i \qquad \frac{1}{d_{av}} = \sum_i \frac{x_i}{d_i}$$

The comparison with experimental data revealed that 90% of the observed u_{if} and 85% of the u_{ff} showed percentage deviations within $\pm$ 35%. It may be pointed out that the authors themselves acknowledged that these correlations based on the oversimplification of bed average properties may be regarded as satisfactory only for first estimates.

More recently Carsky et al.[34] constructed diagrams where, maintaining the analogy with phase equilibria, the grid region composition where assumed to be in equilibrium with the bulk composition of the upper region. They stated the beds were in one of three regions – segregation, transient or mixing - depending mainly on the value of the factor u/u_{mf}. The relationship between the lower and upper layer composition was observed to be strongly affected by the superficial velocities. However it is interesting to note that in the segregation region, that is in the range of gas velocity where the transition from the packed to the fluidized state occurs, the relationship between these two compositions resembles that of the phase transition in liquid-vapor equilibrium when the relative volatility is constant.

2.4 INDEPENDENT VARIABLES AFFECTING THE FLUIDIZATION PROPERTIES OF MIXTURES

As comprehensively discussed in a recent work[35], any criterion aiming to establish an equivalence between a two-component bed and a monosolid system with the same u_{mf} gives place to a misleading approach, fated to overlook important aspects of the binary fluidization phenomenology. The most important of them is the gradual nature of the

process, which results from the interaction between the progress of particle suspension and that of the segregation-mixing phenomena to which the two solids are subjected. Accordingly, a different method of analysis must be followed. On the ground of it, there is the idea that no incipient fluidization velocity can be defined with reference to a two-component bed, since its fluidization takes place along an extended velocity interval whose boundaries are defined as the initial and the final fluidization velocity of the mixture, u_{if} and u_{ff}, respectively. A valuable characteristic of this approach is that it facilitates the identification of the variables that determine the fluidization pattern of the two-solid bed, as their variations are clearly reflected by a change of either u_{if} or u_{ff}. The number of these parameters, here listed in Table 2.1 taken from the aforementioned study, is rather large; that constitutes a serious complication for the development of a model of binary fluidization endowed with general validity.

Table 2.1: Independent variables of binary fluidization

SOLID PROPERTIES	
solid densities	ρ_f , ρ_j
particle diameters	d_f , d_j
particle shape	ϕ_f , ϕ_j
MIXTURE PROPERTIES	
composition	x_f
bed voidage	ε
fluidization velocity	u
packed bed distribution	*mixed, segregated (f/j or j/f),*
other	

Being the initial and final fluidization velocity two values that characterize the behavior of binary mixtures with respect to segregation, a systematic investigation of the dependence of

both velocities on independent variables (particle density and size distribution, composition, bed diameter and height, initial distribution, etc.) is of great importance for an accurate description of fluidization properties of the binary bed.

The effect of bed voidage is by far the key-feature of gas-particle interaction inside the binary bed, whose recognition proves essential to the interpretation of two-component segregating fluidization. From a theoretical point of view, bed voidage should not be looked at as an independent variable, as a relationship exists with other system properties (volume fractions, size ratio, particle sphericity, etc.) as comprehensively illustrated by Yu and Standish (1987) out of the field of particle fluidization and verified in following works dealing with fluidized systems[18, 27, 35-38]. In practice, however, this possibility is limited only to binary beds of free-flowing spheres.

Among these variables operating velocity, composition, densities and diameters surely play a major role. A series of experiments performed separately on density and size segregating systems have been recently the object of a paper by Formisani et al.[35]. Through the examination of diagrams of the two velocity thresholds at varying composition of the mixture, they have recently demonstrated that the differences in size and density between the components are not equivalent factors of segregation. This diversity of behavior is illustrated in Figures 2.6-9. They also affirmed that the fluidization dynamics of any binary mixture is determined by the initial arrangement of the fixed bed. The trends of u_{if} and u_{ff} at varying flotsam fraction x_{f0} are thus reported for the well-mixed arrangement (Figures 2.6 and 2.8) and for an initially segregated one (Figures 2.7 and 2.9) .

The comparison between Figures 2.5 and 2.6 obtained for a density segregating system clearly shows that the dependence of u_{ff} on x_{f0} is practically unaffected by the initial arrangement of the bed. Despite some unavoidable but altogether slight differences in system voidage, the curve of the final fluidization velocity u_{ff} is practically insensitive to the initial state of mixing of the two components in the fixed state. It can be stated, on this basis, that the gas flow rate required for ensuring full support to the particle mass is, in all cases, determined only by the overall amount of the two solids. $u_{ff,}$ for a wide range of

compositions assumes values which are close to that of the minimum fluidization velocity of the jetsam component, with a visible decrease at high flotsam concentrations.

As regards the dependence of u_{if} on x_f, when the initial mixture is homogeneously distributed, the initial fluidization velocity of the bed is practically coincident with its u_{mf} (i.e. with the weighted average of the minimum fluidization velocities of the two solids). When the initial bed is segregated fluidization starts in the upper bed layer where the flotsam components are, so that u_{if} is always practically equal to the minimum fluidization velocity of the flotsam.

The same authors have also shown that the shape of the velocity diagram for any two-density systems does not change with the density ratio. These results have general validity and the value of the ratio ρ_j / ρ_f does not alter the general dynamics of fluidization, although it determines the absolute amplitude of the velocity interval along which it takes place. The similarity of behavior of mixtures of two solids of different density is likely to facilitate the development of a quantitative theory of segregating fluidization.

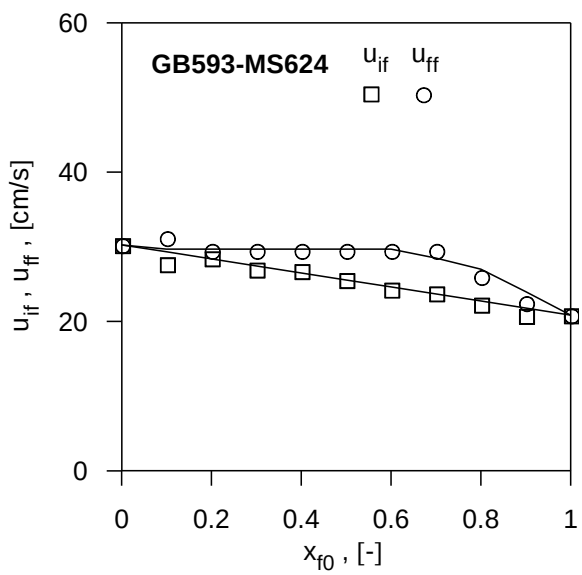

Figure 2.6: Typical dependence of u_{if} and u_{ff} on composition for a two-density system. Well-mixed bed.

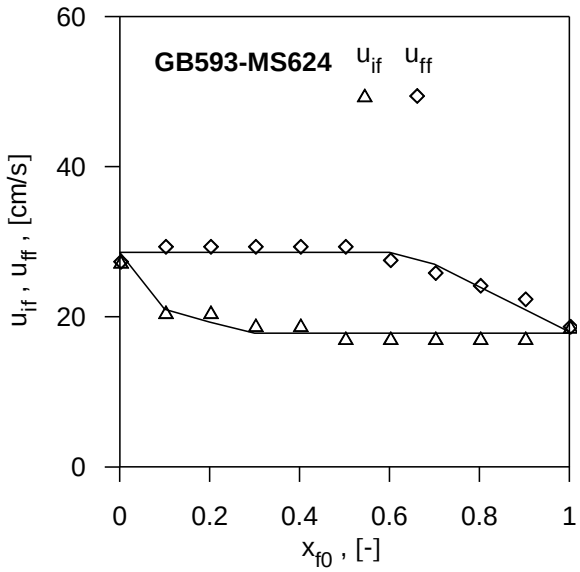

Figure 2.7: Typical dependence of u_{if} and u_{ff} on composition for a two-density system. Segregated bed.

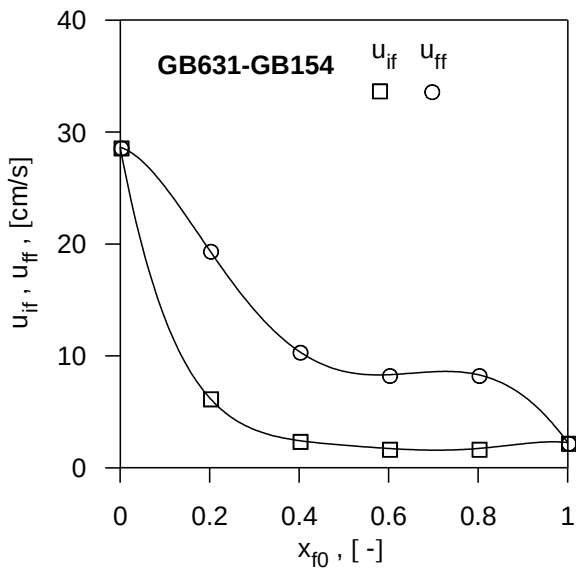

Figure 2.8: Typical dependence of u_{if} and u_{ff} on composition for a two-size system. Well-mixed bed.

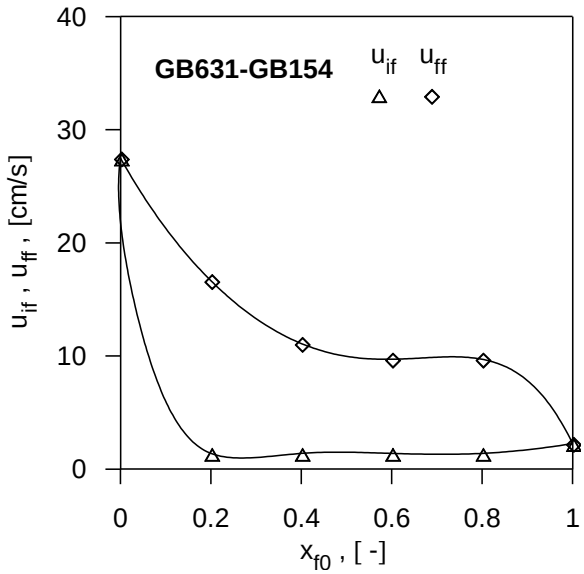

Figure 2.9: Typical dependence of u_{if} and u_{ff} on composition for a two-size system. Segregated bed.

In other words this result suggests that, if properly developed, the analysis of the dependence of the difference u_{ff}–u_{if} on composition can highlight the substantial analogy of behaviour of all density- segregating beds and provides a basis for a generalized theory of segregating fluidization.

The same analysis was performed on size segregating systems by examining the results reported in Figures 2.8 and 2.10 for mixed and segregated beds, respectively. As previously reported for two-density systems, the curve of u_{ff} is not related to the initial arrangement of the mixture components. On the contrary, the initial fluidization velocity of the mixed bed is higher than that of the stratified one, particularly at low flotsam fractions. Fluidization starts at the free surface of the bed so that when its upper layer is fluidized, the rapid fall of u_{if} observed in the diagram of Figure 2.8 is mainly due to the voidage reduction accompanying the increase of the flotsam fraction. Beyond the value of x_{f0} that corresponds to the minimum of each curve in Figure 1.8, the mixture voidage increases again, but the surface per unit volume of particles in the bed increases as well, so that u_{if} approaches its ultimate

value (i.e. $u_{mf,f}$, at x_{f0}=1) more gradually. In contrast, for the segregated systems, u_{if} coincides, at practically all x_{f0s}, with the minimum fluidization velocity of the flotsam component, below which the jetsam layer acts as a passive gas distributor. That explains why the values of u_{if} in Figure 2.7 are practically unaffected by the mixture composition.

Given these trends of the characteristic velocities, the amplitude of the fluidization field is found to depend on the mixture composition as well as on the initial state of mixing of the two solids. For both categories of mixtures, the velocity range of fluidization, i.e. the difference u_{ff} - u_{if}, measures the amplitude of the transient phenomenon during which the two components change from the fixed state to suspension. The difference between the two velocity is therefore also connected to the extent of the segregation phenomena during this transition. Respect to this issue the two diagrams of Figures 2.6 and 2.8 show the substantial difference which exists between the two types of mixtures, clearly highlighted by the variation of the amplitude u_{ff}–u_{if} of their fluidization velocity intervals. When the phenomenon is driven by a difference in particle density, the transition to the fluidized state is shorter for jetsam-rich systems, whose final fluidization velocity is never too higher of that at which the process of suspension starts. The opposite is true for size segregating mixtures, as a narrower interval of velocity has to be crossed at high flotsam fractions. This justifies the authors' considerations on the existence of a substantial difference of the mechanisms by which differences in size and density of particles can determine stratification. Compared to that of two-density systems, the fluidization pattern of size-segregating mixtures is in fact further complicated by the local voidage reduction resulting from the mixing of the two solids, an effect influencing the dependence of both u_{if} and u_{ff} on system composition. The strong relationship between d_j/d_f and $\varepsilon_{mf,m}$ at any mixture composition is the main element of difference between the mechanisms of size and density segregating fluidization.

Furthermore, with mixtures of fully dissimilar solids the shape of the fluidization diagram can make clear which of the two factors of segregation, i.e. the difference in particle density or size, plays a major role in determining the mixing–segregation pattern that accompanies bed suspension. This is another peculiar advantage of this approach.

As regards the influence of the geometric factors (height, diameter or aspect ratio of the bed) on the values of the characteristic velocities u_{if} and u_{ff}, no visible effects have been ascertained in the same work[35]. Like u_{mf} of a monodisperse bed, the amplitude of the fluidization velocity interval is independent on bed height, although a perceptible diminution of u_{if} is generally observed with shallow beds, namely when *H/D* is lower than 1, probably due to the fact that a large portion of the particle bed is affected by the fluid-dynamic singularity of the grid region of the column.

Compared to the traditional methods of analysis, the potentiality of the approach developed in the present investigation is witnessed by its capacity to recognize the effect of all the variables that, for the fact of playing an independent role in the fluidization process, can be thought to affect the mixing– segregation equilibrium of the solid species.

2.5 FURTHER REMARKS

From what presented so far it appears evident that it is possible to develop a clearer approach, closer to the actual phenomenology of fluidization, based on definition of the "initial" and "final fluidization velocity" of binary mixtures. These parameters are the lower and upper boundary, respectively, of a characteristic fluidization velocity range whose amplitude, measured by the difference between u_{ff} and u_{if}, is mainly determined by the diversity in density or size between the two components as well as by the mixture composition and component distribution within the fixed bed. The definition of a minimum fluidization velocity of the binary system, widely used in most literature studies, can result in a misleading analysis of its fluidization behavior: although it can be calculated by rewriting theoretical equations such as Carman- Kozeny's in a form suitable for taking the specific nature of each mixture into account, u_{mf} does not represent the actual fluidization condition. As a consequence, it also constitutes a source of error for models which relate segregation to the bubble flow rate measured by the excess gas velocity u-u_{mf}.

Though the two characteristic velocities assume the same importance of the minimum fluidization velocity for the mono-component fluidization and represent a simple measure of the tendency to segregate for binary beds, the literature is lacking of model capable of predicting them. As it has been reported in the previous section, Vaid and Sen Gupta proposed the only two equations for calculating u_{if} and u_{ff} for a binary mixture. However their equations do not take into account segregation at all, since the properties which appear in the dimensionless numbers are evaluated at the average flotsam concentration. So doing they do not consider that a top-to-bottom variation in concentration exists along the axis of bed and the use of a mean Reynolds number is allowed only if the bed is actually mixed. Maintaining only the viscous term in eqns (2.4.1) and (2.4.2), the calculated values of u_{if} and u_{ff} are equivalent to those obtained by using the equation for u_{mf}, namely eqn (1.2.4) or (1.2.6), if a constant value for the voidage equal to 0.388 for the u_{if} and 0.476 for the $u_{ff.}$ is employed. This is equivalent to state that u_{ff} is greater than u_{if} only because related to a condition of higher voidage. In any case these equations provide unsatisfactory estimates and do not give the value of the minimum fluidization velocity of the individual components when applied to x_{f0}=0 and x_{f0} =1.

It is interesting however to note that these correlations were obtained using data from both gas-solid and liquid-solid systems. In fact it should be noted that segregation phenomena are not peculiar only to gas-solid fluidization, but they occur as in liquid-solid systems as well, even if no bubbles are present. In liquid-solid fluidization a bed made of two or more different particles often shows a tendency toward segregation that results in significant changes in the concentration of individual components along the height, with the coarse or heavier component preferentially occupying the lower region of the bed if the two solids differ only in size or density respectively. If the smaller particles are also the denser, depending on the component density or size ratio, the well-known phenomenon of layer inversion can be observed: the smaller an denser particles may be jetsam at low liquid velocity and become flotsam when the flow rate is increased.

Further to the work of Vaid and Sen Gupta, it is possible to mention only another study, due to Noda et al.[26], in which the authors recognized that the final fluidization velocity is the most appropriate variable to represent the threshold of binary fluidization, so abandoning the way of determining the minimum velocity of fluidization as defined for monodisperse systems. They proposed an empirical equation for its calculation which however has not been demonstrated capable of providing satisfactory predictions.

The lack of accurate equations for predicting the fluidization velocity boundaries is probably due to the fact this approach has been substantially abandoned after its first developments and only recently resumed by few authors[29,35-38]. The reason for which the efforts have been diverted should be search out in the aforementioned study on the phase equilibrium of acrylic and dolomite particles by Yang and Keairns[32], where the authors concluded that the final fluidization velocity u_{ff} has no physical significance in term of the state of particle mixing or separation, because at u_{ff} the bed may be in ''final fluidization,'' but far from being perfectly mixed. However even if for many systems u_{ff} does not coincide with the velocity of full mixing, its measure is a quantification of the segregation phenomena. The real challenge is to explain the relationship between total fluidization and the equilibrium concentration profile at the end of the gradual suspension process. In this regard an attempt to introduce the role played by segregation on the progress of binary fluidization is accomplished in the next chapter, where a parametric model for the velocity interval is derived extending the classical equations for predicting the pressure drop in monosolid beds.

Chapter 3

A MODEL FOR THE FLUIDIZATION VELOCITY INTERVAL

In this chapter the complex mechanism by which homogeneous mixtures of two solids achieve fluidization is subjected to theoretical analysis, in order to elaborate relationships capable to provide the final fluidization velocity. It is shown how the equation that describes the force equilibrium of fluidization can be rewritten in forms that account for the distribution assumed by the components of density- and/or size segregating mixtures during the transition to the fluidized state. This is accomplished by applying the force balance to a realistic structure, i.e. realizing that at u_{ff} the system is characterized by a certain level of segregation and the usual procedure of averaging properties is no longer valid. At the time being the extent of segregation is taken into account by introducing a single adjustable parameter *k.*

In section 1 the previous mentioned mathematical model is derived, assuming a homogeneous initial state of mixing of the fixed bed. In section 2 the experimental apparatus and procedure are briefly described as well as the properties of the single solids are reported. In section 3 the validation for density segregating bed is first addressed, whereas in section 4 the comparison between model predictions and experimental data is focused on beds composed of two solids differing only in size. The choice of illustrating the results relevant to this two types of mixtures in different sections is related to an important

difference which exists between them. A peculiar feature of the size segregating systems is in fact that bed voidage depends on component diameter ratio and local composition[28, 35], whereas the voidage of mixtures of spherical particles having the same average diameter but different densities does not significantly change with composition or axial component distribution[36]. For this reason, to understand and describe some essential differences of behavior between the two types of mixtures, a separate analysis is required. Because of its simplicity with respect to the other kind of mixture, the analysis of density segregating systems is the first to be carried out. Finally in section 5 the study of mixture of thoroughly dissimilar solid is addressed, showing the high extent of generality of the model proposed.

3.1 MODEL EQUATIONS

3.1.1 THE INITIAL FLUIDIZATION VELOCITY

The initial fluidization velocity can be simply defined as the value at which somewhat is observed to happen in the fixed bed. If the solids are initially loaded in a well mixed arrangement it coincides with the establishment of a fluidization traveling front near the free surface of the bed, where at the same time a small stratum of solids undergoes complete separation (see again Figure 2.1). At higher velocities this stratum grows in thickness until all the system is brought into the fluidized state. Thus for a homogeneous mixture u_{if} represents the starting point both for suspension and segregation. As reported in recent papers[35,36], it can be calculated by equating the gas pressure drop with the total weight of the bed per unit section and this means that instantaneously all the bed is supported to allow segregation phenomena to take place. It is thus necessary to correctly compute the drag friction in a multisize assembly to successfully predict this velocity. As discussed in the previous chapter, this is accomplished by introducing into the well known Carman-Kozeny equation the relationship which relates the packing porosity to the

composition and the size ratio. In the light of these considerations, the expression to calculate u_{if} is the following:

$$\frac{180\mu_g u_{if}}{d_{av}^2}\frac{\left(1-\varepsilon_{mf,m}\right)^2}{\varepsilon_{mf,m}^3}=\left(\rho_{av}-\rho_g\right)\left(1-\varepsilon_{mf,m}\right)g \qquad (3.1.1)$$

where

$$\rho_{av}=\rho_f x_{f0}+\rho_j\left(1-x_{f0}\right) \qquad \frac{1}{d_{av}}=\frac{x_{f0}}{d_f}+\frac{1-x_{f0}}{d_j}$$

Thus, as it is possible to verify by comparing eqn (3.1.1) and (1.2.10), the initial fluidization turns out to coincide with the conventional minimum fluidization velocity for an initially well-mixed bed. However this a peculiar result for homogeneous system and does not have a general validity. In fact for a initially segregated bed, with the less dense or smaller component on top, fluidization starts when the gas velocity is raised to the value of the u_{mf} of the flotsam solid. This value is different from that calculated by eqn (1.2.7) which provides the minimum fluidization velocity for a stratified system. Even more evident is the case where the solids are different only in density: in this case u_{mf} is the same whether calculated for a well- mixed arrangement or a totally segregated one, showing the inadequacy of this variable of characterizing mixtures with respect to their segregation behavior.

3.1.2 THE FINAL FLUIDIZATION VELOCITY[40]

In order to analyze the dependence of u_{ff} on the composition and on the constitutive properties of the two solids, a force balance can be written. At any operating velocity intermediate to u_{if} and u_{ff} the axial distribution of mixture components is approximately that sketched in Figure 3.1, an idealized version of Figure 2.1b with sharp interfaces between the three layers, whose heights are indicated as h_f, h_j and h_m, respectively.

Neglecting the little error on h_f due to the presence of bubbles in the flotsam layer, when particle segregation is driven only by the difference in solid density, the total drag force on the three sections of the bed can be expressed as

$$F_d = 180\mu_g Au\left[\frac{\left(1-\varepsilon_{mf,f}\right)^2}{d_f^2\varepsilon_{mf,f}^3}h_f + \frac{\left(1-\varepsilon_{mf,j}\right)^2}{d_j^2\varepsilon_{mf,j}^3}h_j + \frac{\left(1-\varepsilon_{mf,m}\right)^2}{d_{av}^2\varepsilon_{mf,m}^3}h_m\right] \tag{3.1.2}$$

and has to balance, at u_{ff}, the buoyant weight:

$$W = gA\left[\left(\rho_f - \rho_g\right)\left(1-\varepsilon_{mf,f}\right)h_f + \left(\rho_j - \rho_g\right)\left(1-\varepsilon_{mf,j}\right)h_j + \right.$$
$$\left. + \left(\rho_{av} - \rho_g\right)\left(1-\varepsilon_{mf,m}\right)h_m\right] \tag{3.1.3}$$

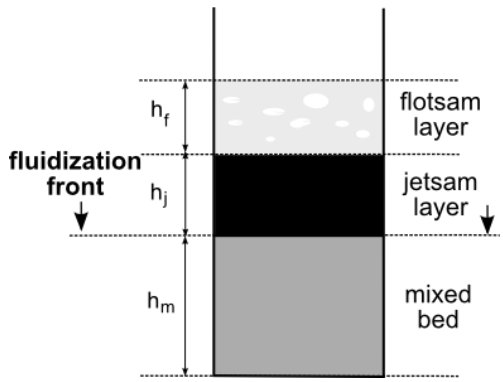

Figure 3.1: Simplified scheme of the fluidization phenomenology.

Given that since its formation at u_{if} the top layer of flotsam particles finds itself over its incipient fluidization point, at any velocity higher than u_{if} but lower than u_{ff} the condition:

$$\frac{180\mu_g u}{d_f^2}\frac{\left(1-\varepsilon_{mf,f}\right)^2}{\varepsilon_{mf,f}^3}Ah_f = \left(1-\varepsilon_{mf,f}\right)\left(\rho_f - \rho_g\right)gAh_f \tag{3.1.4}$$

holds. This means that a force balance only on the two bottom layers would provide the same result.

A mass balance on the jetsam shows that its segregated amount is related to the decrease of the height of the homogeneous portion of the binary bed occurred past u_{if}:

$$h_j = (h_0 - h_m)(1 - x_{f0}) \frac{(1 - \varepsilon_{mf,m})}{(1 - \varepsilon_{mf,j})} \tag{3.1.5}$$

Equating eqns (3.1.2) and (3.1.3) provides the expression of u_{ff}:

$$u_{ff} = \frac{\left[(\rho_f - \rho_g) x_{f0} h_m + (\rho_j - \rho_g)(1 - x_{f0}) h_0\right] g}{180 \mu_g \left[\frac{(1 - \varepsilon_{mf,m})}{(\varepsilon_{mf,m}^3 d_{av}^2)} h_m + \frac{(1 - \varepsilon_{mf,j})}{(\varepsilon_{mf,j}^3 d_j^2)} (h_0 - h_m)(1 - x_{f0}) \right]} \tag{3.1.6}$$

The final fluidization velocity therefore results only dependent on the single solid properties and the residual height of the homogeneous mixture h_m.

At the same time, the minimum fluidization velocity of either solids is calculated as

$$u_{mf,f/j} = \frac{(\rho_{f/j} - \rho_g) d_{f/j}^2 \varepsilon_{mf,f/j}^3 g}{180 \mu (1 - \varepsilon_{mf,f/j})} \tag{3.1.7}$$

so that substitution of eqns (3.1.7) into (3.1.6) yields

$$u_{ff} = \frac{u_{mf,f}\dfrac{\left(1-\varepsilon_{mf,f}\right)}{\left(\varepsilon_{mf,f}^{3}d_{f}^{2}\right)}h_m x_{f0} + u_{mf,j}\dfrac{\left(1-\varepsilon_{mf,j}\right)}{\left(\varepsilon_{j}^{3}d_{j}^{2}\right)}h_0\left(1-x_{f0}\right)}{\dfrac{\left(1-\varepsilon_{mf,m}\right)}{\left(\varepsilon_{mf,m}^{3}d_{av}^{2}\right)}h_m + \dfrac{\left(1-\varepsilon_{mf,j}\right)}{\left(\varepsilon_{j}^{3}d_{j}^{2}\right)}\left(h_0-h_m\right)\left(1-x_{f0}\right)} \tag{3.1.8}$$

that expresses u_{ff} as a function of the fluidization properties of either solid.

Equation (3.1.6) relates the upper boundary of the fluidization velocity interval of a mixture of known average composition to the quantitative effect of segregation up to the moment the gas drag force begins to support the whole bed mass. For a bed of initial height h_0, this effect is measured by h_m, the residual height of the original mixture left at the bottom of the bed.

As it is not easy, for the time being, to establish a reliable relationship between the progress of binary fluidization from u_{if} to u_{ff} and the variation of the height h_m of the residual homogeneous mixture, a correlation has been devised to correlate data at the final fluidization velocity:

$$\frac{h_{m,ff}}{h_0} = k\frac{\left(1-\varepsilon_{mf,m}\right)}{\left(1-\varepsilon_{mf,j}\right)}\frac{\varepsilon_{mf,j}^{3}}{\varepsilon_{mf,m}^{3}}\sqrt{x_{f0}\left(1-x_{f0}\right)} \tag{3.1.9}$$

In it, k is a fitting parameter typical of each mixture but independent of its composition, to be determined from the comparison of the predictions of the theoretical equation (4.2.7) with the experimental curves of u_{ff} versus x_{f0}. Since the prediction of u_{ff} is addressed in this chapter, from now on the subscript ff in h_m that indicates the final fluidization condition will be omitted.

The height ratio $h_{m,}/h_0$ in equation (3.1.9) is a measure of the tendency of the mixture to remain, at u_{ff}, in the homogeneous state; this seems related to the gain in drag force effectiveness provided by the void condition typical of the mixed state, expressed by the ratio:

$$\frac{\left(1-\varepsilon_{mf,m}\right)}{\left(1-\varepsilon_{mf,j}\right)}\frac{\varepsilon_{mf,j}^{3}}{\varepsilon_{mf,m}^{3}}$$

A more effective utilize of the gas rate could be at the basis of this behavior.

Equation (3.1.9) has therefore to be looked at as a relationship that links these variables to a function of mixture composition capable to give the best fit of data. Although it is not possible to provide a theoretical justification to the function of solid fractions that appears in eqn (3.1.9), a few comments can still be made. As it will be discussed in more detail in the next chapter, the height ratio h_m/h_0 is also a measure of the interactions between the two components and the product of concentration $x_{f0}(1- x_{f0})$ is the simplest functional form that gives a zero value at the extremes of the concentration domain. In fact, like any interaction, it must disappear when only a component is present. The product of solid fractions would provide a sufficient good fit of the experimental data, but this functionality produces model curves such that for x_{f0}=1 the velocity of flotsam is not found. The introduction of the square power in the correlation, that is the geometric mean of solid fractions, allows avoiding this seemingly unphysical result.

Values of voidage relevant to the pure jetsam component ($\varepsilon_{mf,j}$) and to the mixture ($\varepsilon_{mf,m}$) are taken from the experiments and substituted into eqn (3.1.9). Depending on whether the components of the bed differ in density or size, $\varepsilon_{mf,m}$ results practically constant with x_{f0} or varies with mixture composition. With the former type of beds, made of spheres of the same size, whatever the composition the difference between $\varepsilon_{mf,j}$ and $\varepsilon_{mf,m}$ is practically negligible so that the voidage function in the right hand side of eqn (3.1.9) may always be assumed equal to 1.

3.2 EXPERIMENTAL

3.2.1 EXPERIMENTAL EQUIPMENT AND PROCEDURE

In Figure 3.2 the experimental apparatus is shown. All the experiments of this study were carried out in a transparent fluidization column of 10 cm ID (1), equipped with a 4-mm-thick plastic porous distributor, ensuring high head loss and good gas distribution. The pressure drop across the column was measured by means of a U-tube water manometer (2) connected to a tap located 1 mm above the distributor plane. The fluidizing gas was compressed air, whose flow rate was monitored in the range 0-25000 Nl/h through a bench of rotameters (3).

The fluidization diagram of the single solids and mixture, that is the Δp vs u curve, were obtained performing all the experiments on well-mixed binary mixtures. To ensure homogeneity of the fixed bed, each mixture was fractioned into various portions (6 to 8) each of which was mechanically premixed and then poured onto the column by means of a long-legged funnel. The effectiveness of this procedure, validated by previous work, was checked by occasionally determining the axial profile of bed composition according to the method described in detail in Chapter 4.

Bed heights were evaluated by averaging the values read on three graduated scales put at 120°C around the column wall, and then used for determining bed void fractions:

$$\varepsilon_0 = 1 - \frac{m}{\rho A h_0} \tag{3.2.1}$$

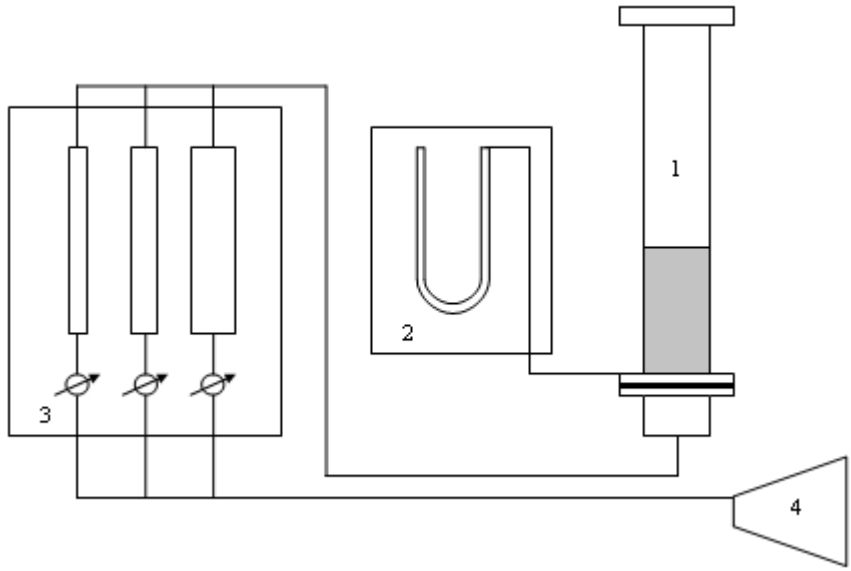

1. *Column*
2. *U-tube manometer*
3. *Rotameters*
4. *Compressor*

Figure 3.2: Experimental apparatus

Because all the solids used in the experiments, with only one exception, belong to group B of Geldart's classification[39] and show no homogeneous expansion when fluidized, the fixed bed voidage ε_0 was always considered equal to ε_{mf}.

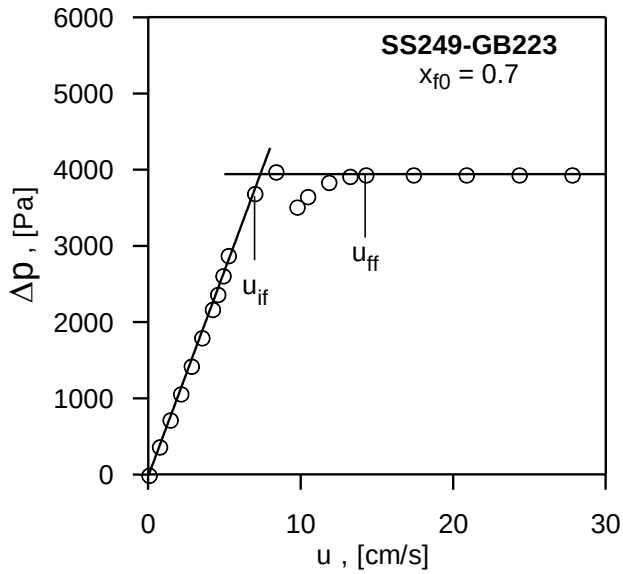

Figure 3.3: Pressure drop vs u relationship for a binary mixture.

A typical experimental pressure drop diagram is shown in Fig. 3.3, where two characteristic velocity thresholds can be recognized. They are the:

- "initial fluidization velocity", u_{if} , at which Δp first deviates from the fixed bed curve, and the

- "final fluidization velocity", u_{ff} , at which the ultimate value of Δp is first attained.

These two limits identify the velocity range within which the entire particle system undergoes suspension into the gaseous stream. Although it refers to a particular type of mixture (obtained by the complete mixing of spheres differing only in density), the diagram of Figure 3.3 shows a common feature of any binary fluidization process, i.e. that their transition to the fluidized state is never instantaneous.

With all mixtures the aspect ratio h_0/D of the fixed bed was set equal to 1.7, so that their composition was varied by adjusting the mass of their components under this constraint.

3.2.2 MATERIALS AND MIXTURES

Measurements involved mixtures of various spherical solids, closely sieved; their granulometric characterization was performed by a Sympatec Helos laser diffractometer, and a Quantachrome helium pycnometer was used to determine particle densities. Measurements were performed on four types of spherical solids: glass ballotini (GB), molecular sieves (MS), and steel shots (SS), ceramics beads (BE). The properties of each cut are listed in Table 2.1. It provides as well as information on particle density and size, also the experimental u_{mf} of the monodisperse solids, determined at the intersection of the fixed bed curve with the horizontal line representing the bed weight per unit section ($u_{if} \approx u_{ff} \approx u_{mf}$).
Among the solids, GB46 belongs to group A of the Geldart classification of particles, so it may exhibit a little expansion at the incipient fluidization point. However this phenomenon proved to be of limited importance, and the assumption $\varepsilon_0 \approx \varepsilon_{mf}$ keeps on being valid.
From the cuts of Table 2.1, the mixtures listed in Table 2.2 were prepared, in a way that density and size ratios between components cover fairly wide ranges. As for the density segregating beds, three mixtures with the same density ratio but with different average diameter have been investigated, namely systems SS439-GB428, SS318-GB322 and SS243-GB223. On the other hand the mixtures GB593-MS624, CE605-GB593 and CE654-M624 made of materials having approximately the same average diameter, are used to investigate the role of density difference on binary fluidization keeping constant the absolute size of the particles.

Tab.2.1 – Properties of the experimental solids

Solid	**Density** [g/cm^3]	**Sieve size** [μm]	**Sauter mean diameter** [μm]	**Experimental u_{mf}** [cm/s]
Molecular sieves (MS)	1.46	710-900	800	31.9
		600-710	624	20.8
Glass ballotini (GB)	2.48	600-710	631	32.5
		500-710	593	30.8
		500-600	521	20.5
		350-600	499	20.2
		400-500	428	17.9
		300-355	322	8.40
		250-300	271	5.70
		200-250	239	4.00
		200-250	223	4.30
		150-180	172	2.80
		150-180	168	2.30
		125-180	154	2.20
		25-50	46	0.232
Ceramics (CE)	3.76	600-710	654	50.1
		500-710	605	43.3
		355-400	376	16.7
Steel shots (SS)	7.60	400-500	439	47.7
		300-355	318	26.2
		200-250	243	17.3

Tab.2.2 – Properties of the experimental mixtures

Type	**Mixture (JETSAM/FLOTSAM)**	ρ_j/ρ_f [-]	d_j/d_f [-]
Density-segregating	CE605-GB593	1.52	1.02
	GB593-MS624	1.70	0.95
	CE654-MS624	2.58	1.04
	SS439-GB428	3.06	1.03
	SS318-GB322	3.06	0.99
	SS243-GB223	3.06	1.09
Size-segregating	GB521-GB271	1	1.94
	GB499-GB172	1	2.90
	GB521-GB168	1	3.10
	GB631-GB154	1	4.10
	GB239-GB46	1	5.20
Dissimilar solids	CE376-GB271	1.52	1.39
	MS631-GB154	0.59	4.10
	SS439-MS800	5.20	0.55

The size segregating beds in Table 2.2 are all made of particles having the same density, i.e. glass ballotini. However different density values should not alter the dynamics of this category of systems which is regulated mainly by the size ratio, which in this study varies approximately from two to five. Finally the mixtures of dissimilar solids, i.e. where both diversity in size and density are present, have been chosen in order to investigate the tendency of the two aforementioned segregating factors to strengthen or balance out.

3.3 VALIDATION

3.3.1 DENSITY SEGREGATING MIXTURES

With respect to the abundant literature on mixtures of differently sized solids those that have addressed two-density beds are much less numerous, so that very little is known on the peculiar behavior of these systems when subjected to fluidization. This persistent lack of information is also one of the sources of uncertainty in evaluating the degree of similarity of the two mechanisms of segregation in view of a unified approach to the problem.

The voidage of mixtures of spherical particles having the same average diameter but different densities does not significantly change with composition or axial component distribution[36]. Under the assumption of constant voidage, the initial fluidization velocity of a mixture of two solids of equal size and different density coincides with the weighted average of the minimum fluidization velocity of its components:

$$u_{if} = x_{f0} u_{mf,f} + \left(1 - x_{f0}\right) u_{mf,j} \qquad (1.2.5)$$

The above equation is basically the one proposed by Otero and Corella[14], after the substitution of u_{if} with u_{mf}, and coincides with the definition of the minimum fluidization velocity of a monodisperse system. These authors have attributed to the velocity value obtained from (3.3.1) the meaning of minimum fluidization velocity of the mixture, which is valid according to their point of view, for any binary system. However, the previous expression is valid only when the components differ only in density, and its value marks the transition from the packed bed state to the velocity region in which both a fixed portion of the bed and a fluidized one are simultaneously present.

Eqn (1.2.5) is in turn equivalent to the equation of Carman-Kozeny rewritten as follows:

$$\frac{180\mu_g u_{mf}}{d^2}\frac{(1-\varepsilon_{mf})^2}{\varepsilon_{mf}^3}=(\rho_{av}-\rho_g)(1-\varepsilon_{mf})g \tag{1.2.6}$$

If the voidage is assumed constant eqn (3.1.6) results only dependent on the single solid properties and the residual height of the homogeneous mixture h_m:

$$u_{ff}=\frac{\{(\rho_j-\rho_g)h_0(1-x_{f0})+(\rho_f-\rho_g)h_m x_{f0}\}g\varepsilon_{mf}^3 d^2}{180\mu_g(1-\varepsilon_{mf})[h_0(1-x_{f0})+h_m x_{f0}]} \tag{3.3.1}$$

Whereas u_{ff} as a function of the minimum fluidization velocity of either solid is expressed:

$$u_{ff}=\frac{u_{mf,f}h_m x_f+u_{mf,j}h_0(1-x_{f0})}{h_m x_f+h_0(1-x_{f0})} \tag{3.3.2}$$

Finally substitution of eqn (3.1.9) in (3.3.2) with the voidage function set equal to 1, gives:

$$u_{ff}=\frac{k\cdot u_{mf,f}\sqrt{x_{f0}^3}+u_{mf,j}\sqrt{1-x_{f0}}}{k\cdot\sqrt{x_{f0}^3}+\sqrt{1-x_{f0}}} \tag{3.3.3}$$

Eqn (3.3.3) generates a family of curves at varying k if the values of the u_{mf}s are provided. Although it was clear that forcing the model curves of u_{if} and u_{ff} to match the end points of the velocity diagram would introduce (but not always, perhaps) a slight improvement in the general fit, it has been deliberately decided to treat the results at x_{f0}=0 and x_{f0}=1 just like those relevant to intermediate concentrations. Calculation of u_{ff} can then be based on the constitutive properties of the two components of the mixture, rather than on their u_{mf}. Although somewhat unaesthetic, this choice is worth to show that the level of the error of prediction at all concentration is fully comparable with that encountered with

monocomponent beds when a well established relationship, like that of Carman-Kozeny or that of Ergun, is used.

The ability of the theory proposed in this paper to interpret the fluidization behavior of binary mixtures can be evaluated by comparing the values of u_{if} and u_{ff} drawn from experiments at varying x_{f0} with those calculated by the model equations. Over the whole range of composition, the two series of values provide the general fluidization diagram of each system, either in the experimental or in the calculated version. On it, at any concentration, the vertical distance between the curve of u_{ff} and that of u_{if} represents the width of the velocity interval along which the binary bed is entirely brought into the fluidized state. During this process, its internal component distribution goes through a succession of equilibrium states, each of which is typical of the specific value of u. Unlike the model curves of u_{if}, obtained from the theoretical equation (1.2.6) that of u_{ff} are derived from a relationship, namely the equation (3.3.1), that cannot be looked at as fully predictive. In it the presence of h_m (the height of the homogeneous portion of the bed at the final fluidization condition) requires the association of eqn (3.1.9), in which the value of k is that capable to provide the best fit of the experimental data over the whole field of x_{f0}.

In Figures 3.4-3.9 the initial and the final fluidization velocity of six density-segregating binary beds are plotted versus the volumetric fraction of their flotsam component. The density ratio of their solids ranges from 1.45 to 3.08 covering nearly all the situations encountered in the applications of two-component fluidization. The properties of these systems are reported in Table 3.2. In it the values of k and of the voidage used throughout the concentration range are shown.

Table 2.3: k-values and other properties used in the model.

Mixture (JETSAM/FLOTSAM)	ε_{mf} [-]	$u_{mf,j}$-$u_{mf,f}$ [cm/s]	k [-]
CE605-GB593	0.405	12.5	0.39
GB593-MS624	0.410	10.0	0.69
CE654-MS624	0.405	29.3	0.24
SS439-GB428	0.415	29.8	0.21
SS318-GB322	0.406	17.8	0.31
SS243-GB223	0.426	13.0	0.42

The assumption made with density-segregating mixtures, i.e. that the variation of ε_{mf} with layer composition is negligible, is well verified in a large number of cases. Just occasionally the two components of the mixture happen to exhibit, at x_{f0}=0 and x_{f0}=1, a limited difference of voidage. Even in these cases it has been preferred to assume ε_{mf} to be constant at an arithmetic average value all over the field of x_{f0} instead of using a weighted average and accounting for the fact that the trend of ε_{mf} versus x_{f0} is that of a slightly inclined line. The resulting errors are however negligible (normally about 1 or 2%), whereas the model equations result noticeably simpler. In any case such an assumption has to be looked at as not indispensable, since the model can incorporate, when required, any relationship between ε_{mf} and x_{f0}. On the other hand, the availability of a reliable relationship between ε_{mf} and x_{f0} is a key-factor in modeling the behavior of size-segregating beds. Similarly the value of d used in eqns (1.2.6) and (3.3.1) is not the Sauter mean diameter evaluated at every concentration, but it is simply the arithmetic mean of the single component sizes.

As it has already been observed in previous investigations[35,36] in the experimental fluidization diagram of two density mixtures u_{if} is given by the straight line joining component u_{mf}'s , as shown by eqn (1.2.5), whereas the locus of u_{ff} is a curve whose slope

progressively increases with x_{f0}. With no exception the velocity diagram always has the same shape, i.e. that of a curvilinear triangle, revealing as the approach adopted captures the similarity of behavior of mixtures having different density ratios. Consistent with this finding is the fact that variations of the density ratio do not seem to induce significant changes in the phenomenology of fluidization of the mixture.

From the experimental viewpoint, the fluidization diagrams of the two density systems considered demonstrate that the dependence on x_{f0} of both characteristic velocities is not a function of the solid density ratio ρ_j/ρ_f but is dictated by the difference $u_{mf,j}$-$u_{mf,f}$. This difference is related, in turn, to the difference $\rho_j d_j^2$ -$\rho_f d_f^2$, as stated by eqn (3.1.7).

Thus, the amplitude of the fluidization velocity intervals of mixtures CE605-GB593 and SS243-GB223, which have a component density ratios of 1.52 and 3.06 but u_{mf} differences of 12.5 and 13.0, respectively, results practically identical at all compositions.

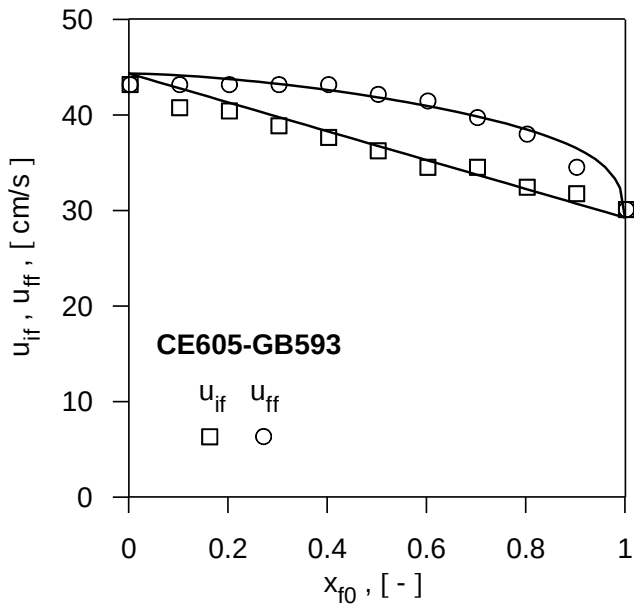

Figure 3.4 Fluidization velocity diagram of the density-segregating mixture CE605-GB593.

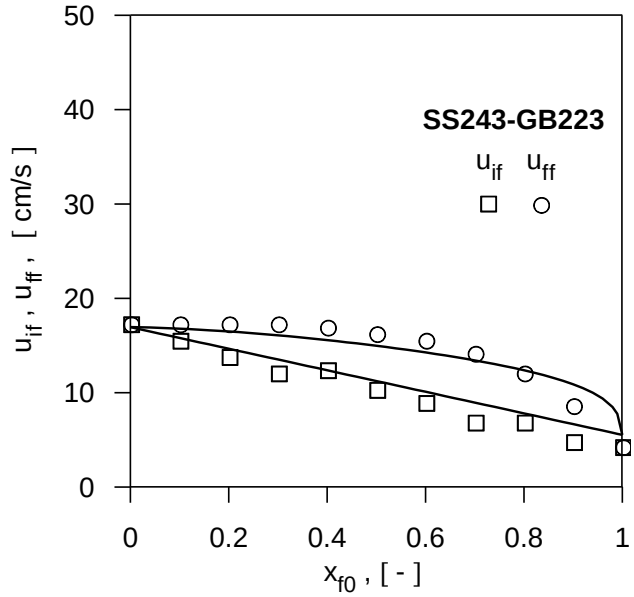

Figure 3.5 Fluidization velocity diagram of the density-segregating mixture SS243-GB223 .

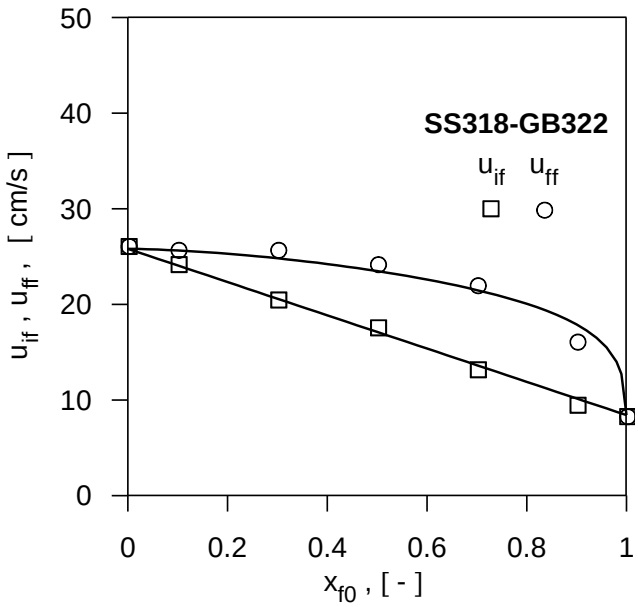

Figure 3.6 Fluidization velocity diagram of the density-segregating mixture SS318-GB322 .

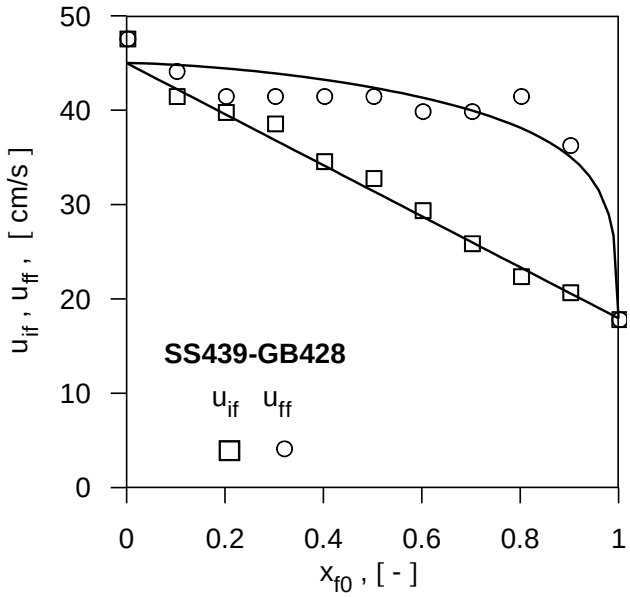

Figure 3.7 Fluidization velocity diagram of the density-segregating mixture SS439-GB428 .

At the same time, the fluidization diagrams of SS243-GB223, SS318-GB322 and SS439-GB428 reported in Figures 3.5-7, exhibit a substantial difference of amplitude, that corresponds to a difference in component u_{mf} equal to 13.0, 17.8 and 29.8, respectively. That occurs notwithstanding that the ratio ρ_j/ρ_f is equal to 3.06 for all three systems. Almost the same width of the fluidization range is instead observed with mixtures SS439-GB428 and CE654-MS624, which have a similar u_{mf} difference. As for the mixture GB593-MS624, its fluidization diagram appears to be the narrowest of all without its density ratio, equal to 1.70, being the smallest.

Subtracting eqn (1.2.5) from eqn (3.3.2) yields an expression for the amplitude of the fluidization interval:

$$\left(u_{ff} - u_{if}\right) = \frac{x_{f0}\left(1-x_{f0}\right)\left(h_0 - h_m\right)}{h_m + \left(h_0 - h_m\right)\left(1-x_{f0}\right)}\left(u_{mf,j} - u_{mf,f}\right) \qquad (3.3.4)$$

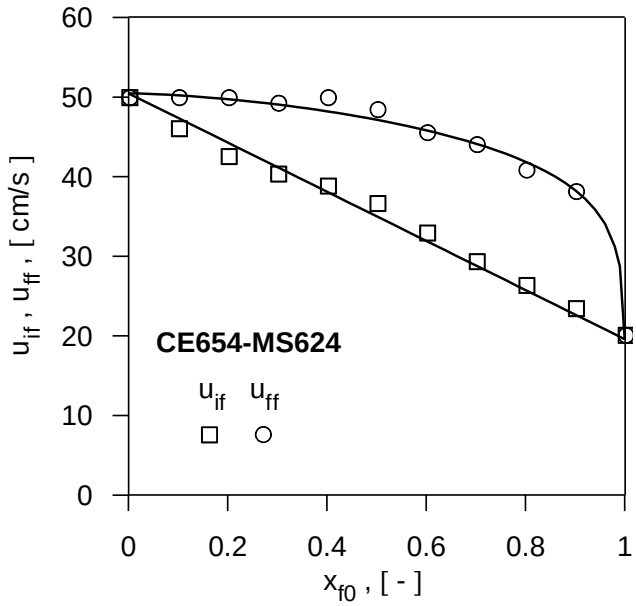

Figure 3.8 Fluidization velocity diagram of the density-segregating mixture CE654-MS624 .

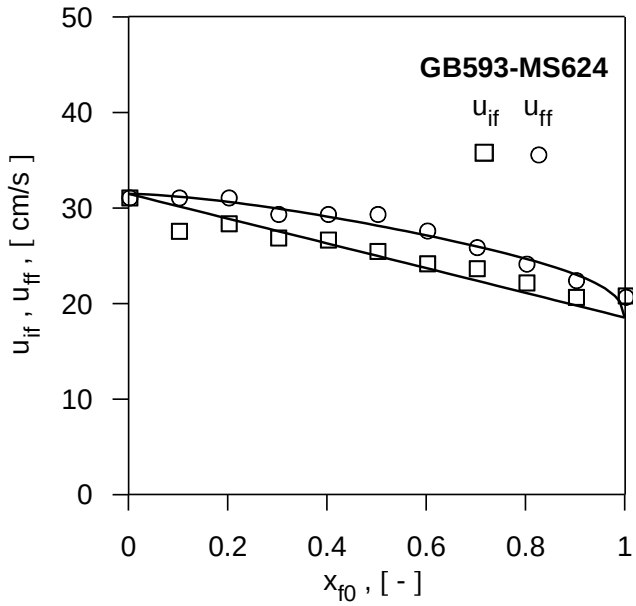

Figure 3.9 Fluidization velocity diagram of the density-segregating mixture GB593-MS624 .

Eqn (3.3.4) may bolster the conclusion that the area of the velocity diagram increases with the difference in component $u_{mf.}$

The fitting procedure of the experimental curves of u_{ff} with the equations (3.3.1) and (3.1.9) provides the values of the parameter *k*, also reported in Table 3.3, to be used in the latter relationship at all compositions. The role played by the difference $u_{mf,j}$-$u_{mf,f}$ in the binary fluidization process is successfully reflected by the model parameter *k*, whose values result very close for mixtures CE605-GB593 and SS243-GB223 (0.39 and 0.42, respectively), and for mixtures SS439-GB428 and CE654-MS624 (0.21 and 0.24, respectively), whereas they are noticeably different for SS243-GB223, SS318-GB322 and SS439-GB428 (0.42 and 0.21, respectively), In Fig. 3.10 the dependence of *k* on $u_{mf,j}$-$u_{mf,f}$ is reported, observing that a smaller difference in component u_{mf} corresponds to a higher value of *k,* which in turn means an enhancement in component mixing.

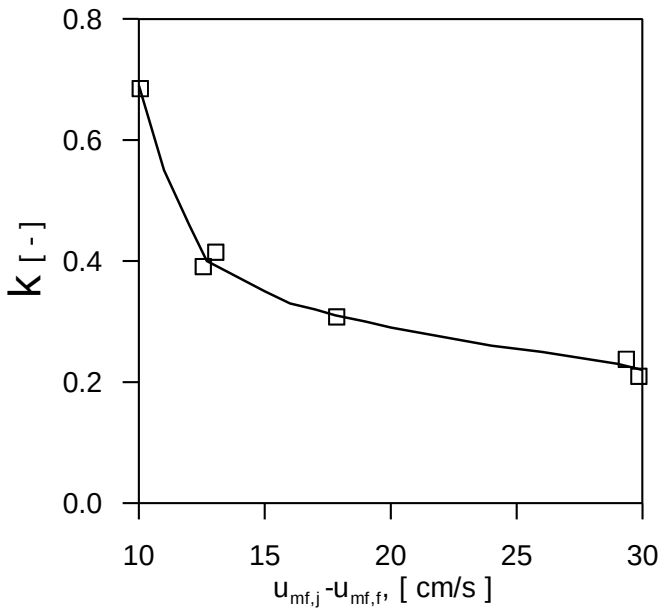

Figure 3.10: Variation of k with the u_{mf} difference between solids.

The ability of the theory proposed in Sec.3 to interpret the binary fluidization pattern is illustrated by the comparison between experimental and calculated values of u_{ff}: as observable in Fig.3.8, the error of prediction always falls within the limit of 10%.

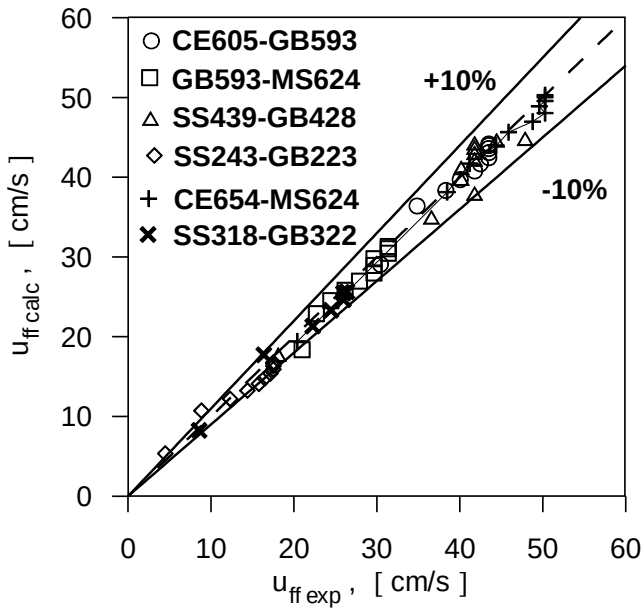

Figure 3.11: Comparison between experimental and calculated values of the final fluidization velocity. Density-segregating mixtures.

3.3.2 SIZE SEGREGATING MIXTURES

Unlike what is a distinctive feature of beds of particles of different density, namely the fact that system voidage is practically unaffected by any other variable, with two-size mixtures any change of composition or of the state of mixing of their components is followed by a variation of voidage. As a consequence of that, the progress of segregation phenomena

induced by fluidization causes these beds to continuously change their axial profile of local voidage.

Given the homogeneous nature of the particle assembly, the initial fluidization velocity is equivalent to the u_{mf} of the mixture. It can be obtained by writing Carman-Kozeny equation in the form:

$$\frac{180\mu u_{if}}{d_{av}^2}\frac{\left(1-\varepsilon_{mf,m}\right)^2}{\varepsilon_{mf,m}^3}=\left(\rho_s-\rho_g\right)\left(1-\varepsilon_{mf,m}\right)g \tag{3.3.5}$$

and the value of bed voidage $\varepsilon_{mf,m}$ drawn from the experimental curve of $\varepsilon_{mf,m}$ versus x_{f0}.

From eqns (3.1.7) and (3.3.5) it is possible to relate the initial fluidization of the mixture to the component fluidization properties:

$$u_{if}=u_{mf,\ f}\ \frac{d_{av}^2}{d_f^2}\frac{\varepsilon_{mf,m}^3\left(1-\varepsilon_{mf,f}\right)}{\varepsilon_{mf,f}^3\left(1-\varepsilon_{mf,m}\right)}=u_{mf,\ j}\ \frac{d_{av}^2}{d_j^2}\frac{\varepsilon_{mf,m}^3\left(1-\varepsilon_{mf,j}\right)}{\varepsilon_{mf,j}^3\left(1-\varepsilon_{mf,m}\right)} \tag{3.3.6}$$

As for the final fluidization velocity eqn (3.1.6) reduces to:

$$u_{ff}=\frac{\left(\rho_s-\rho_g\right)g\left[\left(h_0-h_m\right)\left(1-x_{f0}\right)+h_m\right]}{180\mu\left[\frac{\left(1-\varepsilon_{mf,j}\right)}{\left(\varepsilon_{mf,j}^3 d_j^2\right)}\left(h_0-h_m\right)\left(1-x_{f0}\right)+\frac{\left(1-\varepsilon_{mf,m}\right)}{\left(\varepsilon_{mf,m}^3 d_{av}^2\right)}h_m\right]} \tag{3.3.7}$$

Eqn (3.3.7) can be written in the dimensionless form:

$$\frac{u_{ff}}{u_{mf,j}}=\frac{\left(h_0-h_m\right)\left(1-x_{f0}\right)+h_m}{\left(h_0-h_m\right)\left(1-x_{f0}\right)+f_{DR}h_m} \tag{3.3.8}$$

showing that the reduction of the final fluidization velocity with respect to $u_{mf,j}$ is a function of the extent of segregation, namely of the height h_m, and of the gain in terms of drag experienced by the jetsam when it is in mixture with the other solid:

$$f_{DR} = \frac{\left(1-\varepsilon_{mf,m}\right)\varepsilon_{mf,j}^3}{\left(1-\varepsilon_{mf,j}\right)\varepsilon_{mf,m}^3}\frac{d_j^2}{d_{av}^2} \tag{3.3.9}$$

The fluidization velocity diagrams and the experimental dependence of $\varepsilon_{mf,m}$ on x_{f0} for the systems under investigation are plotted in Figs 3.12-21, together with the relevant model curves. Both the initial and the final fludization velocity exhibit curvilinear trends at varying x_{f0}, determined by both the difference $u_{mf,j}$-$u_{mf,f}$ and the peculiar shape of the $\varepsilon_{mf,m}$ versus x_{f0} curve, in turn determined by the particle size ratio d_j/d_f.

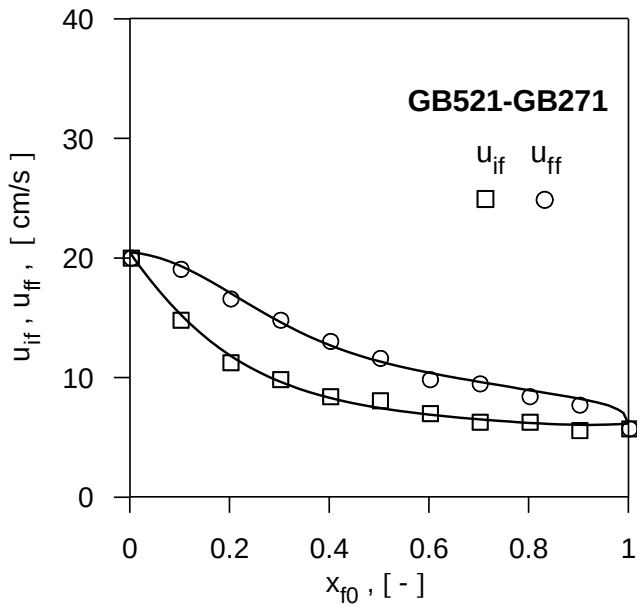

Figure 3.12: Fluidization velocity diagram of the size-segregating mixture GB521-GB271.

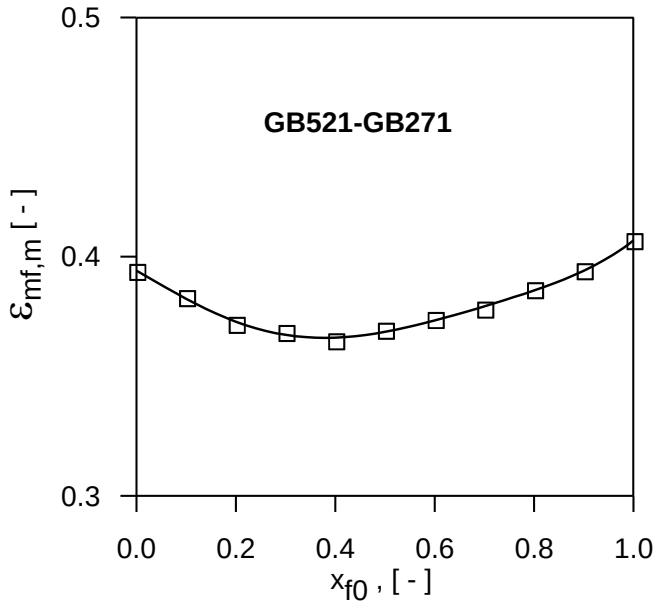

Figure 3.13: Voidage of the homogeneous size-segregating mixture GB521-GB271 at varying composition.

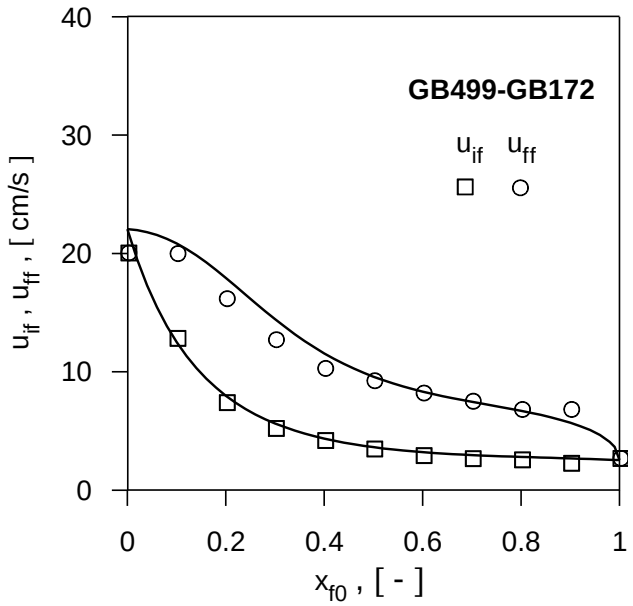

Figure 3.14: Fluidization velocity diagram of the size-segregating mixture GB499-GB172.

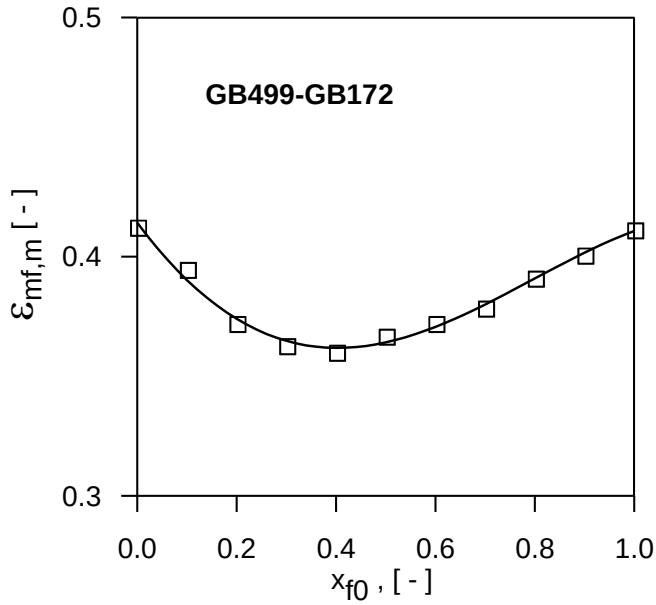

Figure 3.15: Voidage of the homogeneous size-segregating mixture GB499-GB172 at varying composition.

All the voidage curves show a minimum at about the same concentration x_{f0}=0.3~0.4, but the value of voidage in this condition decrease almost proportionally to the size ratio. The fluidization have also the same shape, even if as a consequence of the strong reduction in voidage both u_{if} and u_{ff} decrease very rapidly when the size ratio d_i/d_f is high. This behavior makes the amplitude of the velocity interval increasing with higher size ratios.

Figure 3.21 may appear a little strange: the voidage relevant to GB46 is appreciably higher than that of the other solids. This is due to the fact that it belongs to group A of the Geldart classification and the presence of surface forces may cause particles to form a more loose packed bed. Even if the model is valid rigorously only for group B powders, it works well revealing that surface forces can be neglected in this case, or better, they can be taking into account simply using an higher value for the voidage.

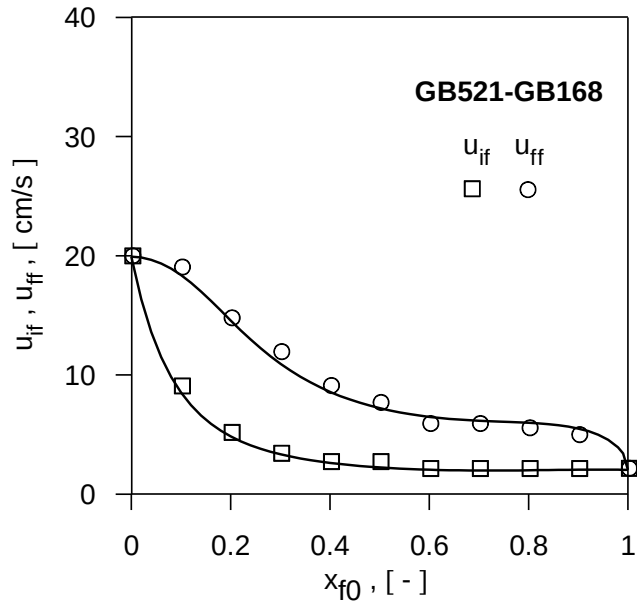

Figure 3.16: Fluidization velocity diagram of the size-segregating mixture GB521-GB168.

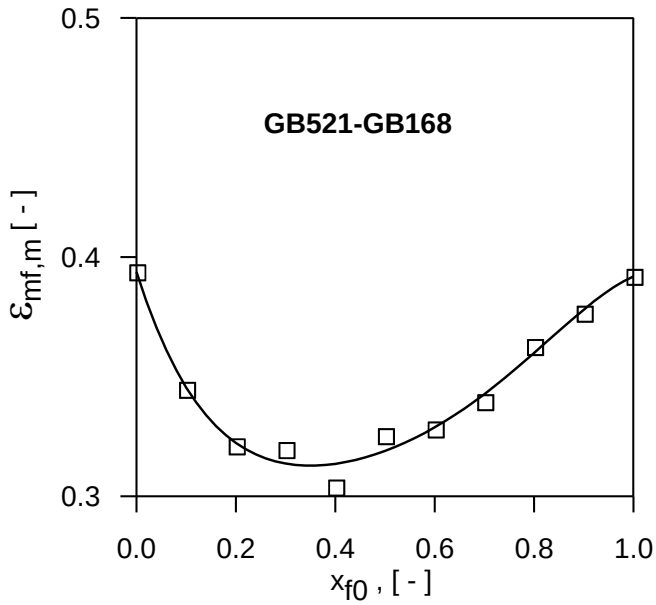

Figure 3.17: Voidage of the homogeneous size-segregating mixture GB521-GB168 at varying composition.

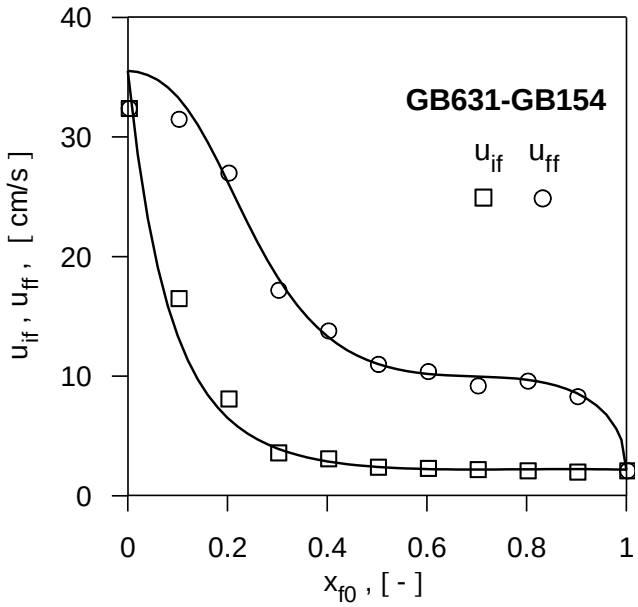

Figure 3.18: Fluidization velocity diagram of the size-segregating mixture GB631-GB154.

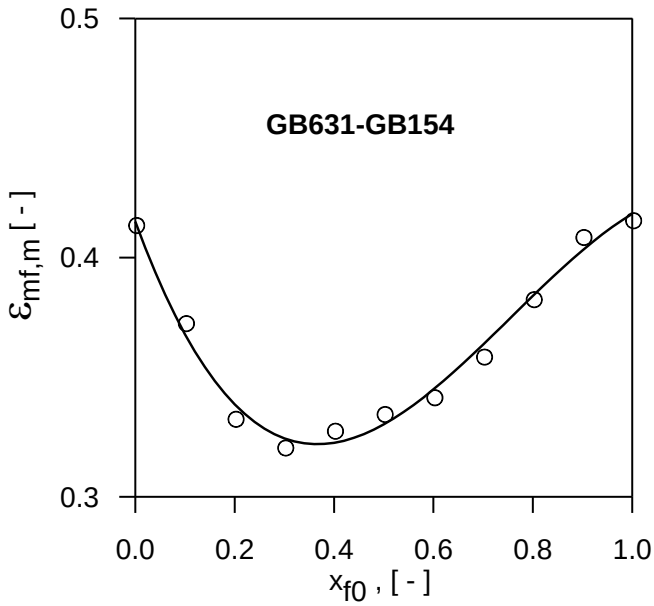

Figure 3.19: Voidage of the homogeneous size-segregating mixture GB631-GB154 at varying composition.

Values of $\varepsilon_{mf,m}$ drawn from these curves have been used when applying eqn (3.3.4) to predict the initial fluidization velocity u_{if} of these mixtures (a point already treated in a recent paper[36]), and eqns (3.3.6) and (3.1.9) to fit the experimental data of their u_{ff}. Notwithstanding that the complication associated to the voidage change introduces a new variable into the problem of segregating fluidization, the ability of the model equations to represent the dependence of u_{ff} on x_{f0} once that the value of k has been defined, is remarkable for a wide range of the component size ratio. This varies from 1.94 to 5.2, as reported in Table 2.4. However the need for the knowledge of voidage can be overcome by using some of the correlations that have developed by many authors in literature, of which eqn (1.2.11) is an example. In this study it has been preferred to employ the experimental values of $\varepsilon_{mf,m}$, in order to avoid any sources of error which derive from the unavoidable degree of approximation of the empirical correlations.

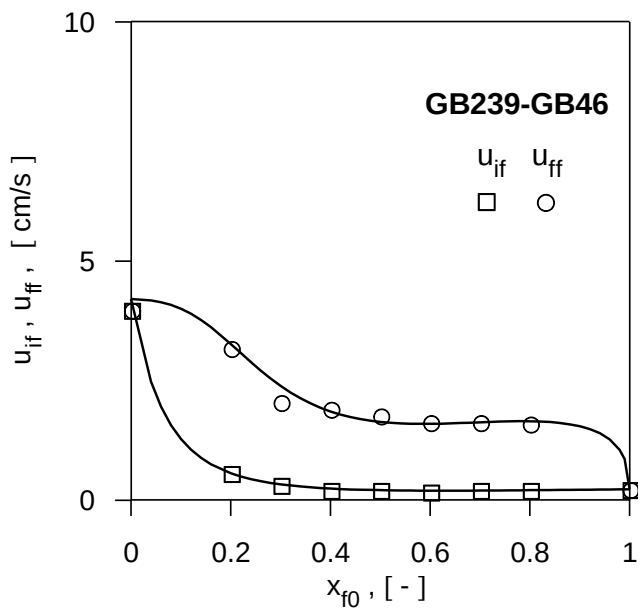

Figure 3.20: Fluidization velocity diagram of the size-segregating mixture GB239-GB46.

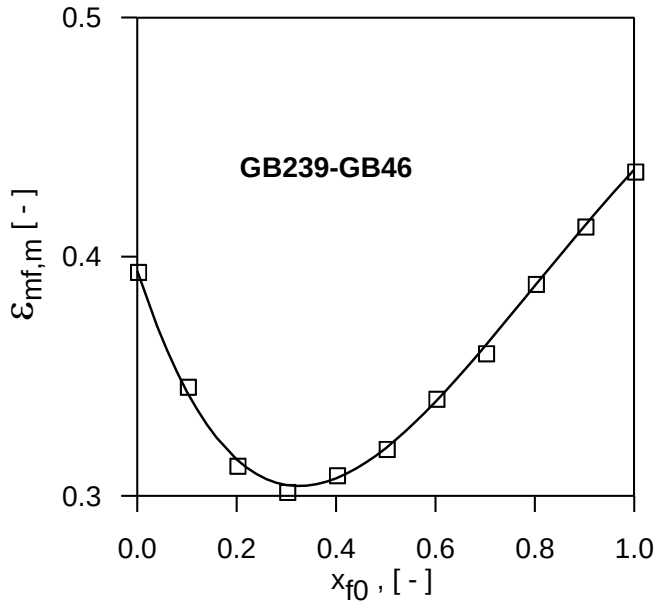

Figure 3.21: Voidage of the homogeneous size-segregating mixture GB239-GB46 at varying composition.

For the five mixtures under scrutiny the values of k are reported in Table 2.4: it diminishes when the component size ratio of the mixture d_j/d_f grows. Owing all the solids the same density, k decreases with component u_{mf} difference as well. Working out the result obtained by subtracting eqn (3.3.5) form (3.3.7), a corresponding relationship to eqn (3.3.4) is:

$$\left(u_{ff} - u_{if}\right) = \frac{\left(1-x_{f0}\right)\left(h_0 - h_m\right)\left(f_{DR} - 1\right)}{f_{DR}h_m + \left(h_0 - h_m\right)\left(1-x_{f0}\right)} u_{mf,j} \qquad (3.3.10)$$

The straight proportionality with $u_{mf,j}$-$u_{mf,f}$ is thus not found with this category of mixtures and it is more appropriate to set a relationship between k and f_{DR}, or equivalently with the size ratio, on which f_{DR} practically only depends. In Figure 3.22 the trend of k with d_j/d_f is reported, showing a dependence that could be a power law, similar to that obtained in Figure (3.11).

Table 2.4 – k-values used in the model

Mixture	**d_j/d_f**	**k**
(JETSAM/FLOTSAM)	[-]	**[-]**
GB521-GB271	1.94	0.48
GB499-GB172	2.90	0.18
GB521-GB168	3.10	0.12
GB631-GB154	4.10	0.077
GB239-GB46	5.20	0.041

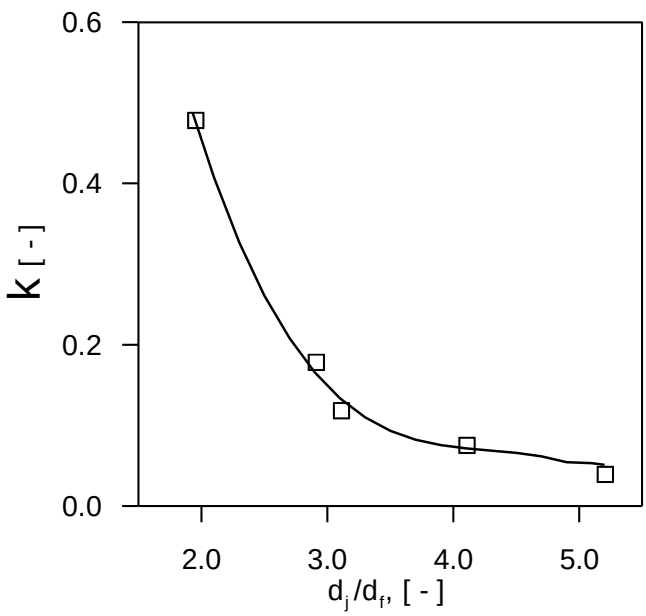

Figure 3.22: Variation of k with the size ratio between solids.

Similarly to what observed with density-segregating systems, a general comparison between experimental and calculated values of u_{ff}, carried out in Figure 3.23, confirms that the error is generally lower than 10%.

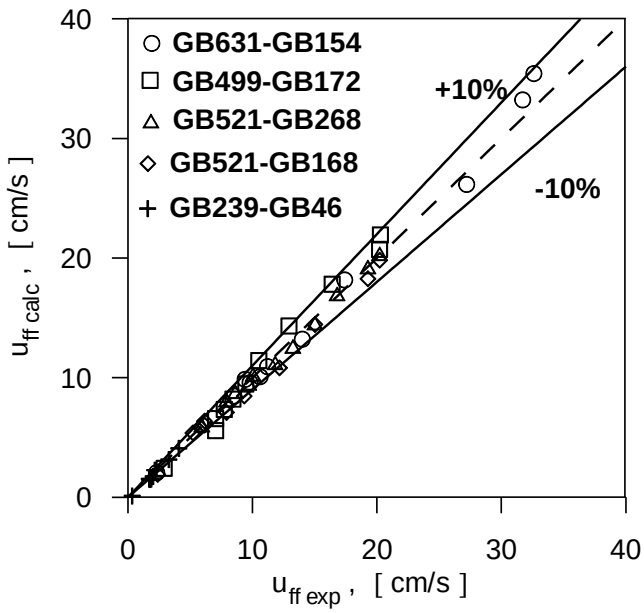

Figure 3.23: Comparison between experimental and calculated values of the final fluidization velocity. Size-segregating mixtures.

3.3.3 MIXTURES OF DISSIMILAR SOLIDS

When mixture components differ both in density and diameter, the action of each segregation factor may tend to either strengthen or balance out that of the other. The former case occurs when the jetsam component is both denser and coarser than the flotsam, and is marked by an enhanced attitude to particle stratification. The latter situation,

instead, gives rise to more than one pattern of segregation, depending on which of the two parameters, density or size, prevails in assigning the role of "flotsam" and "jetsam" to either solid. To illustrate this point, Figure 3.25 reports the curves of u_{if} and u_{ff} versus x_{f0} for the mixture SS439–MS800, whose flotsam component is the lighter but also the bigger material (molecular sieves). Notwithstanding that the particle diameter ratio of this mixture is 0.55, causing a significant reduction in voidage shown in Figure 3.26, the shape of the fluidization velocity diagram is very similar to the curvilinear triangle typical of equal size systems, a circumstance that makes clear that the high density ratio (here equal to 5.2) is by far the prevailing factor that influences the fluidization process.

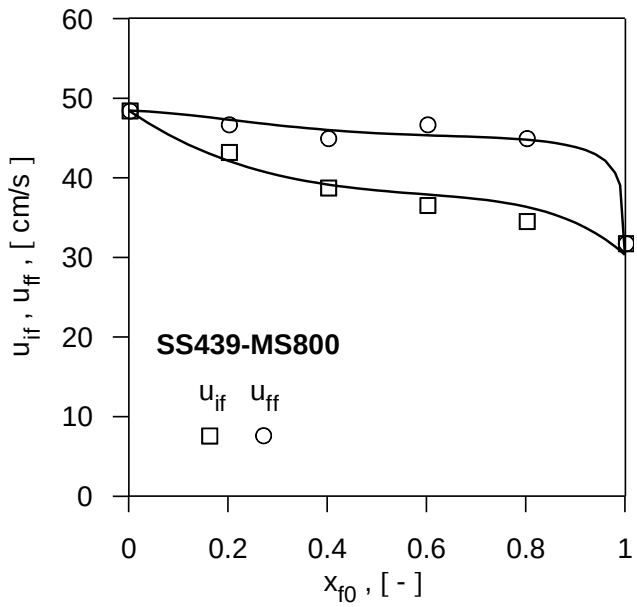

Figure 3.25: Fluidization velocity diagram of the mixture SS439-MS800.

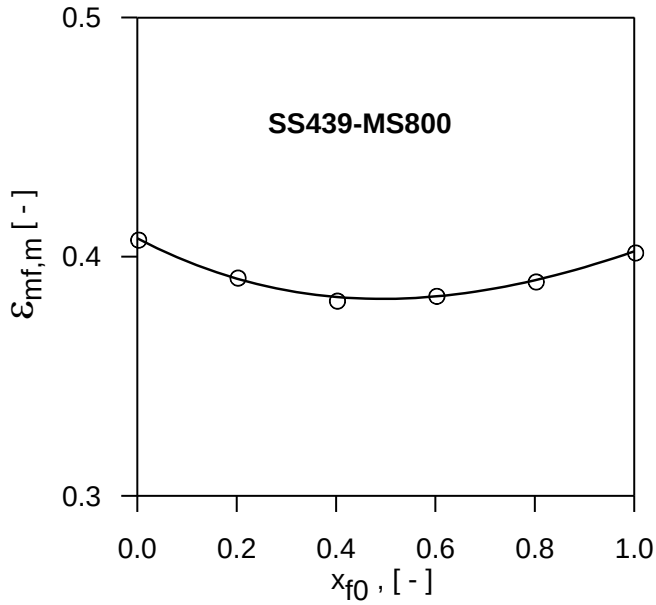

Figure 3.26: Voidage of the homogeneous mixture SS439-MS800 at varying composition.

An opposite behavior, shown in Figure 3.27, is encountered with mixture MS624–GB154, whose flotsam component (glass ballotini) is the denser, albeit smaller, material. For this system, whose size and density ratios are equal to 4.1 and 0.59, respectively, size-segregation prevails, and its relative weight results greater at low flotsam concentrations. More than that, the phenomenon is strongly attenuated in flotsam rich beds (x_{f0}>0.6), whose fluidization velocity range is narrow. Compared with the diagram of GB631–GB154 reported in Fig. 3.18, the reduction of u_{ff}–u_{if} at high flotsam fractions is apparently due to the lower density of the jetsam solid. In fact in both systems the voidage reduction affects the fluidization dynamics in the same extent, as it can be observed comparing Figure 3.19 and 3.28. Altogether, these results indicate that for a given density ratio of the two solids, a limit size ratio has to be reached for the denser solid to assume the role of "flotsam". When this occurs, the increase of the flotsam fraction over the minimum of $\varepsilon_{mf,m}$ tends to counterbalance that of the total bed weight, in a way that the full fluidization velocity of the whole system does not significantly vary.

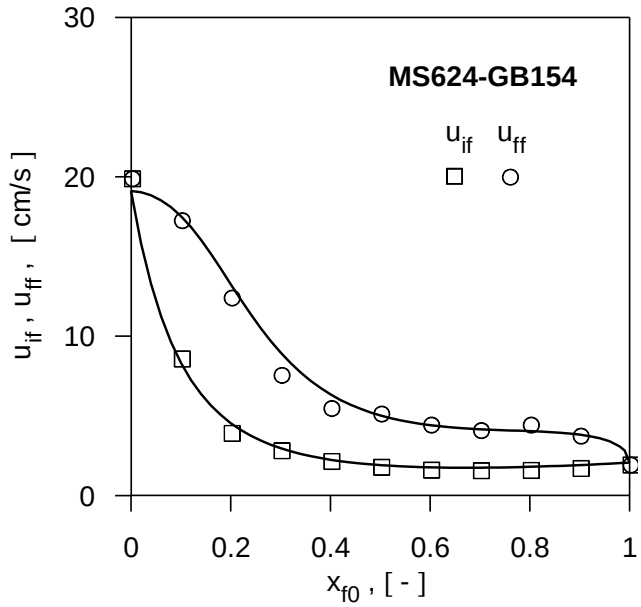

Figure 3.27: Fluidization velocity diagram of the mixture MS624-GB154.

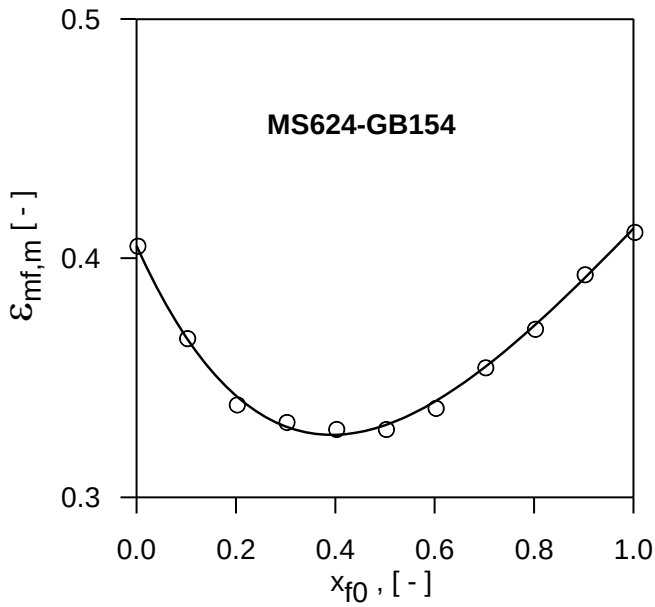

Figure 3.28: Voidage of the homogeneous mixture MS624-GB154 at varying composition.

The mixture CE376-GB271, which is characterized by a limited component size ratio equal to 1.39, exhibits experimental values of $\varepsilon_{mf,m}$ that allow assuming this variable as practically unaffected by system composition. Accordingly, an average value of $\varepsilon_{mf,m}$ drawn from the experiments and equal to 0.405, has been used to model their fluidization pattern. Figure 3.29 shows the variation of the initial and final fluidization velocity with composition for this system, whose shape is not dramatically different from the diagram of Figure 3.4 relevant to the bed CE605-GB593. However, a limited variation of the size ratio has made the fluidization diagram of Figure 3.29 a little bit more curvilinear.

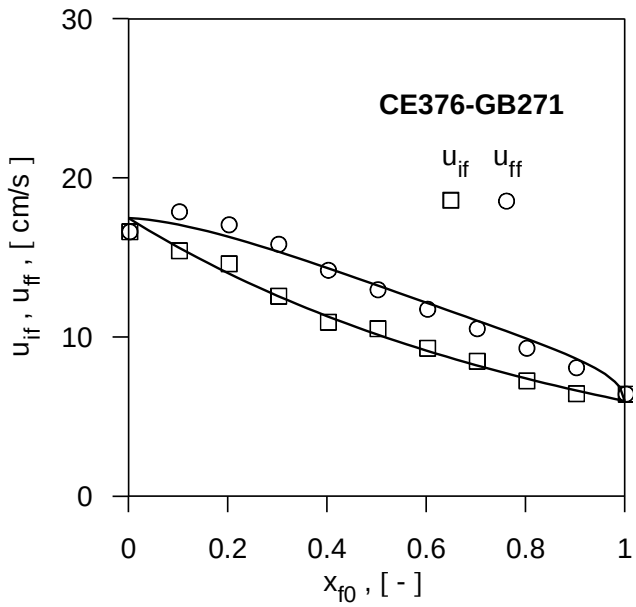

Figure 3.29: Fluidization velocity diagram of the mixture CE376-GB271.

The velocity diagram of the previous figures have been obtained by using the fully theoretical equation (3.1.1) for u_{if} and eqns (3.1.6) in conjunction with eqn (3.1.9) for u_{ff}.

The values of *k* used to fit the data are reported in Table 2.5, where these values are also compared with those of similar systems previously reported.
In all three systems of dissimilar solids the tendency to mix up is enhanced as can be found by the inspection of the higher values used for the parameter k, which have increased:

- in system CE376-GB271 with respect to CE605-GB593 (with k equal to 0.65 and 0.39 respectively) as a consequence of having introduced a limited variation of the size ratio and of having decreased the values of the component diameters (which in turn has determined a lower component u_{mf} difference);
- in MS624-GB154 in comparison with GB631-GB154 (with *k* equal to 0.14 and 0.077 respectively) as a result of having decreased the density of the jetsam solid and hence the difference $u_{mf,j}$-$u_{mf,f}$;
- in SS439-MS800 compared to SS439-GB428 (with *k* equal to 0.33 and 0.21 respectively). Also in this case the overall effect of having reduced the density and increased the size of the flotsam component results in a lower difference $u_{mf,j}$-$u_{mf,f.}$

The systems CE376-GB271 and SS439-MS800 exhibit a behavior that is essentially that of a density segregating mixture: their *k* values seem to follow the same trend of this latter category of systems as reported in Figure 3.30.

Table 2.5: Comparison with previous systems.

Mixture (JETSAM/FLOTSAM)	**k [-]**	**$u_{mf,j}$-$u_{mf,f}$** [cm/s]	**Mixture (JETSAM/FLOTSAM)**	**k [-]**	**$u_{mf,j}$-$u_{mf,f}$** [cm/s]
CE376-GB271	0.65	11.0	CE605-GB593	0.39	12.5
MS624-GB154	0.14	18.6	GB631-GB154	0.077	30.3
SS439-MS800	0.33	15.8	SS439-GB428	0.21	29.8

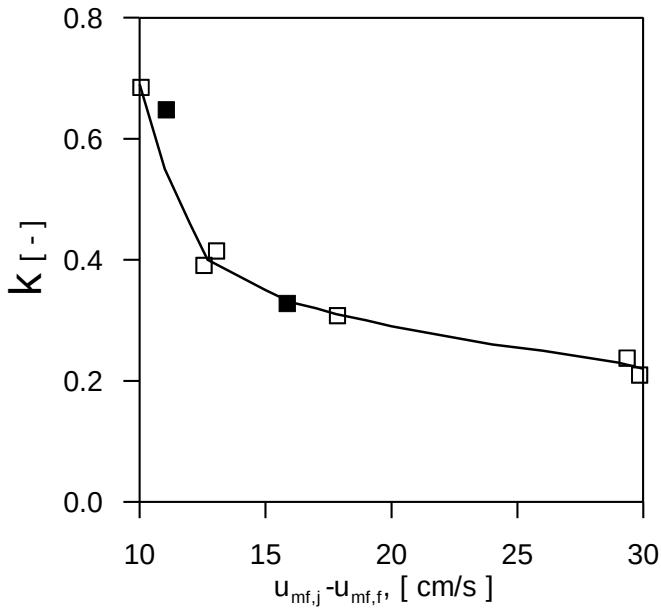

Figure 3.30: Variation of k with the u_{mf} difference between solids.
□Density segregating beds; ■ mixtures CE376-GB271 and SS439-MS800.

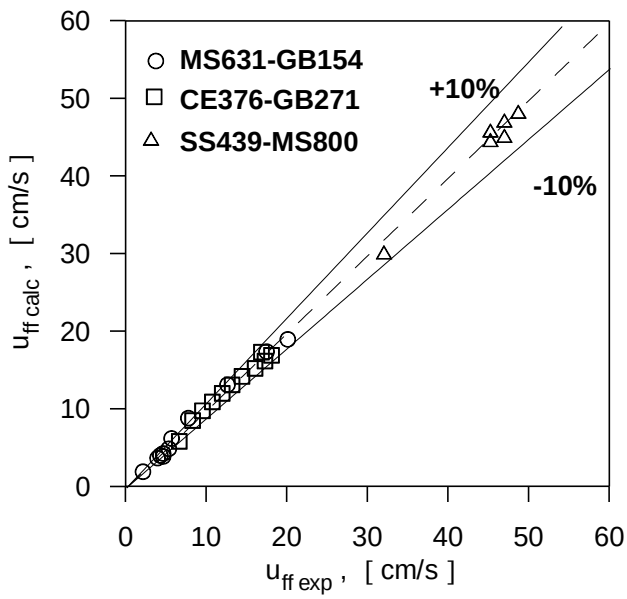

Figure 3.31: Comparison between experimental and calculated values of the final fluidization velocity. Mixtures of dissimilar solids.

As for the system MS614-GB154, for $u_{mf,J}$-$u_{mf,f}$=11 the value of k would be about 0.3 according to Figure 3.30, whereas for d_J/d_f=4.05 $k\approx$0.08 in Figure 3.22. The value of 0.14 used to fit data is intermediate, even if a stronger dependence on size ratio should be inferred.

Although not yet fully predictive, the theoretical analysis proposed in the present investigation proves capable to give errors of prediction that seldom exceed 10%, as shown in Fig. 6.8 even when both segregation factors act simultaneously. The overall quality of the agreement for these systems is shown in Figure 3.31.

3.4 DISCUSSION

In this chapter it has been proved that a more realistic representation of the structure assumed by any homogeneous two-solid bed during its transition to the fluidized state makes possible to analyze the process in the light of the fundamental theory of fluidization. Whatever the nature of the mixture, i.e. that of the factors that drive the segregation process of its component, the initial and final fluidization velocity of the binary bed can be calculated with good accuracy by reworking the force balance so as to account for the change in the axial distribution of the two solids. However, while the prediction of u_{if} is founded on the knowledge of the relationship between bed voidage and component concentration, that of u_{ff} requires quantifying the extent of segregation. To overcome this difficulty, the model proposed makes use of an experimental parameter, whose value is independent on the mixture composition and valuable from a single experiment.

In front of this apparent limitation, to be overcome by a deeper insight into the mechanisms of particle segregation, stands out the overall ability of the model to interpret the dependence of the amplitude of the fluidization velocity field of a binary mixture on the variables it is function of (component density and diameter, composition, voidage, etc.).

Thus, through the analysis of the behavior of homogeneous systems, this study confirms the possibility of addressing the problem of segregating fluidization in fundamental terms.

The most valuable achievement of the present investigation is probably that implicit in the fact that eqn (3.1.9) can be used with any types of mixtures without any difference in the error level. That demonstrates that application of the fundamental theory makes possible a unique description of segregating fluidization, regardless of the driving force of segregation being the inequality of particle density or size. Out of some other minor effects, a clear evidence has been given that the main difference of behavior between two-density and two-size mixtures arises from the voidage variation experienced by the latter in response to any change in local composition, an added complication in that it introduces a new variable into the phenomenology. Once that this aspect of the problem is properly accounted for, the need for a separated analysis of the behavior of density- and size segregating mixtures is therefore eliminated. This has to be looked at as a novel result in the field such to encourage new efforts towards a fully theoretical model of segregating fluidization.

Chapter 4

SOLID-SOLID INTERACTIONS AND THE SEGREGATION PATTERN IN THE FLUIDIZATION OF TWO DISSIMILAR SOLIDS

As it has been discussed in the previous chapter, when mixture components differ both in density and size, the two segregation factors may act in a compensating way, balancing out their effects. In this case more than one pattern of segregation is possible, depending on which particles assume the role of flotsam and which that of jetsam. The diversity of behavior may be related to the solid-solid interactions which arise in the column as a consequence of the different weight of the species.

The parametric eqn (3.1.9) for h_m that links this variable to the geometric mean of the component volume fractions, may be regarded as a measure of segregation and, at the same, residual interaction. The presence of these interactions provides an explanation for the fact that the fluidization velocity interval is always included between the minimum fluidization velocities of the single solids. In other words the flotsam undergoes a delayed fluidization, with respect of its u_{mf}, because of the presence of the other solid. Conversely, the early suspension of the jetsam is due to the dynamic action of the other component.

A quantification of these interactions is possible only if the fluid drag on each species is known, and the way to divide the friction force is derived theoretically in Section 4.1. Macroscopic balances are carried out in Section 4.2 in order to explicit these interactions

both for a homogeneous bed and a system which has undergone a partial segregation. The expressions derived from these balances show that it is theoretical possible that the component with higher minimum fluidization velocity can behave as jetsam, giving rise to an unusual phenomenology of suspension characterized by the appearance of a the fluidization front at the bottom of the column, which is described in Section 4.3. In the same section it is also shown that, for a mixture where the denser component is also the smaller and for a given density ratio of the two solids, a limit size ratio has to be reached for the denser solid to assume the role of "flotsam". Even in presence of the behavior mentioned above, that is when fluidization starts at the bottom of the column, it is demonstrated in Section 4.4 that the parametric model for the final fluidization velocity presented in the previous chapter keeps on providing good fitting if the simplified three-layer structure is modified conveniently.

4.1 COMPONENT CONTRIBUTES TO THE TOTAL PRESSURE DROP

The frictional pressure drop through a static pile of particles can be correlated in the usual way by defining a friction factor c_f' by the equation[41]:

$$-\frac{dp}{dz} = c_f' \cdot \frac{1}{2}\rho_g v^2 \frac{S_{tot}}{V_g} = c_f' \cdot \frac{1}{2}\rho_g v^2 \frac{S_f + S_j}{V_g} \qquad (4.1.1)$$

v is the interstitial fluid velocity, V_g is the available flow volume, S_t is the total surface area made up of two contributes, the flotsam and jetsam external surfaces. The average velocity through the bed is related to the volumetric flux as follows:

$$v = \frac{u}{\varepsilon_{mf,m}} \qquad (4.1.2)$$

For spherical particles V_g and the ratio S_t/V_g are:

$$V_g = Ah_0\varepsilon_{mf,m} \tag{4.1.3}$$

$$\frac{S_f + S_j}{V_g} = 6\frac{1-\varepsilon_{mf,m}}{\varepsilon_{mf,m}}\left(\frac{x_{f0}}{d_f} + \frac{1-x_{f0}}{d_j}\right) \tag{4.1.4}$$

Substituting eqn (4.1.4) and eqn (4.1.3) in eqn (4.1.1) and redefining a new friction factor $c_f' = 3c_f/2$, yields:

$$-\frac{dp}{dz} = 2c_f\rho_g u^2\frac{1-\varepsilon_{mf,m}}{\varepsilon_{mf,m}^3}\left(\frac{x_{f0}}{d_f} + \frac{1-x_{f0}}{d_j}\right) \tag{4.1.5}$$

The friction factor defined by eqn (4.1.5) is usually correlated in terms of a Reynolds number which is defined in terms of the interstitial fluid velocity and the hydraulic mean depth V_g/S_t. Neglecting a factor 6 that affects only its numerical values, Re is defined as:

$$\mathrm{Re} = 6\frac{\rho_g v}{\mu_g}\frac{V_g}{S_t} = \frac{\rho_g u}{(1-\varepsilon_{mf,m})\mu_g}\left(\frac{x_{f0}}{d_f} + \frac{1-x_{f0}}{d_j}\right) \tag{4.1.6}$$

For low Reynolds numbers the Carman-Kozeny equation gives:

$$c_f = \frac{90}{\mathrm{Re}} \tag{4.1.7}$$

After substitution of eqn (4.1.7) into eqn (4.1.5) the following expression for the pressure drop is obtained:

$$-\frac{dp}{dz}=\frac{180\mu u\left(1-\varepsilon_{mf,m}\right)^2}{\varepsilon_{mf,m}^3}\left(\frac{x_{f0}}{d_f}+\frac{1-x_{f0}}{d_j}\right)^2=\frac{180\mu u\left(1-\varepsilon_{mf,m}\right)^2}{\varepsilon_{mf,m}^3 d_{av}^2} \qquad (4.1.8)$$

Eqn (4.18) provides the theoretical justification of having introduced the Sauter mean size in the model presented in the previous chapter.

The procedure that has just been illustrated to derive eqn (4.1.8) provides the means through which the drag force on the single species can be evaluated. In fact eqn (4.1.1) allows to split up two contributions:

$$-\frac{dp}{dz}=c_f{}'\cdot\frac{1}{2}\rho_g v^2\frac{A_f}{V_g}+c_f{}'\cdot\frac{1}{2}\rho_g v^2\frac{A_j}{V_g}=\left(-\frac{dp}{dz}\right)_f+\left(-\frac{dp}{dz}\right)_j \qquad (4.1.9)$$

obtaining

$$\left(-\frac{dp}{dz}\right)_f=\frac{180\mu u\left(1-\varepsilon_{mf,m}\right)^2}{\varepsilon_{mf,m}^3 d_{av}}\frac{x_{f0}}{d_f} \qquad (4.1.10)$$

$$\left(-\frac{dp}{dz}\right)_j=\frac{180\mu u\left(1-\varepsilon_{mf,m}\right)^2}{\varepsilon_{mf,m}^3 d_{av}}\frac{1-x_{f0}}{d_j} \qquad (4.1.11)$$

The same result could be derived by intuitively scaling the friction force between solids according to the surface fraction of each species, that is:

$$\frac{S_f}{S_t}=\frac{x_{f0}/d_f}{x_{f0}/d_f+\left(1-x_{f0}\right)/d_j}=\frac{d_{av}}{d_f}x_{f0} \qquad (4.1.12)$$

$$\frac{S_j}{S_t} = \frac{\left(1-x_{f0}\right)/d_j}{x_{f0}/d_f + \left(1-x_{f0}\right)/d_j} = \frac{d_{av}}{d_j}\left(1-x_{f0}\right) \tag{4.1.13}$$

In the simplified case of a two-density bed the frictional pressure drop on each species is proportional to their volumetric abundance.

4.2 SOLID-SOLID INTERACTIONS

4.2.1 HOMOGENEOUS BED

For a well mixed bed u_{if} can be calculated from the relation introduced in Chapter 3:

$$\frac{180\mu_g u_{if}}{d_{av}^2}\frac{\left(1-\varepsilon_{mf,m}\right)^2}{\varepsilon_{mf,m}^3} = \left(\rho_{av}-\rho_g\right)\left(1-\varepsilon_{mf,m}\right)g \tag{3.1.1}$$

Eqn (3.1.1) can be obtained by a simple macroscopic force balance on the entire bed including all individual contributions in order to quantify the interaction between the two solids. This is accomplished by carrying out separate force balances on each individual solid:

$$-\left(\rho_f-\rho_g\right)g + f_{D,f} + f_{j\to f} = 0 \tag{4.2.1}$$

$$-\left(\rho_j-\rho_g\right)g + f_{D,j} + f_{f\to j} = 0 \tag{4.2.2}$$

In the previous expressions, written per unit volume of solid component, four types of force appear: the gravitational force, the buoyancy, the fluid-solid interaction f_D and the interaction between the two solids. As shown in the previous section a theoretical way to

distribute the friction exerted by the fluid between flotsam and jetsam is that of scaling it proportionally to the component external surface. So doing the drag forces per unit volume become:

$$f_{D,f} = \frac{180\mu u_{if}\left(1-\varepsilon_{mf,m}\right)}{\varepsilon_{mf,m}^3 d_{av} d_f} \tag{4.2.3}$$

$$f_{D,j} = \frac{180\mu u_{if}\left(1-\varepsilon_{mf,m}\right)}{\varepsilon_{mf,m}^3 d_{av} d_j} \tag{4.2.4}$$

Note as eqns (4.2.3) and (4.2.4) become equal for two-density systems. The terms $f_{f\to j}$ and $f_{j\to j}$ represent the interactions between the two species, and therefore necessarily:

$$f_{f\to j} A h_0 \left(1-\varepsilon_{mf,m}\right)\left(1-x_{f0}\right) = -f_{j\to f} A h_0 \left(1-\varepsilon_{mf,m}\right) x_{f0} = F_I \tag{4.2.5}$$

where h_0 is the initial height of the bed, kept constant in all experiments of fluidization, and F_I is the total force, per unit area, acting between the two solids, flotsam and jetsam. For the convention used here F_I is positive if the flotsam particles produce an upward force which acts over the jetsam ones. Therefore a positive value of F_I means that the flotsam tends to segregate to the top, whereas the jetsam tends to sink to the bottom.

Substituting eqns (4.2.3)-(5) in eqns (4.2.1) and (4.2.2) provides:

$$-\left(\rho_f - \rho_g\right)g + \frac{180\mu u_{if}\left(1-\varepsilon_{mf,m}\right)}{\varepsilon_{mf,m}^3 d_{av} d_f} - \frac{F_I}{A h_0 \left(1-\varepsilon_{mf,m}\right) x_{f0}} = 0 \tag{4.2.6}$$

$$-\left(\rho_j - \rho_g\right)g + \frac{180\mu u_{if}\left(1-\varepsilon_{mf,m}\right)}{\varepsilon_{mf,m}^3 d_{av} d_j} + \frac{F_I}{A h_0 \left(1-\varepsilon_{mf,m}\right)\left(1-x_{f0}\right)} = 0 \tag{4.2.7}$$

In eqns (4.2.6) and (4.2.7) there are two unknowns u_{if} and F_I. Solving for them eqn (3.1.1) is again obtained along with the expression for the interaction force:

$$F_I = \left[\frac{\left(\rho_j - \rho_g\right)}{d_f} - \frac{\left(\rho_f - \rho_g\right)}{d_j} \right] A h_0 \left(1 - \varepsilon_{mf,m}\right) d_{av} x_{f0} \left(1 - x_{f0}\right) g \tag{4.2.8}$$

For a density segregating system this force is proportional to the density difference between the species:

$$F_I = \left(\rho_j - \rho_f\right) h_0 \left(1 - \varepsilon_{mf}\right) x_{f0} \left(1 - x_{f0}\right) g \tag{4.2.9}$$

whereas for a size segregating bed it results mainly dependent on the component difference of the specific surface:

$$F_I = \left(\frac{1}{d_f} - \frac{1}{d_j} \right) \left(\rho_s - \rho_g\right) h_0 \left(1 - \varepsilon_{mf,m}\right) x_{f0} \left(1 - x_{f0}\right) d_{av} g \tag{4.2.10}$$

Inspection of Eqn (4.2.8) allows making some considerations. First of all it simply states that the drag exerted on the flotsam which exceeds its weight results in a net force transferred to the denser component. Similarly the jetsam component has an effective weight that burdens on the other species. This interaction force can be zero if:

$$\left(\rho_j - \rho_g\right) d_j = \left(\rho_f - \rho_g\right) d_f \tag{4.2.11}$$

Setting F_I=0, eqns (4.2.1) and (4.2.2) can be solved separately for the initial fluidization velocity. This procedure provides two identical results, where the u_{if} is expressed as a function of the flotsam component or, alternatively, of the jetsam one:

$$u_{if} = \frac{(\rho_f - \rho_g) d_{av} d_f \varepsilon_{mf,m}^3 g}{180\mu(1-\varepsilon_{mf,m})} = \frac{(\rho_j - \rho_g) d_{av} d_j \varepsilon_{mf,m}^3 g}{180\mu(1-\varepsilon_{mf,m})} \quad (4.2.12)$$

Eqn (3.1.1) can be rearranged in the form:

$$u_{if} = \frac{(\rho_s - \rho_g) d_{av} d_f \varepsilon_{mf,m}^3 g}{180\mu(1-\varepsilon_{mf,m})} \left(\frac{d_{av}}{d_f} x_{f0} \right) + \frac{(\rho_s - \rho_g) d_{av} d_j \varepsilon_{mf,m}^3 g}{180\mu(1-\varepsilon_{mf,m})} \left[\frac{d_{av}}{d_f} (1 - x_{f0}) \right] \quad (4.2.13)$$

In view of eqn (4.2.13), the initial fluidization velocity of the bed can be considered as the external surface weighted mean of the minimum fluidization velocities of its components in an "*ideal*" mixture:

$$u_{if} = u_{mf,f}^* \frac{A_f}{A_{tot}} + u_{mf,j}^* \frac{A_J}{A_{tot}} \quad (4.2.14)$$

where $u^*_{mf,f}$ and $u^*_{mf,j}$ are equal respectively to the first and second expression for u_{if} given in eqn (4.2.12). They can be also defined as the component fluidization velocities in the mixed state if no interactions were present. In other words if no segregation occurred and no solid-solid interactions were present, the flotsam would begin to fluidize at $u_{mf,f}^*$ (and so the mixture, $u_{if} = u_{mf,f}^*$) while the jetsam would fluidize at $u_{mf,j}^*$ (and $u_{ff} = u_{mf,j}^*$). However interactions are not present only if the condition (4.2.11) is satisfied. Thus in this special case and in absence of segregation, the mixture would fluidized completely at a single velocity point at each composition:

$$u_{if} = u_{ff} = u_{mf,f}^* = u_{mf,j}^* \quad (4.2.13)$$

Being the fluidization interval a measure of particle segregation, eqn (4.2.11) could thus be regarded as a criterion to promote mixing, at least if the presence of interactions determines a contributory cause to segregation. In the next section it is shown than in some cases the when the component ρd are similar, segregation phenomena appear to be limited, but this criterion has no general validity.

Another important issue arises from the fact interaction force expressed by eqn (4.2.8) is positive if:

$$(\rho_j - \rho_g)d_j > (\rho_f - \rho_g)d_f \tag{4.2.14}$$

For our sign convention, the positive value of the force F_I indicates that the flotsam component exerts a force directed upwards on the jetsam, which in turn hinders the flotsam migration to the upper regions of the bed opposing a downward force. In other words if F_I>0 the flotsam component will tend to rise, whereas the jetsam will sink. This would mean that the role of jetsam and flotsam have been correctly assigned. Even if eqn (4.2.14) seems to provide a criterion for identifying which is the role played by each component, it has been derived for a well mixed bed at its u_{if} and gives only information on the initial tendency of particles to segregate. As in the case of the layer inversion phenomenon in liquid fluidized beds the particle tendency to rise or fall might depend on particle properties as well as the operating velocity. For a better insight on this topic, a force balance has been carried out on a system whose internal component distribution is no longer homogeneous.

Finally it is worth noticing that when gas velocity is increased above u_{if} instantaneously the force exerted by the flotsam on the other solid is unbalanced in each layer: the cumulative upward force increases along the column height being the highest at the bed free surface. This effect could be an explanation for the fact that segregation is observed to start at the top of the bed.

4.2.2 PARTIAL SEGREGATION

The expression for the u_{ff} derived in the previous chapter is:

$$u_{ff} = \frac{\left[\left(\rho_f - \rho_g\right)x_f h_m + \left(\rho_j - \rho_g\right)\left(1-x_f\right)h_0\right]g}{180\mu_g\left[\frac{\left(1-\varepsilon_{mf,m}\right)}{\left(\varepsilon_{mf,m}^3 d_{av}^2\right)}h_m + \frac{\left(1-\varepsilon_{mf,j}\right)}{\left(\varepsilon_{mf,j}^3 d_j^2\right)}\left(h_0 - h_m\right)\left(1-x_f\right)\right]} \qquad (3.1.6)$$

Eqn (3.1.6) can be also obtained following a procedure similar to that carried out in section 4.2.1. Bearing in mind the simplified scheme of Figure 3.1, reported again below, we can formulate a force balance on the jetsam in the layer h_j and on both components in the layer h_m. Writing each balance per unit volume of component in that layer yields:

Jetsam layer:

$$-\left(\rho_j - \rho_g\right)g + f_{D,j}^{j} + f_{m\to j,j} = 0 \qquad (4.2.15)$$

Mixed layer, flotsam:

$$-\left(\rho_f - \rho_g\right)g + f_{D,f}^{m} + f_{j\to m,f} + f_{j\to f}^{m} = 0 \qquad (4.2.16)$$

Mixed layer, jetsam:

$$-\left(\rho_j - \rho_g\right)g + f_{D,j}^{m} + f_{j\to m,j} + f_{f\to j}^{m} = 0 \qquad (4.2.17)$$

where $f_{D,k}^{l}$ is the drag force on the component *k* in the layer *l*, $f_{l\to s,k}$ is the interaction force that layer *l* exerts on the component *k* in the layer *s*, $f_{k\to i}^{l}$ is the force exerted by the component *k* on component *i*, both species being in the layer *l*.

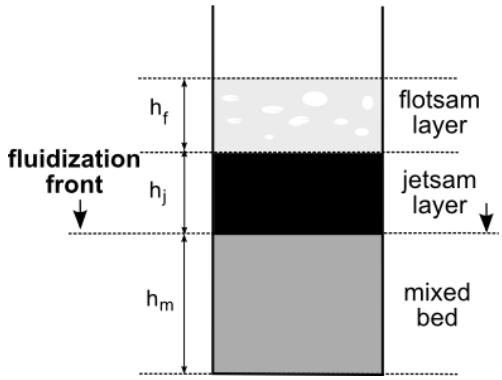

Figure 3.1: Simplified scheme of the fluidization phenomenology.

Moreover the following relationships must be satisfied:

$$f_{m\to j,j}A\left(1-\varepsilon_{mf,j}\right)h_j = -f_{j\to m,f}A\left(1-\varepsilon_{mf,m}\right)h_m x_f = F_{I,l} \tag{4.2.18}$$

$$f_{m\to j,j}A\left(1-\varepsilon_{mf,j}\right)h_j = -f_{j\to m,j}A\left(1-\varepsilon_{mf,m}\right)h_m\left(1-x_{f0}\right) = F_{I,l} \tag{4.2.19}$$

$$f_{f\to j}Ah_m\left(1-\varepsilon_{mf,m}\right)\left(1-x_{f0}\right) + f_{j\to f}Ah_m\left(1-\varepsilon_{mf,m}\right)x_{f0} = F_{I,l} \tag{4.2.20}$$

where $F_{I,l}$ is the total force exchanged between the two layers and the layers h_j and h_m are related by eqn (3.1.5).

Furthermore the expressions for the terms $f_{D,k}^{l}$ are:

$$f_{D,k}^{l} = \frac{180\mu u_{ff}\left(1-\varepsilon_{mf,l}\right)}{\varepsilon_{mf,l}^{3}d_{av}^{l}d_k} \tag{4.2.21}$$

In it d_{av}^{l} is the Sauter mean diameter in the layer *l*.

Now we can solve the previous system of equations obtaining eqn (3.1.6), along with the expressions for the layer-layer interaction and the forces exchanged by the two component in the layer h_m:

$$F_{I,l} = (1-\varepsilon_{mf,m})g\frac{h_m(h_0-h_m)\{f_{DR}(\rho_j-\rho_g)-(\rho_{av,m}-\rho_g)\}}{[f_{DR}h_m+(h_0-h_m)(1-x_{f0})]} \tag{4.2.22}$$

$$f_{f\to j} = x_{f0}g\frac{f_{DR}\left[\frac{(\rho_j-\rho_g)}{d_f}h_0-\frac{(\rho_f-\rho_g)}{d_j}h_m\right]+(h_0-h_m)(\rho_f-\rho_g)}{[f_{DR}h_m+(h_0-h_m)(1-x_{f0})]} \tag{4.2.23}$$

$$f_{j\to f} = (1-x_{f0})g\left\{-\frac{f_{DR}\left[(\rho_j-\rho_g)\frac{d_{av}}{d_f}-(\rho_f-\rho_g)\frac{d_{av}}{d_j}\right]h_m}{[f_{DR}h_m+(h_0-h_m)(1-x_{f0})]}+\right.$$
$$\left.+\frac{\left[f_{DR}\frac{d_{av}}{d_j}-1\right](\rho_j-\rho_g)(h_0-h_m)(1-x_{f0})}{[f_{DR}h_m+(h_0-h_m)(1-x_{f0})]x_{f0}}\right\} \tag{4.2.24}$$

Inspection of eqns (4.2.22) and (23) shows as these forces are always positive when eqn (4.2.11) is satisfied, that is they are directed upwards according to our convention. This means that the mixed layer supports the jetsam layer and the flotsam in the stratum h_m always exerts an upward thrust.

Eqn (4.2.24) indicates that the force exerted by the jetsam component on the flotsam one is negative when h_m is large, i.e. near to h_0, whereas it becomes positive for smaller values of h_m. Since h_m decreases with velocity, the previous analysis states that up to a certain velocity

value the jetsam in the homogeneous layer is supported by the flotsam included in h_m whereas for higher velocities the jetsam concurs with the flotsam to support the layer h_j.
The value of h_m that marks this transition is:

$$\left.\frac{h_m}{h_0}\right|_{f_{j\to f}=0} = \frac{\left(\rho_j-\rho_g\right)\left(1-x_{f0}\right)\left(f_{DR}\frac{d_{av}}{d_j}-1\right)}{\left(\rho_j-\rho_g\right)\left(1-x_{f0}\right)\left(f_{DR}\frac{d_{av}}{d_j}-1\right)+f_{DR}x_{f0}\left[\left(\rho_j-\rho_g\right)\frac{d_{av}}{d_f}-\left(\rho_f-\rho_g\right)\frac{d_{av}}{d_j}\right]} \quad (4.2.25)$$

The corresponding velocity at which this transition occurs is found by substituting the value of h_m from eqn (4.2.25) in eqn (3.1.6). The final result is:

$$u\big|_{f_{j\to f}=0} = u^*_{mf,j} \quad (4.2.26)$$

Eqn (4.2.26) proves what it would be easily guessed without derivation, that is the jetsam begins to push upward when it has no residual weight in the mixed zone. Another point to stress is that when eqn (4.2.12) is satisfied the reversal of sign in equation (4.2.24) is predicted for h_m=h_0, i.e. when the bed is mixed. According to eqn (4.2.24) if for any reason the bed starts to segregate forming a defluidized layer in the middle of the bed (see again Figure 3.2), then immediately both components in the mixed layer below starts to support this defluidized stratum. Thus, if the component ρd difference is not very large, the solid which initially behaves as jetsam, once segregation has progressed to a minor extent, starts to push upwards, thus rendering the distinction between flotsam and jetsam less clear.
The balance proposed can appear cumbersome and of minor interest, however it demonstrates as interactions contribute to the fluidization of the mixture. The presence of these interactions provides a theoretical explanation of the fact that u_{if} is always observed to be higher than the minimum fluidization velocity of the flotsam and that u_{ff} is generally lower than the minimum fluidization velocity of the jetsam component. In fact the role played by

interactions is that of hindering the fluidization of the flotsam component and facilitating that of the jetsam one. Furthermore these balances show that the assignment of the role of jetsam and flotsam can depend on the concentration profile along the column axis determined by the operating velocity.

4.3 SEGREGATION PATTERNS

4.3.1 EXPERIMENTAL

In this section several concentration profiles along the column height are presented. In order to obtain these data, a solenoid valve on the feed line was employed to cut the air flux off instantaneously, thus "freezing" the particulate bed in the mixing state associated to a given steady fluid dynamic condition; subsequently, the solid was gently drawn from the top of the column by means of a vacuum device, in horizontal layers of particles generally 2 cm thick (or 1 cm thick, when a higher resolution was needed). Each of these layers was then sieved to measure, by weighing, the mass fraction of either solid component. Concentration values were then referred to the average height of the relevant layers and used to trace the respective profiles in function of height. Owing to the absence of free fine percolation after the interruption of the gas flow, the technique employed, used by many research groups[8-12, 35,37] and widely accepted in the field, is able to ensure reliable results.

The properties of the solids employed are reported in Table 2.1 of the previous chapter and in Table 4.1.

Table 4.1 – Properties of the experimental solids (see also Table 2.1).

Solid	**Density** [g/cm^3]	**Sieve size** [μm]	**Sauter mean diameter** [μm]	**Experimental u_{mf}** [cm/s]
Glass ballotini (GB)	2.48	800-900	838	45.6
		500-600	570	24.5
Ceramics (CE)	3.76	533	43.3	30.5
Steel shots (SS)	7.60	150-200	170	6.90
Bronze (BR)	8.86	200-300	243	17.5

4.3.2 THE TENDENCY TO RISE OR FALL

In a gas fluidized bed it is not always possible to know a priori which component will sink and which will float. If the particles differ only in density or size, it is obvious that the jetsam component will be the denser or the larger respectively. In some cases, whether the particular component will behave as flotsam or jetsam will have to be determined experimentally. This is especially true for a bed of multi-component mixtures with a wide size and density distribution or when the components differ both in density and size with the heavier being also the smaller. For a two-component binary system, Chiba et al.[4] suggested the general rules presented in Table 4.2. In a gas fluidized bed of a mixture of wide size and density distribution, the distinction between flotsam and jetsam becomes less clear because one particular component may be flotsam with respect to some components in the bed, while simultaneously it is also jetsam relative to other components.

According to the rules of Table 4.2, for spherical particles and neglecting special cases, i.e. when the bed is made up almost exclusively by just one component, the denser solid is always jetsam unless it is more than ten times smaller. This is equivalent to state that, out of the case where percolation becomes important (that is approximately when the component size ratio is greater than 6) the denser component is always jetsam.

Table 4.2: Classification of Jetsam and Flotsam[4].

CASE *I* $d_B/d_S \leq 10$		
Ia	$\rho_B=\rho_S$	Jetsam=bigger component
Ib	$\rho_B \neq \rho_S$	Jetsam=heavier component
CASE *II* $d_b >> d_s$ and bed material → 100% smaller component		
IIa	$\rho_B > (\rho_S)_B$	Jetsam=bigger component
IIb	$\rho_B < (\rho_S)_B$	Jetsam=smaller component
CASE *III* $d_b >> d_s$ and bed material → 100% bigger component		
IIIa	$\rho_B > \rho_S$	Jetsam=bigger component
IIIb	$\rho_B < \rho_S$	Jetsam=either component may be jetsam
CASE *IV* The minor component is platelike with ϕ <0.5		
IVa	Platelike particle is denser	Jetsam=platelike component
IVb	Platelike particle is lighter	Jetsam=either component may be jetsam
	ρ_B , ρ_S: density of the bigger, smaller component	*d_B , d_S: size of the bigger, smaller component*
	$(\rho_S)_B$: bulk density of the smaller component	*ϕ: sphericity*

Figures 4.1-3 demonstrate that this statement is not always true, because in some cases an inversion of the roles of jetsam and flotsam is possible at a lower size ratio. These figures report some experimental profiles obtained at different gas flow rate for an initially well mixed bed. In all three systems examined the two solids are always molecular sieves (MS), as the bigger and lighter component, and glass ballotini (GB) as the smaller and heavier one, with component size ratio equal to 1.64, 2.45 and 5.09 in Figures 4.1-3 respectively, and solid fraction equal to 0.5.

For the mixture GB800-GB521 of Figure 4.1, an unexpected fluidization phenomenology is observed to occur. In this case for $u_{if} < u < u_{ff}$ the system displays as significantly segregated, with the bigger but less dense component MS800 accumulating at the top of the bed, whereas the heavier GB521 sinks to the bottom acting as jetsam. However GB521 is also the solid possessing the lower minimum fluidization velocity and, being almost pure in the bottom region, it appears to be completely fluidized. Thus the bed is made up of three parts: a lower one which is a fluidized bed that consists near only of GB521, a top packed stratum made up of almost exclusively the bigger component, and an intermediate layer supporting the upper defluidized bed.

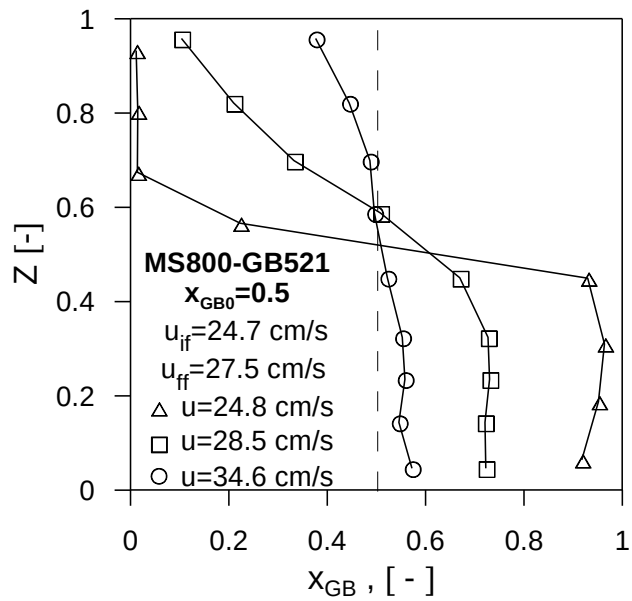

Figure 4.1: Axial concentration profile of the mixture MS800-GB521 at varying velocities.

This apparently surprising experimental observation is predicted by the criterion (4.2.14). In fact this criterion is different from that which identifies the jetsam as the component with the higher minimum fluidization velocity. Assuming equal voidage for the single solids, the jetsam has a higher minimum fluidization if the following condition is satisfied:

$$(\rho_j - \rho_g) d_j^2 > (\rho_f - \rho_g) d_f^2 \qquad (4.3.1)$$

Then It may happen that the component with greater u_{mf} initially segregate on the top of the column, forming a packed layer through which the gas passes with a too low interstitial velocity to fluidize it. This layer is then held supported by the thrust of a stratum where components are still forming a mixture, leading to a phenomenology which is analogous to that shown in Figure 3.1, with the exception however that now the freely bubbling bed is situated near the grid region. The system can be schematized as a bed made up of three layers: a layer composed only of GB521 at the bottom, a mixed middle stratum and MS800 as a pure component at the top. This same pattern is observed in other systems and is also schematized in Figure 4.11, reported later in the text. In this case it is worth pointing out that in the light of eqns (4.2.23) and (24), in which the flotsam is the solid MS800, the top packed layer made up of MS800 is not supported by the other solid GB521, at least in the early stages of segregation, but the particles MS800 themselves exerts an upwards thrust in the mixed layer underneath. The presence of the GB particles, however, has the effect of increasing the drag force in the mixed layer, since the average Sauter diameter and voidage both decrease. At higher gas velocities the GB particles progressively segregate at the bottom so that the forces acting between the two top layers are again balanced out. Another point to notice is that for this system it is necessary to reach a velocity appreciably beyond the value of u_{ff} to obtain a concentration profile that can be considered approximately uniform along the entire bed.

Figure 4.2 shows some experimental profiles at varying velocity for the mixture MS800-GB322. In this case the criterion (4.2.14) fails when predicting that, starting from a homogeneous bed, the solid GB322 tends initially to rise in the bed. Though the role of GB322 as flotsam has in this case no experimental confirmation, at each velocity investigated, the system may be considered homogeneous and thus attributing the role of jetsam or flotsam to a particular component may have no sense in this case. Another

important point to take into account is the following: when the difference of the product ρd is not large, in correspondence of a limited extent of segregation both GB337 and MS800 in the mixed middle layer exerts an upward force (see again eqn (4.2.24)) and this can promote mixing between the two species.

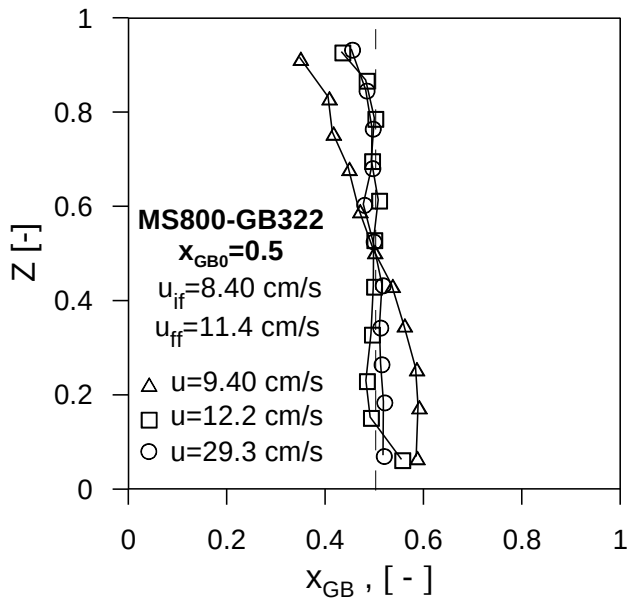

Figure 4.2: Axial concentration profile of the mixture MS800-GB322 at varying velocities.

By further increasing the size ratio it is shown in Figure 4.3 that for the system MS800-GB162 the heavier component, i.e. GB172, becomes flotsam even if the bed undergoes only a weak segregation and easily mixes near its final fluidization point. The inversion of the role of flotsam and jetsam is observed to occur for a size ratio less than 10, unlike indicated in Table 4.1.

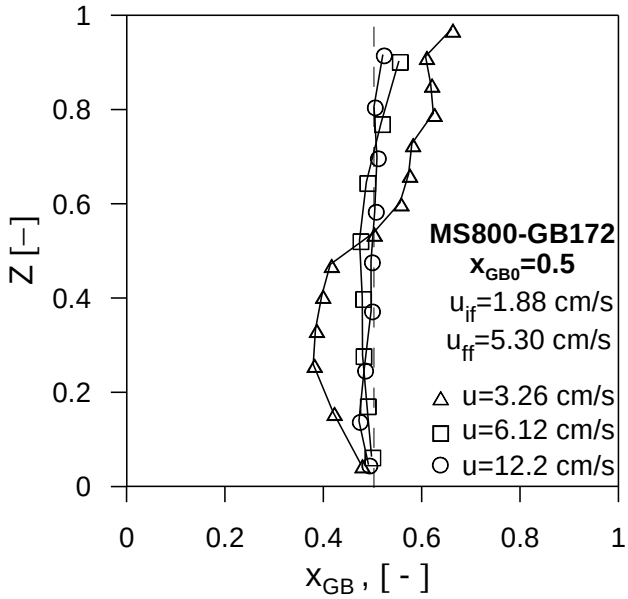

Figure 4.3: Axial concentration profile of the mixture MS800-GB172 at varying velocities.

All the systems so far analyzed have been investigated at a volume fraction equal to 0.5; however, as stated also in Table 4.2, the role of jetsam or flotsam may not depend on the solid fraction, except very near the extremes of the concentration domain. This is also experimentally reported by other authors[42] and by the concentration profiles illustrated in Figure 4.4-4.6. Nevertheless the experimental data are insufficient to draw a final conclusion on this topic. The system GB570-BR243 has been investigated at three different volume fractions of bronze solids 0.2, 0.5 and 0.8. In each case the flotsam component is always GB570, which have a higher u_{mf}, even if for x_{BR}=0.8 the bed is practically mixed at its u_{ff}. When glass richer systems are examined in Figure 4.5 and 4.6, the tendency to segregation is strongly enhanced since much higher velocity than u_{ff} is required to bring the system in a homogeneous state.

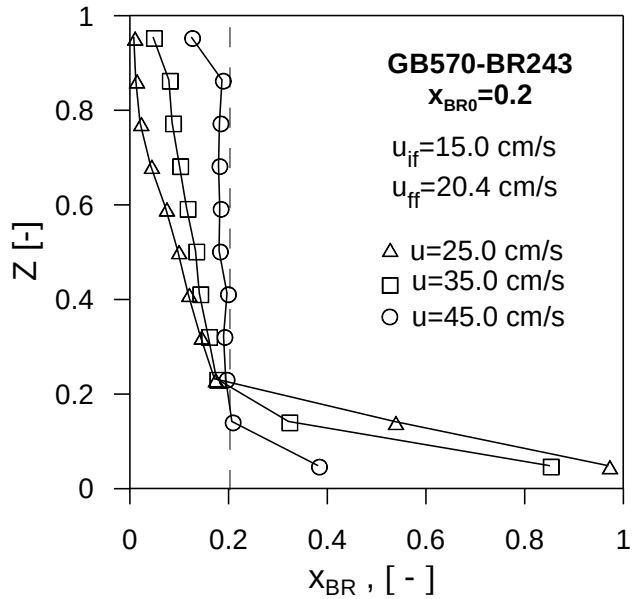

Figure 4.4: Axial concentration profile of the mixture GB570-BR243 at varying velocities.

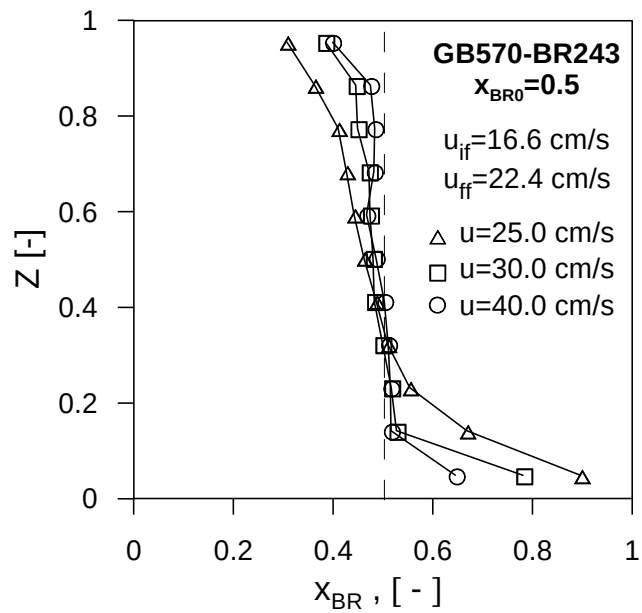

Figure 4.5: Axial concentration profile of the mixture GB570-BR243 at varying velocities.

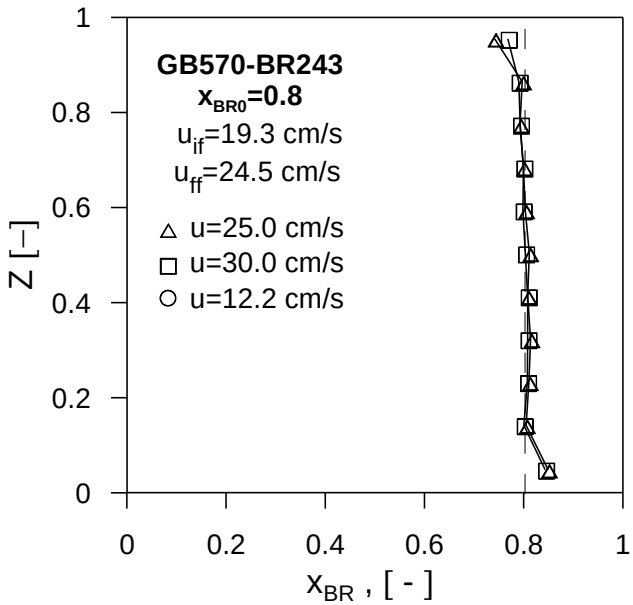

Figure 4.6: Axial concentration profile of the mixture GB570-BR243 at varying velocities.

The phenomenology of fluidization of this system is predicted by the relationship (4.2.14) and is analogous to that of the mixture MS800-GB521.

In all the cases under investigation, when $\rho_{LB}d_{LB} \leq \rho_{HS}d_{HS} \leq \rho_{LB}d^2_{LB}$ appreciable segregation with the heavy and fluid (i.e. with lower u_{mf}) component behaving as jetsam is observed, especially during the transition from the packed to the fluidized state. Further proofs of the general validity of this statement can be searched out in literature (see Table 4.3 later in the text) and in Figure 4.7 where the concentration profiles of an additional system, namely GB593-SS243, are shown. Like the other two beds, GB570-BR243 and MS800-GB521, it reaches a practically mixed state for a velocity higher then u_{ff} .

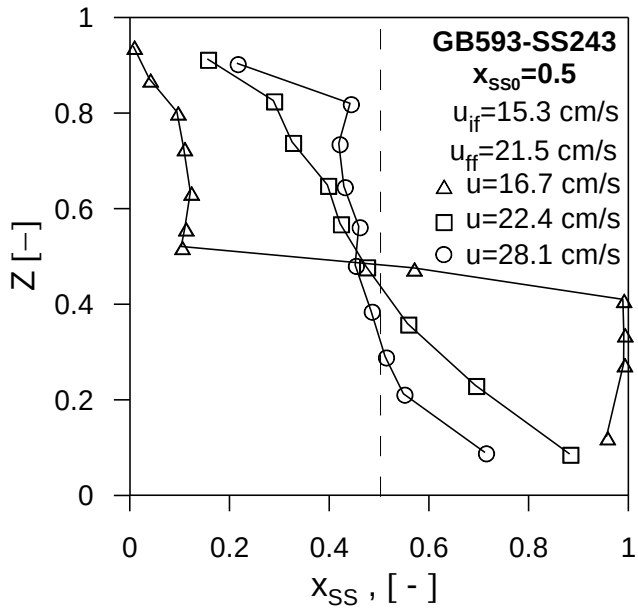

Figure 4.7: Axial concentration profile of the mixture GB593-SS243 at varying velocities.

The condition (4.2.14) fails however in predicting the flotsam behavior of CE533 and SS170 for the systems GB838-CE533 and CE376-SS170 whose experimental concentration profiles are shown below (Figures 4.8-4.11). Like the systems MS800-GB172 and MS800-GB322, both mixtures exhibit an internal component distribution which are not strongly affected by segregation. At velocity moderately higher than its u_{if}, the bed CE376-SS170 practically does not vary its initial homogeneous arrangement and this is observed at different compositions x_{SS}=0.2, 0.5 and 0.8. In this case it may have no sense to know which component is jetsam.

The system GB838-CE533 undergoes a slight segregation during its transition from the packed to the fluidized state, as shown in Figure 4.11 for x_{CE}=0.5. However the two solids may be considered practically mixed at a velocity near the u_{ff} of the mixture.

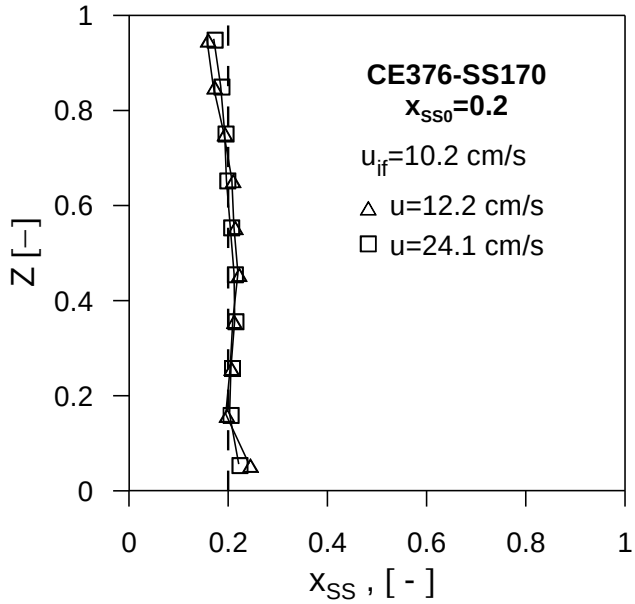

Figure 4.8: Axial concentration profile of the mixture CE376-SS170 at varying velocities.

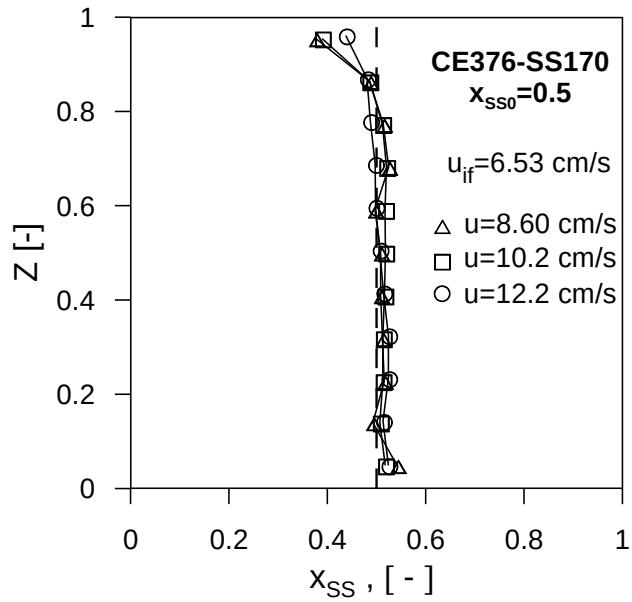

Figure 4.9: Axial concentration profile of the mixture CE376-SS170 at varying velocities.

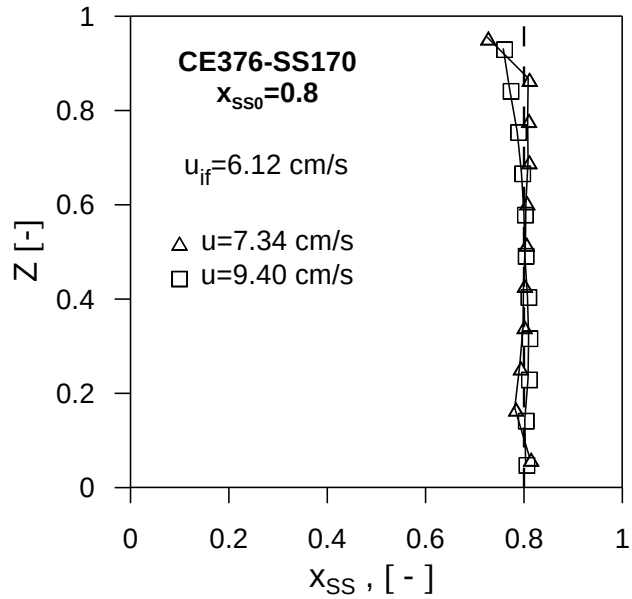

Figure 4.10: Axial concentration profile of the mixture CE376-SS170 at varying velocities.

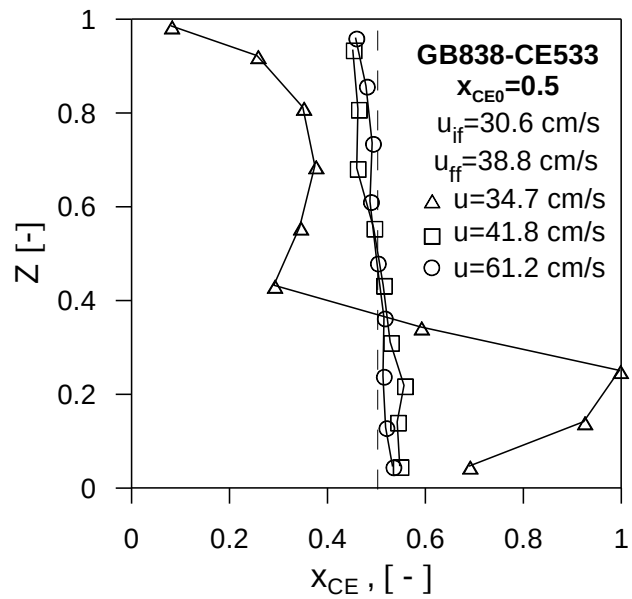

Figure 4.11: Axial concentration profile of the mixture GB838-CE533 at varying velocities.

In both mixtures just presented, the component ρd values are similar (see Figure 4.12). This bolsters the idea that the absence of interactions which is verified when the component ρd are nearly equal, represents a condition that can minimize, in certain cases, the occurrence of segregation phenomena.

Summarizing the results reveals that, at a given density ratio, the condition (4.2.14) dictates the flotsam behaviour of the bigger particles for a component size ratio d_{LB}/d_{HS} (see notation introduced in Chapter 1, L=light or less dense, B=big, H=heavy or denser, S=small) which is lower with respect to what is observed experimentally. This occurs for the system GB-MS and GB-CE, which show the inversion of roles of flotsam and jetsam at d_{LB}/d_{HS} equal to about 4 and 5 respectively, instead of 1.5 and 1.7 as calculated by eqn (4.2.14). For higher density ratio ρ_{HS}/ρ_{LB} it is likely that this inversion does not occur out of the region where percolation becomes important. Nevertheless in all cases investigated, when eqn (4.2.14) fails, the tendency of particles to mix up is greatly enhanced. It is as if the criterion based on the interaction force acts in a contrasting way with the always present propensity of the denser particles to sink, this latter effect probably explainable with arguments related to gravitational stability often invoked in the liquid-solid fluidization studies[43]. According to this interpretation, when $\rho_{LB}d_{LB} \leq \rho_{HS}d_{HS} \leq \rho_{HS}d^2_{HS}$ both factors act in the same direction and segregation is thus intensified. Another consideration arises from the fact that the particle tendency to migrate upwards or downwards can change during segregation, i. e. it may depends on concentration and operating velocities as well.

In the light of these considerations, when the diversity in size an density are contrasting the diagram of Figure 4.12 shows the likely presence of three region into which the density and size ratios domain can be divided:

I. for $\rho_{LB}d_{LB} \geq \rho_{HS}d_{HS}$ mixing is promoted. It is generally sufficient to fluidize the mixture at a velocity near u_{ff} to obtain good mixing, especially when $\rho_{LB}d_{LB}$ and $\rho_{HS}d_{HS}$ are not much different. At the time being it is not possible to know in advance which component will be flotsam.

II. for $\rho_{LB}d_{LB} \leq \rho_{HS}d_{HS} \leq \rho_{LB}d^2_{LB}$ appreciable segregation generally occurs, especially in the velocity interval in which fluidization is achieved. The condition (4.2.11) that marks the transition from region I to II seems to be a boundary where segregation phenomena are abruptly intensified. For the mixtures which belong to this region the velocity must be raised above u_{ff} in order to obtain a state of good mixing. With no exception the HSF component behaves as jetsam in this region.

III. for $\rho_{HS}d^2_{HS} \geq \rho_{LB}d_{LB}$ the segregation pattern is similar to that of Figure 3.2. In the velocity interval $u_{if} < u < u_{ff}$ the bigger component fluidizes independently at the top of the column, whereas the denser one is packed at the bottom.

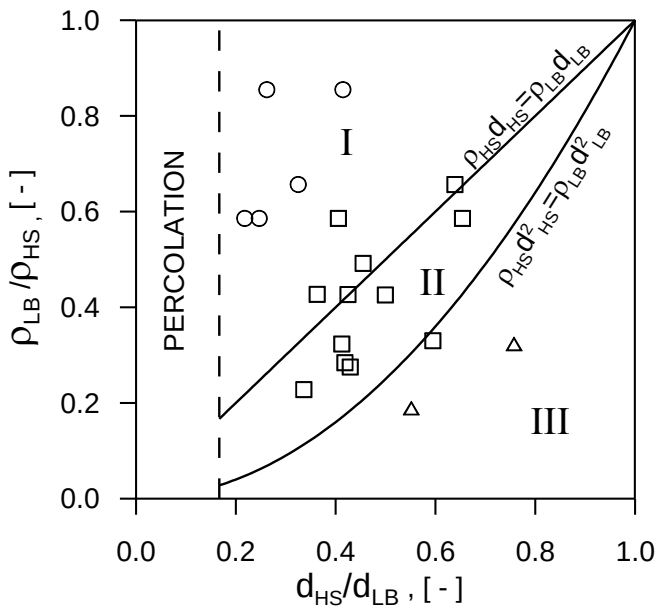

Figure 4.12: Regions in the size and density ratio domain. Circles: Jetsam=LBP; Squares: Jetsam=HSF; Triangles: Jetsam=HSP. P=packed i.e. with higher u_{mf}, F=fluid i.e. with lower u_{mf}.

In Table 4.3 all the systems investigated are again reported together with other systems studied by other authors.

Table 4.3: Density and size ratios of the binary mixtures reported in 4.10. IR=iron; PP=polypropylene; SG=silica gel; HC=hollow char.

Mixture	**Mixture Type** (Tab. 1.1)	d_{HS}/d_{LB} [-]	ρ_{LB}/ρ_{HS} [-]	**Jetsam solid**	**Ref.**
MS800-GB172	LBP-HSF	0.21	0.59	MS	This study
MS631-GB154	LBP-HSF	0.24	0.59	MS	This study*
MS800-GB322	LBP-HSF	0.59	0.4	GB	This study
GB838-CE533	LBP-HSF	0.64	0.66	CE	This study
GB838-CE270	LBP-HSF	0.32	0.66	GB	This study*
CE376-SS170	LBP-HSF	0.45	0.49	SS	This study
SS170-BR70	LBP-HSF	0.41	0.86	SS	This study*
SS170-BR70	LBP-HSF	0.26	0.86	SS	This study*
GB475-IR170	LBP-HSF	0.36	0.43	IR	34
MS800-GB521	LBP-HSF	0.65	0.59	GB	This study
GB593-SS243	LBP-HSF	0.41	0.33	SS	This study
GB570-BR254	LBP-HSF	0.43	0.28	BR	This study
SG375-GB125	LBP-HSF	0.33	0.23	GB	38
GB565-BR235	LBP-HSF	0.42	0.29	BR	44
PP275-GB116	LBP-HSF	0.42	0.43	GB	42
GB461-BR273	LBP-HSF	0.59	0.33	BR	8
HC775-GB385	LBP-HSF	0.50	0.43	GB	13
MS800-SS439	LBF-HSP	0.55	0.19	SS	This study
GB322-SS243	LBF-HSP	0.75	0.33	SS	This study

** visual observation of the mixture's behavior.*

4.4 THE FINAL FLUIDIZATION VELOCITY WHEN THE FLUID COMPONENT IS JETSAM

4.4.1 THE REVISED PARAMETRIC MODEL FOR U_{FF}

When the bed is loaded in the column as an homogeneous arrangement, the initial fluidization velocity can be calculated by eqn (3.1.1) in any case. As for the condition of complete fluidization, it is necessary to know a priori what role each component will assume, i.e. jetsam or flotsam.

In section 4.3 it has been shown as it is theoretically possible that initially the component with higher u_{mf} migrate to the upper portion of the bed forming a fixed bed. Another layer underneath prevents it to fall down, exerting a net force upwards, whereas the other component fluidizes undisturbed near the distributor. If it is assumed that the middle layer is approximately made of jetsam and flotsam in the same proportions as in the initial homogeneous bed, the phenomenology can be sketched as in Fig. 4.11. Following this scheme it is possible to demonstrate that, while the equation for u_{if} remains the same, that for u_{ff} is still obtained by eqn (3.1.6) after permutation of the suffixes '*j*' and '*f*':

$$u_{ff} = \frac{\left[\left(\rho_j - \rho_g\right)\left(1 - x_{f0}\right)h_m + \left(\rho_f - \rho_g\right)x_{f0}h_0\right]g}{180\mu_g\left[\frac{\left(1-\varepsilon_{mf,m}\right)}{\left(\varepsilon_{mf,m}^3 d_{av}^2\right)}h_m + \frac{\left(1-\varepsilon_{mf,f}\right)}{\left(\varepsilon_{mf,f}^3 d_f^2\right)}\left(h_0 - h_m\right)x_{f0}\right]} \tag{4.4.1}$$

At the same time the correlation (3.1.9) becomes:

$$\frac{h_m}{h_0} = k\frac{\left(1-\varepsilon_{mf,m}\right)}{\left(1-\varepsilon_{mf,f}\right)}\frac{\varepsilon_{mf,f}^3}{\varepsilon_{mf,m}^3}\sqrt{x_f\left(1-x_f\right)} \tag{4.4.2}$$

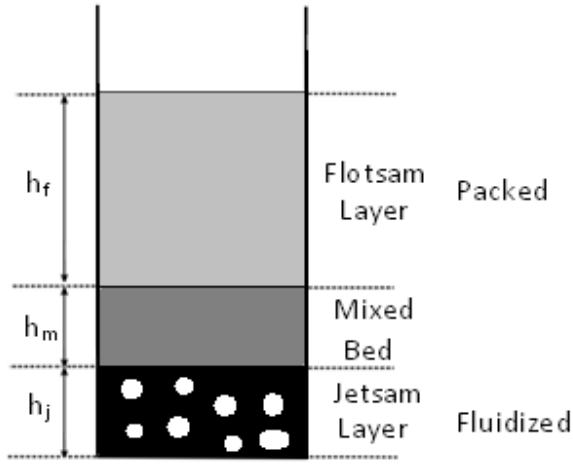

Fig. 4.11: Segregation mechanism in the fluidization process of two-solid beds where the flotsam is the packed component.

For the case $\rho_{LB}d_{LB} \leq \rho_{HS}d_{HS} \leq \rho_{LB}d^2_{LB}$ it has been shown that in all the cases examined in the present study, as well as in the published works found in literature, the heavy and smaller component behaves as jetsam and the bed follows a phenomenology similar to that sketched in Fig. 4.11. Thus for this type of mixture the validation of eqns (4.4.1) and (4.4.2) is addressed in the next section.

4.4.2 VALIDATION

In Table 4.1 the properties of binary mixtures studied are presented. The fluidization behavior of three mixtures has been studied, namely GB593-BR254, GB618-SS243 and MS800-GB521. In reporting the system acronyms the convention to indicate as first species that with higher u_{mf} has been followed.

Figures 4.12-4.16 show the dependence of the fluidization velocities and voidage with composition for all the systems studied. The model curves have been generated using eqn (3.3.1) for the u_{if} and eqns (4.4.1) and (4.4.2) for the u_{ff}.

The values of k introduced in eqn (4.4.2) are again that producing the best fitting of the experimental points and allow comparing the segregation tendency of these systems, with a greater k for systems which lower component ρd difference as shown in Table 4.4. Though the adequacy of the variable $\Delta\rho d$ for carrying out comparisons has no general validity, it is possible here because all the three systems belong to the same region of Figure 4.12, that is these mixtures all exhibit the same fluidization phenomenology.

Even if the phenomenology is quite different from the previous systems and in spite of evident simplifications, the agreement between experimental data and model prediction is sufficiently good.

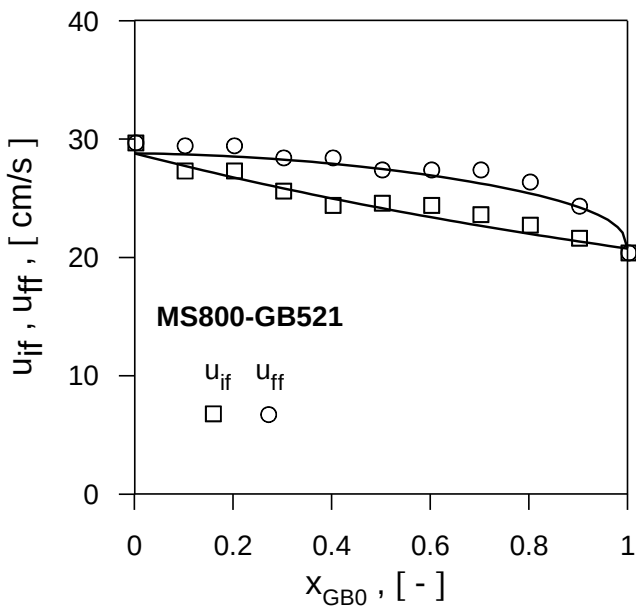

Figure 4.12- Fluidization velocity diagram of the mixture MS800-GB521.

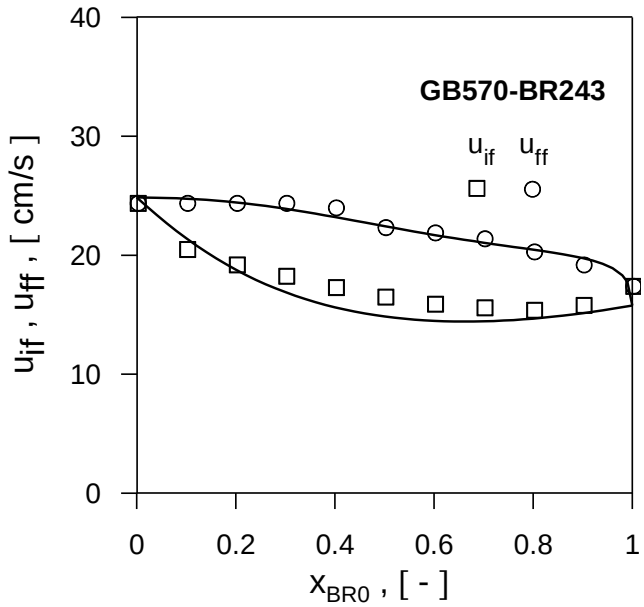

Figure 4.13: Fluidization velocity diagram of the mixture GB570-BR243.

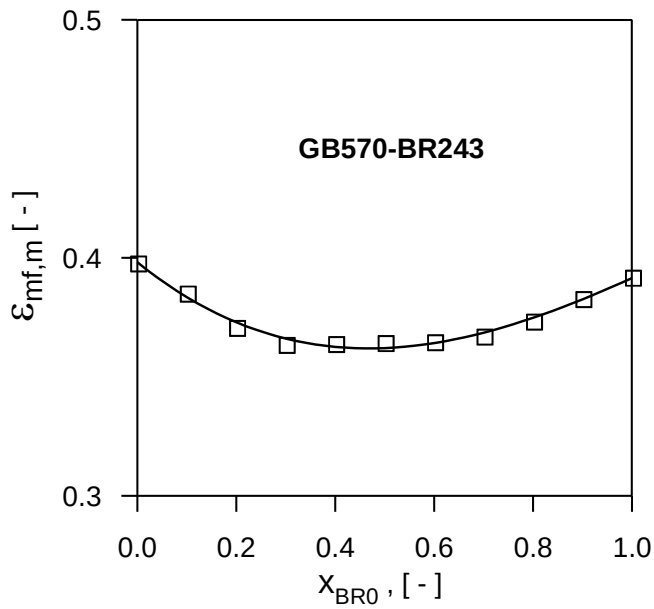

Figure 4.14: Voidage of the homogeneous mixture GB570-BR243 at varying composition.

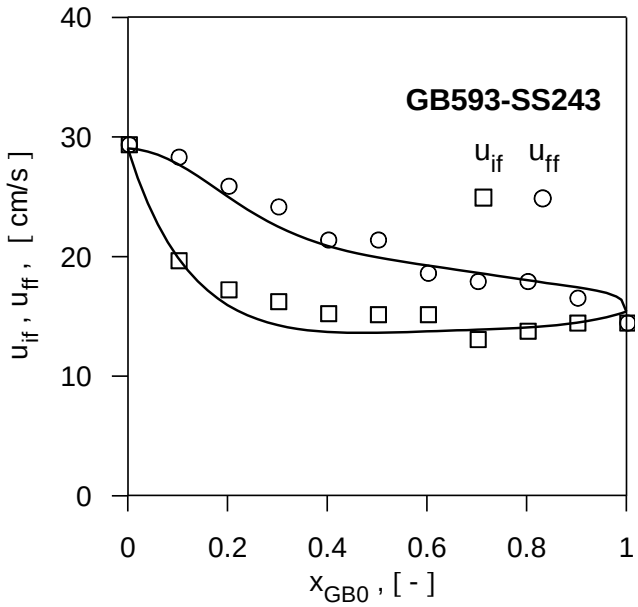

Figure 4.15- Fluidization velocity diagram of the mixture GB593-SS243.

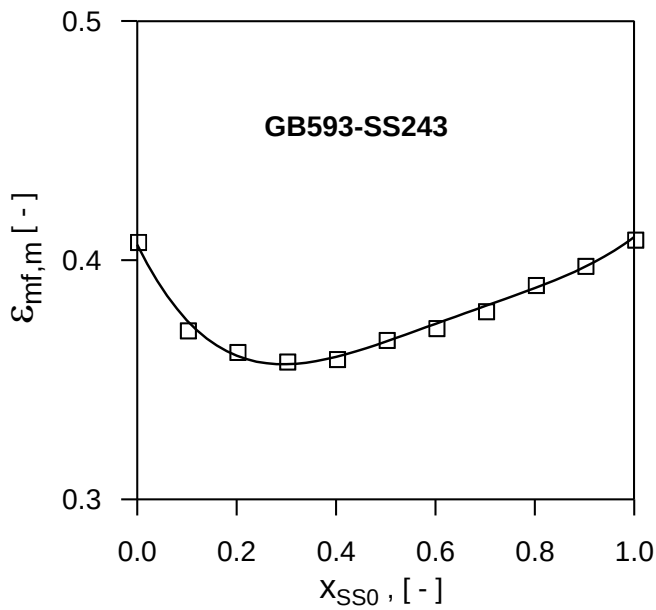

Figure 4.16: Voidage of the homogeneous mixture GB593-SS243 at varying composition.

Table 4.4: Dependence of *k* on the component ρd difference.

Mixture	ε_{mf} [-]	$\Delta\rho d$ [g·μm/cm^3]	k [-]
MS800-GB521	0.398	124	0.22
GB593-SS243	Fig. 4.16	376	0.19
GB570-BR243	Fig. 4.14	739	0.055

Although not yet fully predictive, the theoretical analysis proposed in the present investigation proves capable to give errors of prediction of the u_{ff} that do not exceed 10%, as shown in Fig. 4.17, even when complex systems are studied, such as those which exhibit the fluidization pattern of Fig. 4.11.

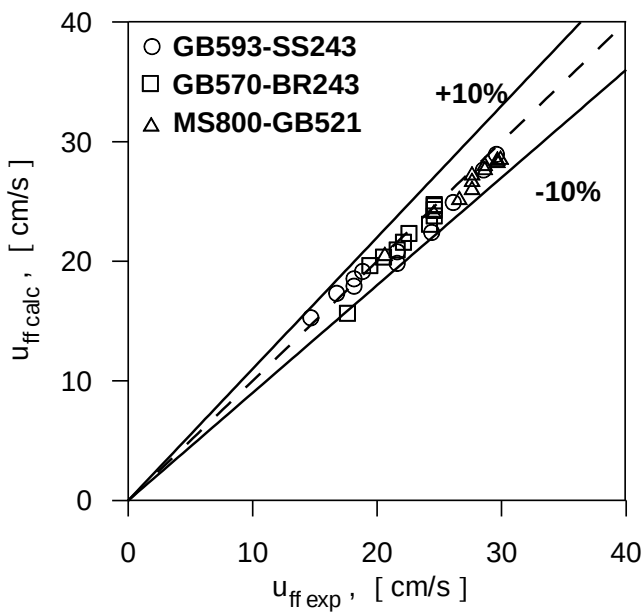

Figure 4.17: Comparison between experimental and calculated values of u_{ff}.

4.5 CONCLUDING REMARKS

In this chapter the complex mechanism of fluidization of mixture of heavy smaller and light bigger particles has been addressed. It has been shown as the solid-solid interactions play an important role in determining the segregation pattern and in assigning the relative role of jetsam and flotsam of different species. The presence of this interaction provides a theoretical explanation of the fact that the two characteristic velocities are always observed to be included between the single component fluidization velocities. Furthermore a criterion has been proposed which, even if unable to predict when the bigger particles behave as flotsam, marks the boundary between a region where segregation occurs to an appreciably extent and a domain of density and size ratios where the mixing tendency of the bed is strongly enhanced, so allowing properly modifying the size of a denser component in order to homogenize, by fluidization, its mixtures with lighter solids.

Finally the three-layer parametric model for the final fluidization velocity has been successfully extended to systems for which the bigger solid has a higher value of the product ρd with respect to the other component. This is accomplished with error levels that are comparable with those relevant to the less complex systems of Chapter 3.

This allows concluding that the analysis based on the fluidization velocity interval is a powerful means for analyzing the behavior of all systems, providing a unified theoretical framework of the segregating fluidization of dissimilar solids.

Chapter 5

PHASE EQUILIBRIUM ANALOGY

As the analysis of the literature presented in Chapter 1 has revealed, many authors have highlighted the similarity of behavior between a liquid and a fluidized bed and at the same time, between the velocity and the phase diagram. This same analogy is developed in Section 1 of this Chapter, showing that the concentration profiles, obtained by slowly defluidizing a fully fluidized bed down to the fixed bed conditions, can be calculated by means of a simple equilibrium relationship that resembles that used in the phase transition of the simplest liquid-vapor equilibrium, that assuming constant relative volatility. In Section 2 it is shown as concentration profiles similar to those calculated using the thermodynamic analogy can be obtained by maximizing a functional that includes the two contrasting particle tendencies for mixing and segregation. The definition of such a functional, even if introduced in a way that may appear quite arbitrary, allows calculating final fluidization curves similar to those experimentally obtained. This latter point is addressed in Section 5.3.

5.1 DEFLUIDIZATION AND PHASE EQUILIBRIUM ANALOGY

5.1.1 CONCENTRATION PROFILE OF A DEFLUIDIZED BED

At progressively decreasing gas flow rate, after the transition from the fully fluidized regime back to the thoroughly packed state, the x_f profile has been measured in the particulate mass with the technique illustrated in section 4.3, that is by vacuuming horizontal layer of particles that are then separated in the individual components. When the two solids were different only in density, not being possible to accomplish the separation by sieving, the solids in each layer were again subjected to fluidization in an auxiliary column of smaller diameter, 3.5 cm ID, which enhanced the segregation by density.

The decrease of gas velocity is accompanied by the progressive defluidization of the coarse (or heavier) component, which sinks together with a certain amount of smaller (or lighter) one; that causes the gradual reduction of the fluidized region of the bed, which becomes increasingly richer in the fine component. As the gas velocity is gradually reduced, a defluidization front travels from the bottom to the top of the column and the fixed bed builds up at the column base by a mechanism of addition of defluidized layers richer and richer in fines; in this way an increasingly larger portion of the bed composition profile assumes the ultimate aspect of the x_f versus z curves of the fixed bed. Such a mechanism is consistent with the reverse one observed during the opposite process of fluidization, whose front starts from the top and travels downwards, up to the deepest region of the particle assembly.

When gradually and slowly defluidized from a condition of full fluidization, any mixture gives place to a fixed bed having a repeatable and characteristic axial composition profile, as a result of the spontaneous tendency of particles to assume a peculiar equilibrium configuration.

5.1.2 PHASE EQUILIBRIUM ANALOGY

The expression used to calculate the final fluidization velocity for a two-density bed, namely eqn (4.2.9), can be rearranged in the form:

$$u_{ff} = u_{mf,f}\frac{h_{m,ff}x_{f0}}{h_{m,ff}x_{f0} + h_0\left(1-x_{f0}\right)} + u_{mf,j}\frac{h_0\left(1-x_{f0}\right)}{h_{m,ff}x_{f0} + h_0\left(1-x_{f0}\right)} \tag{5.1.1}$$

Thus u_{ff} is still an average of the component fluidization velocities even if not longer weighted with the total solid volume fractions. However, the volume fraction of flotsam in the system obtained combining the bottom layers h_m and h_j (see Figure 5.1) is:

$$x_{fb} = \frac{h_{m,ff}x_{f0}}{h_{m,ff}x_{f0} + h_0\left(1-x_{f0}\right)} \tag{5.1.2}$$

Inspection of eqns (5.1.1) and (5.1.2) reveals that the final fluidization velocity turns out to be equivalent to the initial fluidization velocity evaluated at x_{fb}:

$$u_{ff} = u_{mf,f}x_{fb} + u_{mf,j}\left(1-x_{fb}\right) \tag{5.1.3}$$

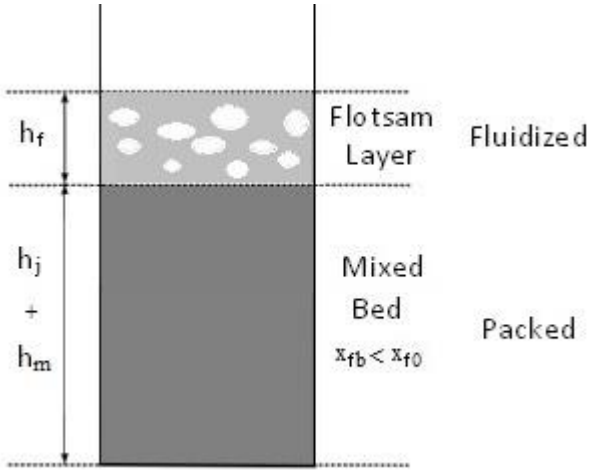

Figure 5.1: Two-layer simplified scheme.

This composition can be determined directly from a graph of the fluidization velocity versus the flotsam volume fraction, as shown in Figure 5.2. The complement to one of this composition is directly the final fluidization velocity, if normalized in the following way:

$$\frac{u_{ff} - u_{mf,f}}{u_{mf,j} - u_{mf,f}} = 1 - x_{fb} \tag{5.1.4}$$

Whereas the following relation holds for the initial fluidization velocity:

$$\frac{u_{ff} - u_{mf,f}}{u_{mf,j} - u_{mf,f}} = 1 - x_{f0} \tag{5.1.5}$$

This way of normalizing velocities for two-density beds is very useful, also in order to obtain directly and easily from the diagram the value of the parameter *k* used to correlate data, for example by the relationship:

$$k = 1 - \frac{1}{2}\left(\frac{u_{ff} - u_{mf,f}}{u_{mf,j} - u_{mf,f}} \right)_{xf\,0=0.5} \tag{5.1.6}$$

Eqn (5.1.3) allows making some considerations on the analogy of the fluidized systems and phase equilibrium relationships. In fact, similarly to the liquid-vapor transition, x_{fb} represents the composition of the ultimate layer which is brought into the fluidized state if the velocity is raised from zero to the final fluidization value, as shown in Figure 5.2. Giving the invariance of u_{ff} with the initial state of mixing of the two solids[35], when the bed is previously fluidized at high velocity and the flow rate is then decreased, it is also likely that this composition turns out to be that of the first layer which becomes packed. This is equivalent to state that at u_{ff} the bed chooses an internal component distribution which is independent on the previous stages of segregation.

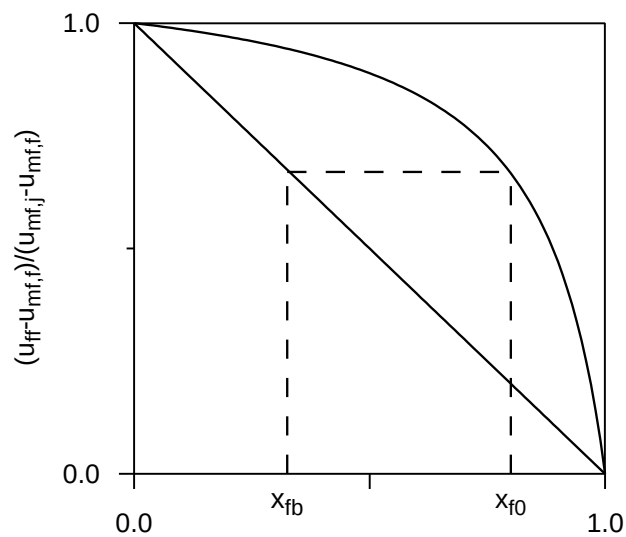

Figure 5.2: Graphical determination of the composition of the lowest layer at u_{ff}.

Thus, providing that the axial concentration profile is an increasing monotone function with respect to the volume fraction of the lighter component, the value of the final fluidization velocity is the same for all the bed having the same flotsam concentration at the bottom of the column, i. e. x_{fb}. For predicting $u_{ff,}$ it would be hence necessary to relate this latter concentration to the average composition x_{f0}. In this regard the functional form of eqn (5.1.3) seems to suggest an equilibrium relationship between these two variables that can be expressed in the following form after the substitution $\alpha=h_0/h_{m,ff}$:

$$x_{f0} = \frac{\alpha \cdot x_{fb}}{\alpha \cdot x_{fb} + \left(1 - x_{fb}\right)} \tag{5.1.7}$$

In (5.1.7) x_{f0} now represents the concentration of the fluidized portion of the bed while an infinitesimal layer near the distributor of composition x_{fb} is still in the packed state. In the light of these considerations, $h_0/h_{m,ff}$ assumes the same role that the relative volatility plays in phase equilibria.

For a two-size mixture the correspondence between u_{if} evaluated at x_{fb} and u_{ff} calculated at the overall concentration x_{f0} for two-size system is valid with good approximation if $d_j/d_f \leq 3$, whereas for higher size ratio this correspondence becomes less strict. In figure 5.3 it has been carried out the comparison between x_{fb} determined directly from the fluidization velocity diagram and the value obtained by eqn (5.1.2), in turn determined by the value $h_{m,ff}$ calculated by means of eqn (3.1.9).

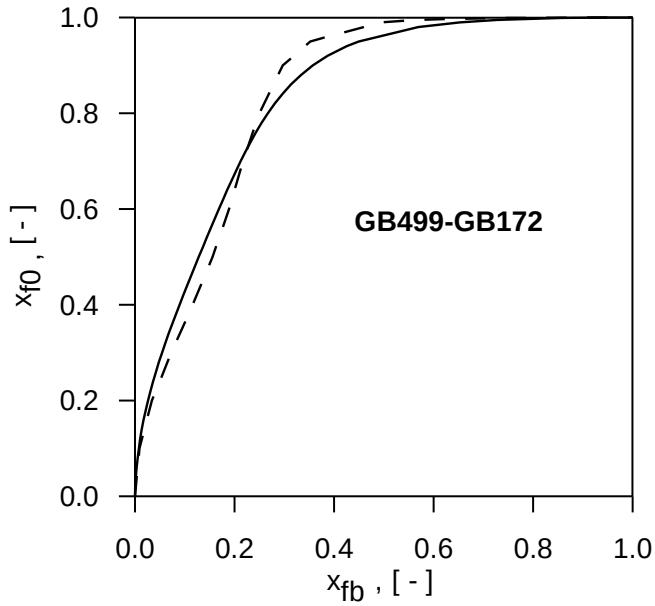

Figure 5.3: Relationship between the total flotsam concentration x_{f0} and the ultimate layer composition x_{fb}. Solid line-x_{fb} evaluated by eqn (5.12). Dashed-evaluated directly from the velocity diagram.

5.1.3 A PRELIMINARY MODEL FOR THE CONCENTRATION PROFILES OF A DEFLUIDIZED BED

Eqn (5.1.6) suggests that a simple equilibrium relationship may link the fluidized and packed portions of the bed when both "phases" contemporary exist. We have verified this statement by measuring the concentration profiles obtained by very slowly defluidizing the bed, previously fluidized well beyond its final fluidization velocity, down to the fixed state. The concentration profile of such a defluidized bed is very repeatable and has the feature to be independent on the state of mixing of the two solids when loaded into the column. Furthermore it provides information about the tendency of particles to assume a distribution along the bed which is the result of their spontaneous dynamics.

When both a packed and fluidized region are present and the defluidization has reached the axial distance z from the distributor, the flotsam fraction of the above fluidized portion is:

$$\overline{y_f} = \frac{\int_z^H \left(1-\varepsilon_{mf}\right) x_f \, dz}{\int_z^H \left(1-\varepsilon_{mf}\right) dz} \tag{5.1.8}$$

where H is the total bed height. The average flotsam fraction $\bar{y}_f$ can be now linked to the concentration x_f of the thin layer which sediments after a little diminution of the gas flow rate. The way how to relate these two variables is suggested by eqn (5.1.7):

$$\overline{y_f} = \frac{\alpha \cdot x_f}{\alpha \cdot x_f + \left(1-x_f\right)} \tag{5.1.9}$$

By using eqns (5.1.8) and (5.1.9) it would be possible to calculate the axial profile of x_f. In order to obtain an analytical solution, a material balance can be written on the scheme of Figure 5.4. With the assumption of constant voidage, the total height of the bed remains constant, i.e. $H=h_0$. When the layer dz becomes packed the amount of solids included in this stratum is transferred to the lower part of the bed. The balance on the flotsam component is:

$$x_f \, dz = -d\left[\left(h_0 - z\right) \cdot \overline{y_f}\right] = -\left(h_0 - z\right) d\overline{y_f} + \overline{y_f} \, dz \tag{5.1.10}$$

Dividing all terms of eqn (5.1.10) for dz gives:

$$x_f = -\left(h_0 - z\right) \frac{d\overline{y_f}}{dz} + \overline{y_f} \tag{5.1.11}$$

which is a first order linear differential equation. Introducing the dimensionless height Z= z/h_0 and considering that:

$$\frac{d\overline{y_f}}{dZ} = \frac{dx_f}{dZ}\frac{d\overline{y_f}}{dx_f} \tag{5.1.12}$$

eqn (5.1.11) can be expressed in the form:

$$\frac{dx_f}{dZ} = \frac{1}{(1-Z)}\frac{\overline{y_f} - x_f}{d\overline{y_f}/dx_f} \tag{5.1.13}$$

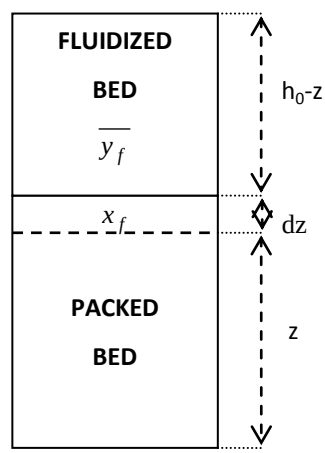

Figure 5.4: Sketch of the defluidization process.

Integration of eqn (5.1.13) gives the concentration profile along the column if a proper equilibrium relationship is provided. Introducing eqn (5.1.9) in eqn (5.1.13) yields:

$$\frac{dx_f}{dZ} = \frac{1}{(1-Z)} \frac{(\alpha-1)}{\alpha} x_f (1-x_f)\left[\alpha x_f + (1-x_f)\right] \tag{5.1.14}$$

With the further assumption of constant α , eqn (5.1.14) can be integrated with the condition $x_f=x_{fb}$ for z=0, obtaining the notable simple result:

$$Z = 1 - \frac{\Pi(x_{fb})}{\Pi(x_f)} \tag{5.1.15}$$

where

$$\Pi(x_f) = \left(\frac{\alpha x_f + 1 - x_f}{1-x_f}\right)^{-1} \left(\frac{1-x_f}{x_f}\right)^{-\frac{\alpha}{\alpha-1}} \tag{5.1.16}$$

Thus the knowledge of x_{fb} allows calculating the concentration profile along the bed using eqn (5.1.15). To obtain an estimate of this starting concentration it is possible to apply eqn (5.1.2), using the parametric correlation for $h_{m,ff}$ proposed in Chapter 3 and evaluating α as $h_0/h_{m,ff}$. In this case from the knowledge of the final fluidization velocity that of the component distribution in the defluidized bed also descend.

In Figure 5.5 some experimental profiles of the system CE605-GB593, at varying total flotsam concentration, are reported together with the relevant model curves obtained from eqn (5.1.15). The same comparison is carried out in Figure 5.6 for the system GB499-GB172. Even if the quantitative agreement is not excellent, this simple model is capable to reproduce the general trend of the component composition profiles, showing the typical change in concavity when the flotsam fraction is increased from low to high values. Note also that the trend of experimental data is similar for density and size segregating systems.

While confirming the potentiality of the approach followed, these preliminary results encourage the effort of addressing segregating phenomena occurring in multi solid systems in the light of the analogy with thermodynamics.

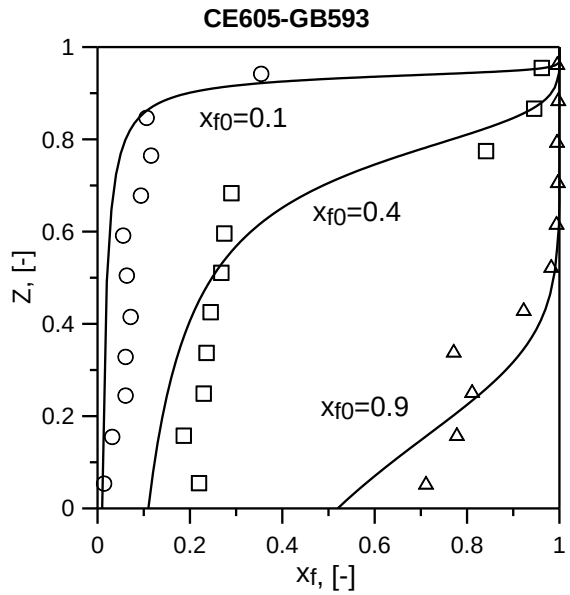

Figure 5.5 - Concentration profiles of the fixed bed at varying flotsam concentration after slow defluidization. CE605-GB593.

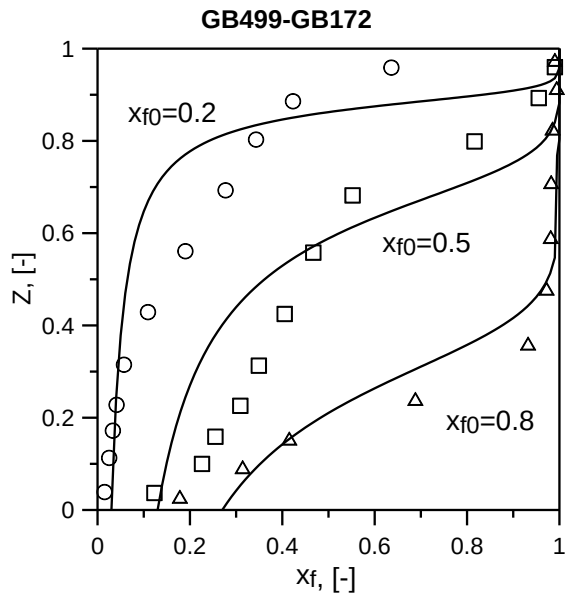

Figure 5.6 - Concentration profiles of the fixed bed at varying flotsam concentration after slow defluidization. GB499-GB172.

Without the assumption of constant voidage, it is possible to differentiate eqn (5.1.8) with respect to *z* obtaining:

$$\frac{d\overline{y_f}}{dz}\int_z^H \left(1-\varepsilon_{mf}\right)dz - y_f\left(1-\varepsilon_{mf}\right) = -x_f\left(1-\varepsilon_{mf}\right) \tag{5.1.17}$$

Since *H* should be found iteratively, eqn (5.1.17) is easier to integrate after the substitution:

$$\int_z^H \left(1-\varepsilon_{mf}\right)dz = \left(1-\varepsilon_{mf,m}\right)h_0 - \int_0^z \left(1-\varepsilon_{mf}\right)dz \tag{5.1.18}$$

Eventually, recalling the eqn (5.1.9), eqn (5.1.17) becomes:

$$\frac{dx_f}{dz} = \frac{\left(1-\varepsilon_{mf}\right)}{\left(1-\varepsilon_{mf,m}\right)h_0 - \int_0^z \left(1-\varepsilon_{mf}\right)dz}\,\frac{(\alpha-1)}{\alpha}\,x_f\left(1-x_f\right)\left[\alpha x_f + \left(1-x_f\right)\right] \tag{5.1.19}$$

Integration of eqn (5.1.19) ends when eqn (5.1.18) is satisfied. In order to analyze the effect of voidage we can assume that the dependence of ε_{mf} on x_f is not different fromt the $\varepsilon_{mf,m}$ vs $x_{f,0}$ curve in the packed state (not necessary a good assumption). For the system GB499-GB172 it is thus possible to draw values of ε_{mf} from Figure 3.15 and substitute them in eqns (5.1.18) and (5.1.19). The concentration profiles obtained with the assumption of constant voidage and those calculated by means of eqn (5.1.19) and Figure 3.15 are compared in Figure 5.7. The assumption of constant voidage leads in this case to negligible errors, except perhaps for x_{f0}=0.2. The greater simplicity of eqn (5.1.13) however makes it preferable.

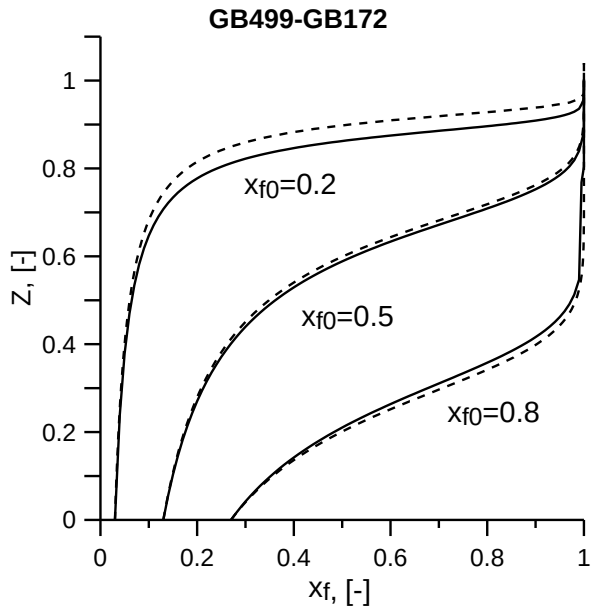

Figure 5.7 - Concentration profiles of the fixed bed at varying flotsam concentration after slow defluidization. Solid line-eqn (5.1.13), Dashed line- eqn (5.1.17) .

5.2 THE MIXING/SEGREGATION EQUILIBRIUM THROUGH THE MAXIMIZATION OF A FUNCTIONAL

Consider the variational problem of finding the maximum scalar value of the functional *F* defined as:

$$F = \int_0^1 x_f Z dZ + \int_0^1 x_f \left(1 - x_f\right)\left(1 - Z\right) dZ \tag{5.2.1}$$

with the mass balance constraint:

$$\int_0^1 x_f \, dz = x_{f0} \tag{5.2.2}$$

Eqn (5.2.1) is made up of two terms: the former is maximized when total segregation occurs, the second when the bed is homogeneous, enhancing the tendency to mix up especially near the distributor. After the maximization procedure, a compromise between this two tendencies will be established accordingly to a mixing-segregation equilibrium.

In order to obtain an analytical solution, x_f must be continuous in its derivative. However, as shown in Figure 5.5, a layer exclusively made up of the flotsam component may establish at the top of the column. In this case the derivative of x_f may be discontinuous at a certain Z value, called here Z^*. Consider then the following modified problem of maximizing F:

$$F = \int_0^{Z^*} \left[x_f Z + x_f \left(1 - x_f\right)\left(1 - Z\right) \right] dZ \tag{5.2.3}$$

and, since only flotsam is present for $Z^* < Z < 1$, with the flotsam mass balance for the remaining bed of height Z^* as a constraint:

$$\int_0^{Z^*} x_f \, dz = x_{f0} - \left(1 - Z^*\right) \tag{5.2.4}$$

When F is at its maximum value the Euler-Lagrange equation applies:

$$\frac{\partial \left[x_f Z + x_f \left(1 - x_f\right)\left(1 - Z\right) + \lambda x_f \right]}{\partial x_f} = 0 \tag{5.2.5}$$

where λ is a Langrange multiplier. Carryout the partial derivative and solving for x_f provides:

$$x_f = \frac{1+\lambda}{2(1-Z)} = \frac{\lambda'}{1-Z} \tag{5.2.6}$$

Since at Z^* =1 x_f=1 and Z=0 x_f=x_{fb} λ' turns out to be:

$$\lambda' = 1 - Z^* = x_{fb} \tag{5.2.7}$$

Substituting eqn (5.2.7) in eqn (5.2.4) yields:

$$x_{f0} - (1-Z^*)\left[1 - ln(1-Z^*)\right] = x_{f0} - x_{fb}\left[1 - ln(x_{fb})\right] = 0 \tag{5.2.8}$$

From eqn (5.2.8) it is possible to calculate Z*, which depends only on the overall composition x_{f0}. This justifies the fact of having neglected in the maximization the portion of the bed included in Z*<Z≤1, because its contribution to the functional F is constant at a given x_{f0}.

Introducing eqn (5.2.7) into eqn (5.2.6) and solving for Z, provides:

$$Z = 1 - \frac{x_{fb}}{x_f} \qquad \text{for } 0<Z\leq Z^* \tag{5.2.9}$$

Note the similarity of eqn (5.2.9) with eqn (5.1.15), the former being much simpler.

At this point it is possible to evaluate if an equilibrium relationship exists between $\bar{y}$ and x_f. From eqn (5.1.7):

$$\overline{y_f} = \frac{(1-Z^*) + \int_Z^{Z^*} x_f \, dz}{1-Z} = \frac{1-Z^*}{1-Z} + \frac{1-Z^*}{1-Z} ln \frac{1-Z^*}{1-Z} = x_f \left(1 - ln\, x_f\right) \tag{5.2.10}$$

Eqn (5.2.10) relates only $\bar{y}$ and x_f and does not depend explicitly on Z. It is actually an equilibrium relationship between the concentration of the fluidized phase and that of the packed one: the similarity with the distribution law when the relative volatility is constant is highlighted in Figure 5.8.

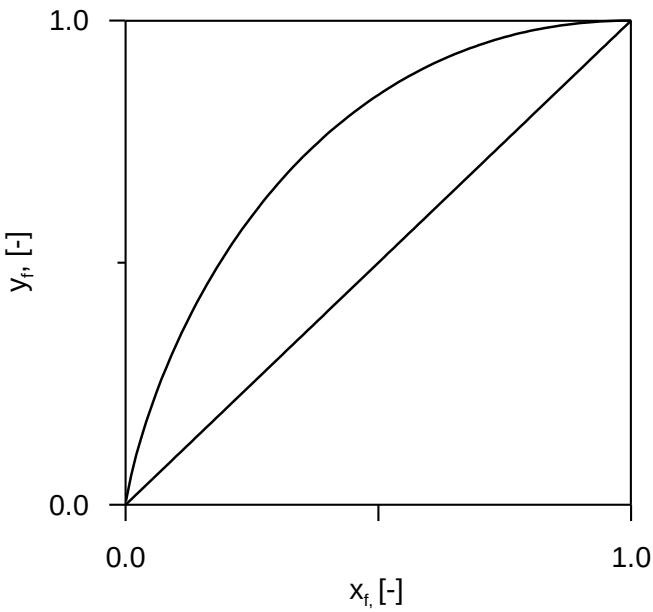

Figure 5.8 -Equilibrium relationship (5.2.10) deriving from the maximization of the functional (5.2.3).

In Figures 5.9 a comparison is made between experimental data and the model curves calculated through the maximization of eqn (5.2.3). For the bed CE605-GB593, the agreement is similar to that illustrated in Figure 5.5.

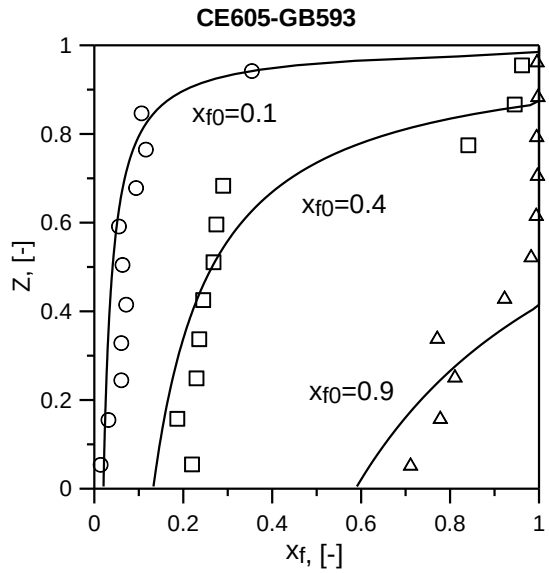

Figure 5.9 - Concentration profiles of the fixed bed after slow defluidization through the maximization of eqn (5.2.3). Mixture CE605-GB593.

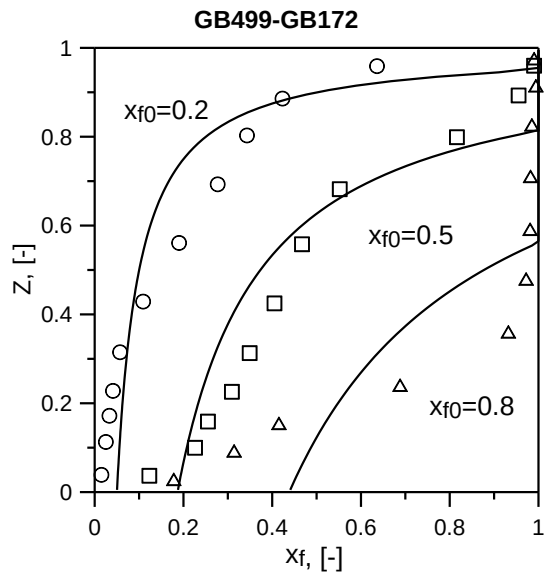

Figure 5.10 - Concentration profiles of the fixed bed after slow defluidization through the maximization of eqn (5.2.3). Mixture GB499-GB172.

The same comparison is reported In figure 5.10 for the system GB499-GB172, showing also in this case a good agreement, except at x_{f0}=0.8 where the fitting is qualitatively worse; however this is probably due to the fact that we have looked for a solution with less regularity.

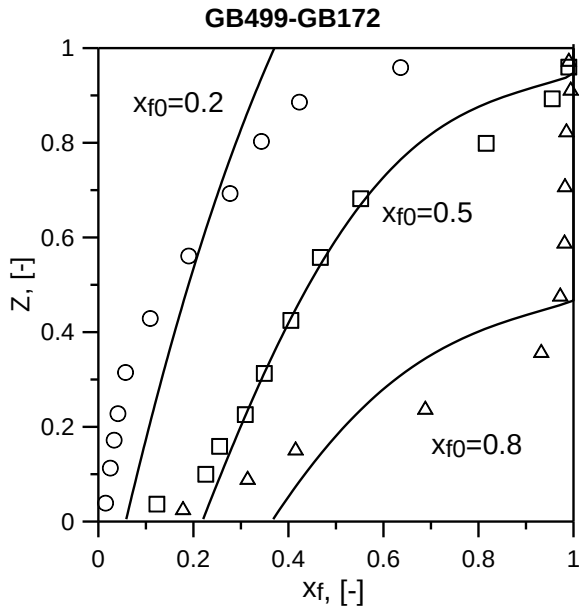

Figure 5.11 - Concentration profiles of the fixed bed at varying flotsam concentration after slow defluidization. GB499-GB172.

For the same system, concentration profiles have been calculated through the maximization of a different functional:

$$F = \int_0^1 \left(\rho_R \frac{d_{av}}{d_j} - \frac{d_{av}}{d_f} \right) \left[\left(1 - x_f^2\right) Z - \left(1 - x_f\right) x_f \right] dZ \qquad (5.2.11)$$

In it ρ_R is the density ratio ρ_f/ρ_j. The result of this procedure is illustrated in figure 5.11. Eqn (5.2.11) has been introduced because it allows calculating velocity diagrams similar to those obtained experimentally, as it is explained in the next section. It is possible to verify that eqn (5.2.11) provides the same concentration profiles of eqn (5.2.1) when the size ratio is 1, thus still providing a unified mathematical description of the process.

5.3 THE FINAL FLUIDIZATION VELOCITY THROUGH THE MAXIMIZATION OF A FUNCTIONAL

Even if this study deals with the determination of the u_{ff} for an initially well-mixed system, other studies have recently reported that it does not depend on the fixed bed arrangement[35, 36]. Thus from the knowledge of the concentration profile of a defluidized bed u_{ff} would derive directly from the bottom layer composition. If the variation in voidage is neglected, this velocity may be calculated from the expression:

$$u_{ff} = u_{mf,f}\, x_{fb} \left(\frac{d_{av,b}}{d_f} \right)^2 + u_{mf,j} \left(1 - x_{fb}\right) \left(\frac{d_{av,b}}{d_j} \right)^2 \qquad (5.3.1)$$

where $d_{av,b}$ is the Sauter mean diameter evaluated at x_{fb}. In this section comparisons are made between experimental data and the curve obtained by maximizing eqn (5.2.11) for the two systems previously investigated. Even if the assumption of constant voidage for a two-size system may appear unjustified, it is likely that when the system is in full fluidization the dependence of voidage on composition is not that of the packed bed, being the particles relatively free to move apart in a well aerated system. The same voidage function that appears in the parametric correlation for $h_{m,ff}$ may have the role to introduce this correction, being exactly the factor by which the value of the minimum fluidization velocity varies when

the voidage changes from that of the mixture to that of the jetsam particles (approximately that of the single component). This assumption, however, must be investigated experimentally and it is likely that a voidage reduction in the dense phase will be still observed but to an attenuated extent.

The expression (5.2.11) comes out quite arbitrarily for the lack of a theory capable to reveal what this functional actually represents. It must be pointed out that it was obtained by trial, looking for an expression that allowed calculating concentration profiles (Figures 5.9 and 5.11) and velocity diagrams with a good qualitative agreement with experimental data.

Figures 5.12-5.17 are relevant to density segregating systems. Being the calculated concentration profiles, and hence dimensionless velocities (see eqns 5.1.4-5), independent on the density ratio (see eqn 5.2.1), the model curves are similar to those generated using an average value of k. When the value of the parameter that gives the best fit is much different from this average value, the agreement becomes unsatisfactory, as in Figures 5.16 and 5.17. In figures 5.18-5.23 the velocity diagrams for size-segregating systems are shown. Except for the bed GB499-GB172, the error of prediction of u_{ff} is never satisfactory, but the calculated curves are similar to those measured experimentally. It should pointed out that the predictions obtained through the maximization of eqn (5.2.11) often overestimates u_{ff}. The presence of an attenuated voidage reduction would lead to an improved fitting.

Finally in Figures 5.24-5.26 the fluidization velocities of binary beds of dissimilar solids are reported. It is interesting to note that the functional (5.2.11) is able to reproduce which of the two segregation mechanisms, by size or density difference, prevails.

These results encourage future work aimed at devising a modified version of eqn (5.2.11) capable of providing a final solution to the problem which does not use any adjustable parameter. The potentiality of this approach is high since it allows determining the relationship between fluidization and the segregation pattern. Even if this has been shown for a particular case, i.e. for the concentration profiles after slow defluidization, it is likely that the same principle based on the maximization of a functional can be applied for determining concentration profiles at different fluidization regimes.

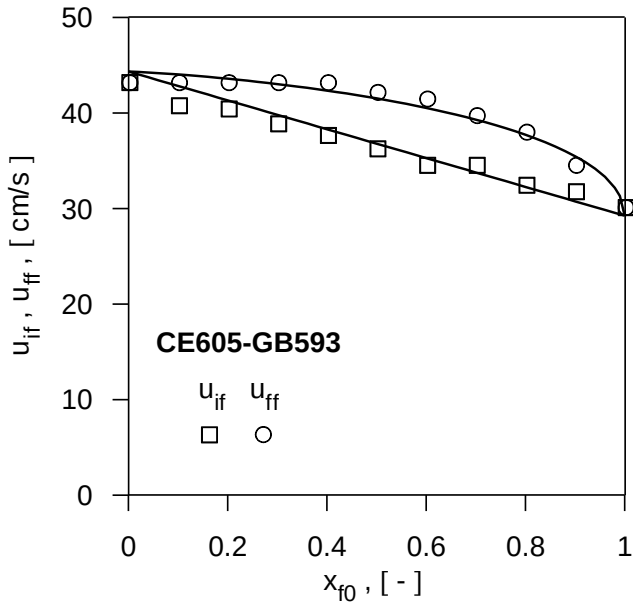

Figure 5.12 –Fluidization velocity diagram of the density segregating mixture CE605-GB593 obtained through maximization of eqn (5.2.11).

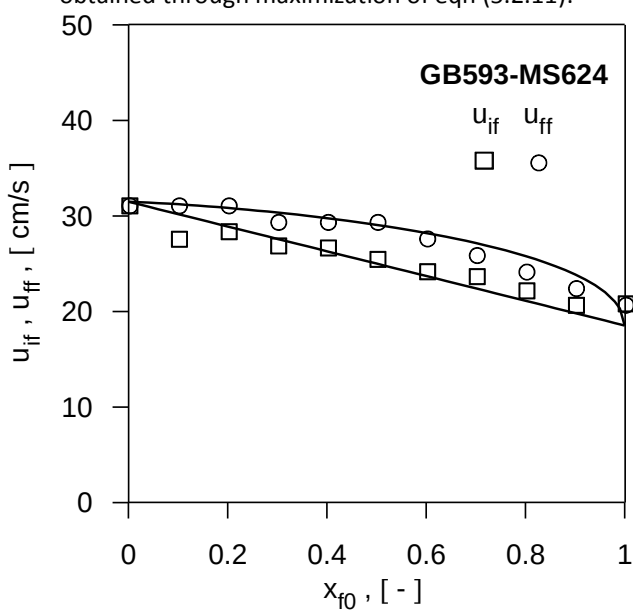

Figure 5.13 —Fluidization velocity diagram of the density segregating mixture GB593-MS624 obtained through maximization of eqn (5.2.11).

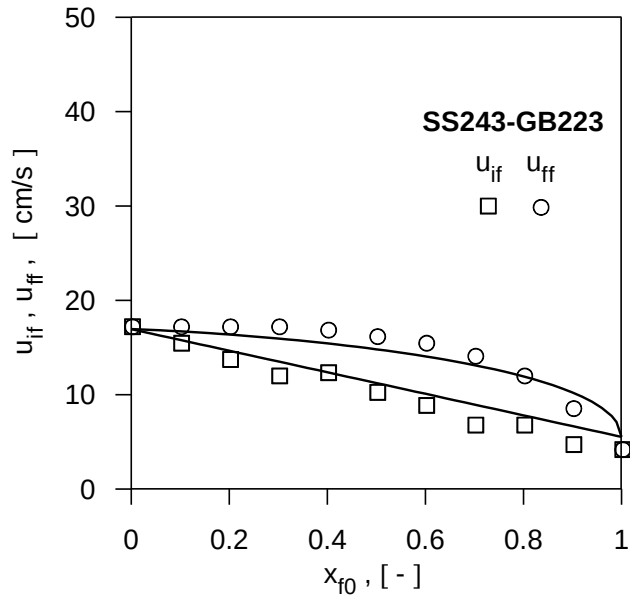

Figure 5.14 –Fluidization velocity diagram of the density segregating mixture SS243-GB223 obtained through maximization of eqn (5.2.11).

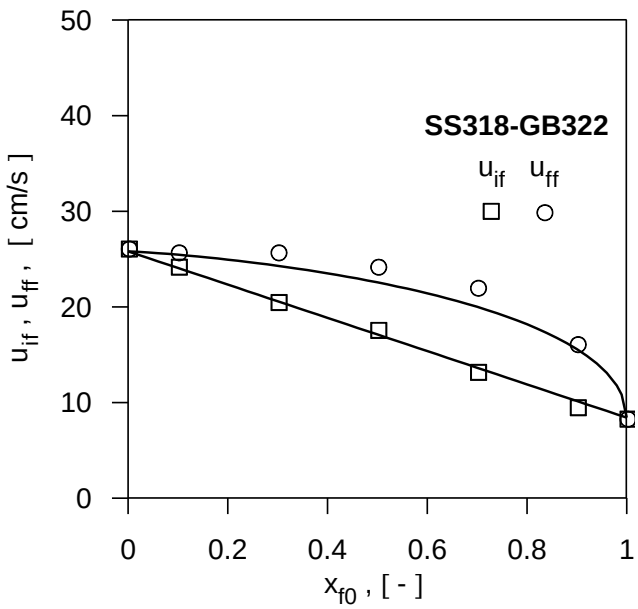

Figure 5.15 –Fluidization velocity diagram of the density segregating mixture SS318-GB322 obtained through maximization of eqn (5.2.11).

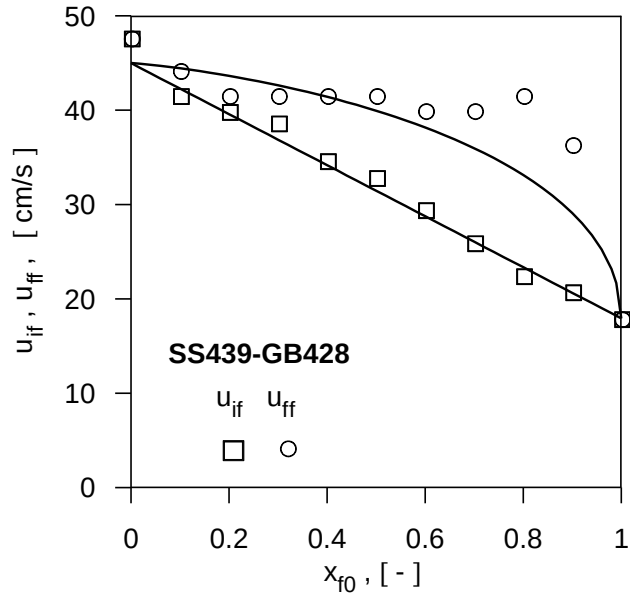

Figure 5.16 –Fluidization velocity diagram of the density segregating mixture SS439-GB428 obtained through maximization of eqn (5.2.11).

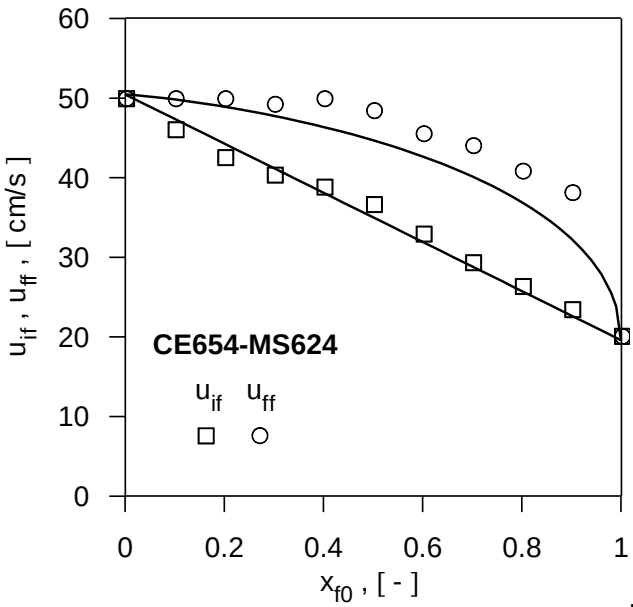

Figure 5.17 –Fluidization velocity diagram of the density segregating mixture CE654-MS624 obtained through maximization of eqn (5.2.11).

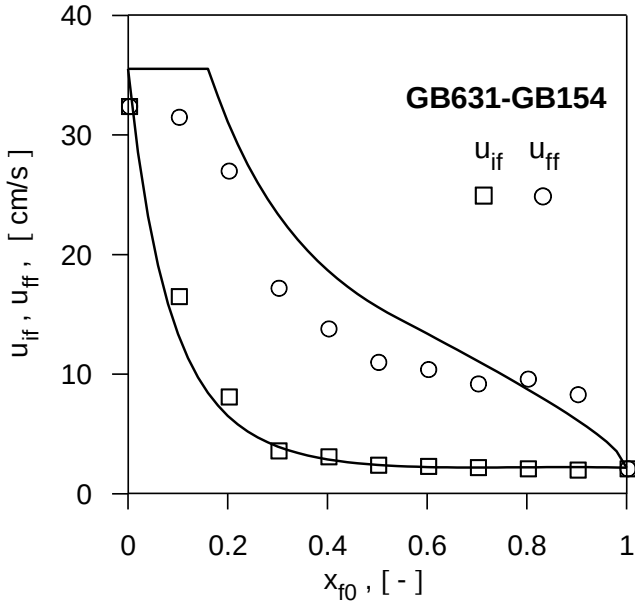

Figure 5.18 – Fluidization velocity diagram of the size segregating mixture GB631-GB154 obtained through maximization of eqn (5.2.11).

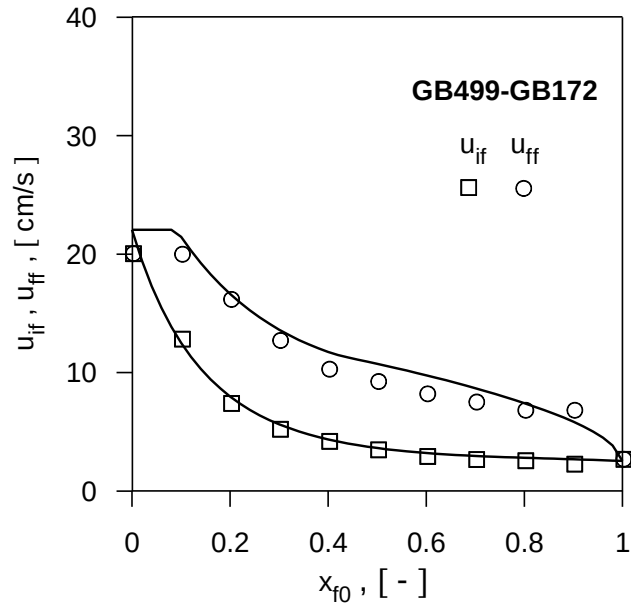

Figure 5.19 – Fluidization velocity diagram of the size segregating mixture GB499-GB172 obtained through maximization of eqn (5.2.11).

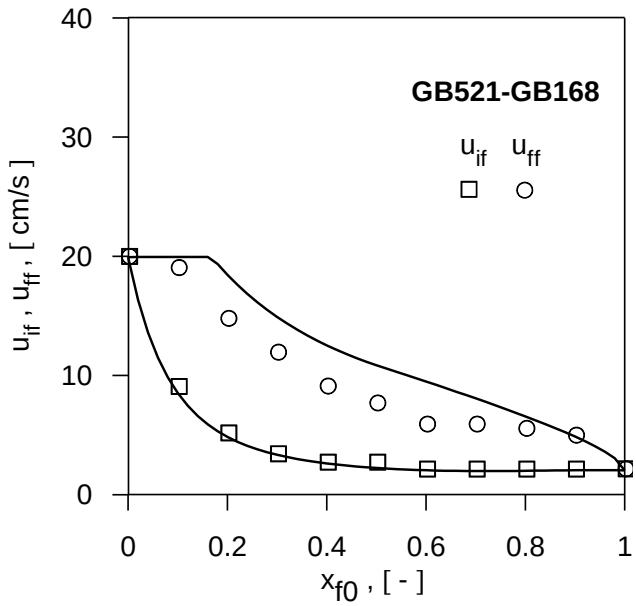

Figure 5.20 – Fluidization velocity diagram of the size segregating mixture GB521-GB168 obtained through maximization of eqn (5.2.11).

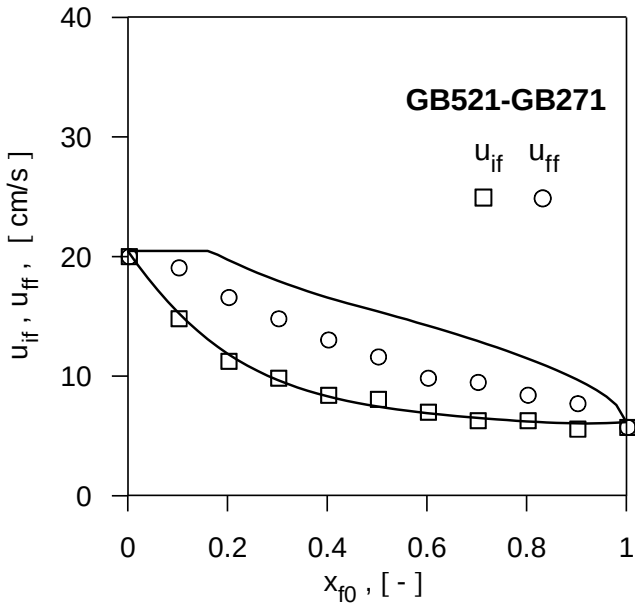

Figure 5.21 – Fluidization velocity diagram of the size segregating mixture GB521-GB271 obtained through maximization of eqn (5.2.11).

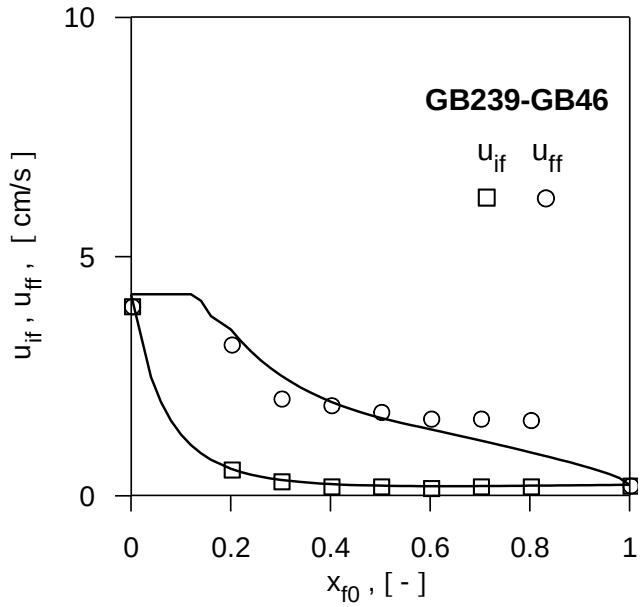

Figure 5.22– Fluidization velocity diagram of the size segregating mixture GB239-GB46 obtained through maximization of eqn (5.2.11).

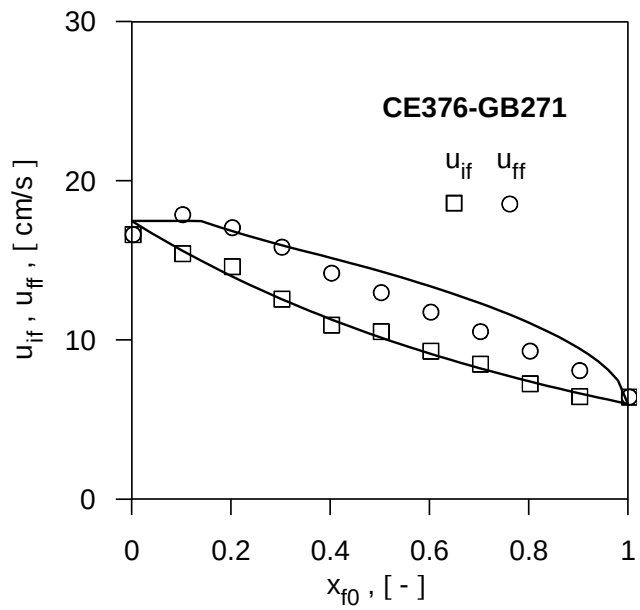

Figure 5.23 – Fluidization velocity diagram of the size segregating mixture CE376-GB271 obtained through maximization of eqn (5.2.11).

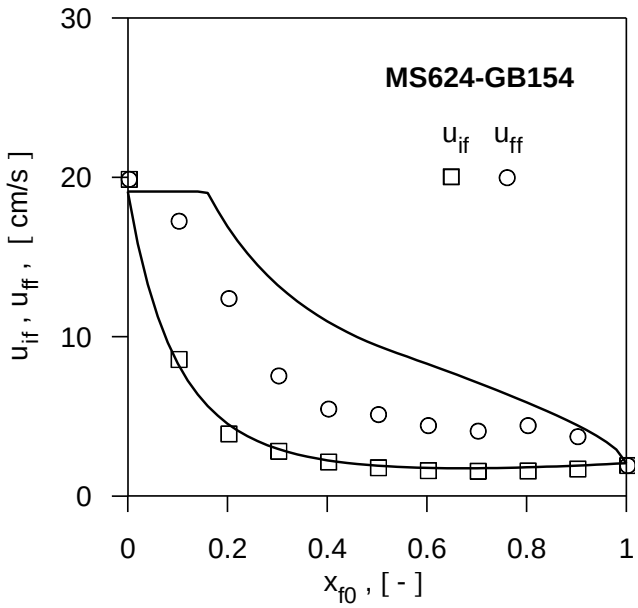

Figure 5.24 –Fluidization velocity diagram of the size segregating mixture MS624-GB154 obtained through maximization of eqn (5.2.11).

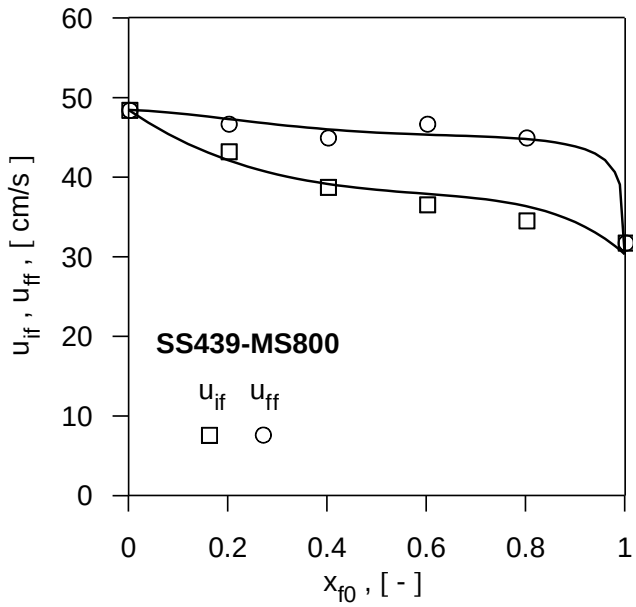

Figure 5.25 – Fluidization velocity diagram of the size segregating mixture SS439-MS800 obtained through maximization of eqn (5.2.11).

In conclusion the analogy between the process of fluidization and the phase transition is evident. The point of the final fluidization can be regarded as the analogous of the dew point of the liquid-vapor multicomponent equilibrium. The difference u_{ff}-u_{if}, i.e. the width of the fluidization velocity interval of the binary bed seems related to the concentration profile obtained from its slow defluidization down to the fixed state. In fact, the relationship between concentration in the fluidized and packed region of the bed seems to be provided by the fluidization diagram. Both u_{ff} and the concentration profiles obtained after defluidization are closely related and they can probably be generated by means of the proper definition of a functional. In regard to this latter topic, all the considerations made in this chapter should be regarded as preliminary and necessitate theoretical justification.

CONCLUSIONS

Based on a critical review of the literature accumulated over the past three decades on fluidization of beds of two solids, this thesis has addressed the characterization of the process by introducing the definition of "fluidization velocity interval". The fluidization phenomenology of systems that starts from the well mixed state is characterized by the simultaneous occurrence of suspension and components segregation. At the "initial fluidization velocity, u_{if} ", the appearance of a fluidization front at the top of the bed is observed; by increasing the gas flow rate, this front travels downwards until all the particulate assembly is brought into the fluidized state at the "final fluidization velocity u_{ff}", which marks the end of the process of suspension. Along this transition, the two components of the beds tend to form distinct layers, to an extent which mainly depends on the difference between their densities and sizes. Over u_{ff} the two solids tend to mix up again, so that in many cases the bed exhibits a new homogeneous state at velocities higher than u_f, that depend on particle properties. Since most of the segregation phenomena occur between u_{if} and u_{ff}, measurement of these variables is a way of characterizing the tendency to segregation of any binary mixture.

The results obtained by the approach adopted in this work are summarized below.

- By accounting for the actual phenomenology of the process, it has been possible to go over the use of empirical equations and carry out a fundamental analysis of

segregating fluidization. A model has been devised capable to interpret the behavior of all types of binary mixtures. This model is based on a force balance by which the classical equations for predicting the pressure drop in mosolid systems, such as Carman-Kozeny's, have been made applicable also to binary beds. Whatever the initial state of mixing of the packed bed, this force balance allows calculating u_{if} by means of a fully predictive equation.

- A more realistic representation of the structure assumed by any homogeneous two-solid bed during its transition to the fluidized state has made possible to highlight the close relationship between particle suspension and segregation. In spite of a certain degree of simplification, a crucial point is that of considering the equilibrium state to give rise to three distinct layers with different composition and height. This simplified structure has proved capable to represent the essential aspects of the suspension mechanism. By reworking the force balance so as to account for the change in the axial distribution of the two solids, a theoretical equation for calculating u_{ff} has been derived which successfully interprets its variation with bed composition:

$$u_{ff} = \frac{\left[\left(\rho_f - \rho_g\right)x_{f0}h_m + \left(\rho_j - \rho_g\right)\left(1-x_{f0}\right)h_0\right]g}{180\mu_g\left[\frac{\left(1-\varepsilon_{mf,m}\right)}{\left(\varepsilon_{mf,m}^3 d_{av}^2\right)}h_m + \frac{\left(1-\varepsilon_{mf,j}\right)}{\left(\varepsilon_{mf,j}^3 d_j^2\right)}\left(h_0 - h_m\right)\left(1-x_{f0}\right)\right]}$$

For a two-size and a two-density bed it becomes, respectively:

$$u_{ff} = \frac{\left(\rho_s - \rho_g\right)g\left[\left(h_0 - h_m\right)\left(1-x_{f0}\right) + h_m\right]}{180\mu\left[\frac{\left(1-\varepsilon_{mf,j}\right)}{\left(\varepsilon_{mf,j}^3 d_j^2\right)}\left(h_0 - h_m\right)\left(1-x_{f0}\right) + \frac{\left(1-\varepsilon_{mf,m}\right)}{\left(\varepsilon_{mf,m}^3 d_{av}^2\right)}h_m\right]}$$

$$u_{ff} = \frac{\left[\left(\rho_j - \rho_g\right)h_0\left(1-x_{f0}\right)+\left(\rho_f - \rho_g\right)h_m x_{f0}\right]g\varepsilon_{mf}^3 d^2}{180\mu_g\left(1-\varepsilon_{mf}\right)\left[h_0\left(1-x_{f0}\right)+h_m x_{f0}\right]}$$

In it, the height h_m of the residual homogeneous mixture represents a measure of the extent of segregation.

- In order to estimate h_m a unique parametric correlation, namely eqn (3.1.9), can be used with all types of mixture without any difference in the error level. This demonstrates that a unique description of segregating fluidization is possible, regardless of the driving force of segregation being the inequality of particle density or size, or both. This correlation utilizes just one parameter, independent of composition, which can be determined by a single measurement. For mixtures of two solids differing only in size or density, the dependence of this parameter on the size ratio of the components and on the difference of their u_{mf} has experimentally been determined.

- A theoretical expression for the component contribute to the total pressure drop in a bed of two solids has been derived. This has allowed carrying out a force balance on bed components that shows that solid-solid interaction is at work in the bed. The presence of this interaction provides a theoretical explanation of the fact that u_{if} is always observed to be higher than $u_{mf,f}$ while u_{ff} is always lower than $u_{mf,j}$. Indeed, solid-solid interaction hinders the fluidization process of the flotsam component while it facilitates that of the jetsam.

- The analysis of this interaction has demonstrated that it is possible to explain theoretically the case of mixtures for which the denser and smaller component achieves the fluidized state at the bottom of the column, while the other solid, bigger and lighter, forms an upper packed layer. The three-layer parametric model

for the final fluidization velocity has been successfully extended to this pecuiliar category of systems, with predictions whose error level is the same of those relevant to beds that exhibit the common phenomenology of fluidization.

• The analogy between the fluidization velocity diagram and a liquid-gas phase diagram has been clearly highlighted, with u_{ff} that plays a role analogous to that of the dew-point temperature. Light has been thrown on the close connection that exists between the final fluidization velocity and the concentration profile of a bed brought back to the packed state by slow defluidization. This profile can actually be calculated from the knowledge of the final fluidization curve.

Despite its results are still incomplete, this work has shown how the approach based on the fluidization velocity interval of a binary mixture is capable to lead to a fundamental description of all aspects of the phenomenology, thus providing a unified theoretical framework of the process of segregating fluidization of dissimilar solids. However, an essential objective of future work is that of going over the parametric analysis and develop a fully predictive theory for the final fluidization velocity. For the time being, it has been shown how both u_{ff} and the axial component distribution after slow defluidization can be generated by the maximization of a functional.

NOTATION

A	column cross section [cm^2]
D	column bed diameter [cm]
D_p	axial dispersion rate in the bulk phase [cm^2/s]
d	particle diameter [μm]
d_{av}	Sauter mean diameter (eqn.4) [μm]
d_B	bubble diameter [cm]
d_{B0}	initial bubble diameter [cm]
F_d	drag force [g cm/s^2]
f_w	wake volume fraction [-]
g	gravity acceleration [cm/s^2]
h	height of the particle layer [cm]
H	total bed height [cm]
k	best-fit parameter [-] or segregation rate constant [cm/s]
m	bed mass [g]
M	mixing index [-]
u_B	bubble rise velocity [cm/s]
u_{if}, u_{ff}	initial, final fluidization velocity [cm/s]
u_{mf}	minimum fluidization velocity [cm/s]
u_{T0}	critical velocity above which mixing predominates [cm/s]
x	solid fraction [-]
w	solids circulation rate [m/s] or mass fraction [-]
W	buoyant weight [g cm/s^2]
$\bar{y}$	average fraction of the fluidized portion of the bed [-]
z	height from gas distributor [cm]

Z	dimensionless height z/h_0 [-]

Greeks

ε	voidage fraction [-]
ε_{mf}	minimum fluidization voidage [-]
μ_g	gas viscosity [g/cm s]
ϕ	particle sphericity [-]
ρ	solid density [g/cm^3]
ρ_g	gas density [g/cm^3]

Subscripts

b	of the layer near the distributor
B	of the bigger particles
f,j	of the flotsam, jetsam component (or layer)
ff	at the final fluidization velocity
H	of the heavy (denser) particles
L	of the light (less dense) particles
m	of the homogeneous mixture
S	of the smaller particles
0	of the initial static bed

REFERENCES

1) Rowe, P.N. and Partridge, B.A. "Particle movement caused by bubbles in a fluidized bed", in Interaction Between Fluids & Particles, Rottenburg, P.A. (Hon. Ed.) Instn Chem. Engrs, London, 135-142 (1962).

2) Rowe, P. N., Nienow, A. W. and Agbim, A. J. (1972). The mechanisms by which particles segregate in gas fluidized beds - binary systems of near spherical particles, *Trans. Inst. Chem. Eng*., **50**, 310-323.

3) Nienow, A.W. and Chiba, T.: "Fluidization of dissimilar solids", in Davidson, J.F., Harrison, D. and Clift, R. (Eds.), Fluidization, Academic Press, London, 357-382 (1985).

4) Chiba, S., Nienow, A.W., Chiba, T. and Kobayashi, H. (1980). Fluidized binary mixtures in which the dense component may be flotsam, *Powder Technol.*, **26**, 1–10.

5) Gibilaro, L.G. and Rowe, P.N. (1974). A model for a segregating gas fluidized bed, *Chem. Eng.ng Sci.,* **29**, 1403-1412.

6) Yoshida, K., Kameyama, H., Shimizu, F.: "Mechanism of particle mixing and segregation", in Grace, J.R., Matsen, J.M. (Eds.), Fluidization, Plenum Press, New York, 1980, 389–396.

7) Burgess, J.M., Fane, A.G., Fell, C.J.D. (1977). Measurement and prediction of the mixing and segregation of solids in gas fluidized beds. *Pac. Chem. Eng. Congr.,* **2**, 1405–1412.

8) Nienow, A.W., Rowe, P.N. and Cheung, L.Y.L. (1978). A quantitative analysis of the mixing of two segregating powders of different density in a gas-fluidized bed, *Powder Technol.*, **20**, 89–97.

9) Rice, R.W. and Brainnovich, Jr J.F. (1986). Mixing/segregation in two- and three-dimensional fluidized beds: binary systems of equidensity spherical particles, *A.I.Ch.E J.,* **32**, 7–16.

10) Peeler, J.P.K. and Huang, J.R. (1989). Segregation of wide size range particle mixtures in fluidized beds, *Chem. Eng. Sci.,* **44**, 1113–1119.

11) Leaper, M. C., Seville, J. P. K., Hilal, N., Kingman, S. W. and Burbidge, A. S. (2004). Examining predictive correlations for equilibrium concentration profiles in jetsam-rich systems, *Adv. Powder Technol.*, **15**, 311-320.

12) Wu, S. Y. and Baeyens, J. (1998). Segregation by size difference in gas fluidized beds, *Powder Technol.,* **98**, 139-150.

13) Chiba, S., Chiba, T., Nienow, A.W. and Kobayashi, H. (1979). The minimum fluidization velocity, bed expansion and pressure-drop profile of binary particle mixtures, *Powder Technol*, **22**, 255–269.

14) Otero, A. R. and Corella, J. (1971). Fluidizacion de mezclas de solidos de distintas caracteristicas, *Anales de la RSEFQ*, **67**, 1207-1219.

15) Wen, C. Y. and Yu, U. H. (1966). Mechanics of fluidization, *Chem. Eng. Prog. Symp. Ser.,* **62**, 100-111.

16) Cheung, L., Nienow, A. W. and Rowe, P. N. (1974). Minimum fluidization velocity of a binary mixture of different sized paticles, *Chem. Eng. Sci.,* **29**, 1301-1303.

17) Yu, A. B. and Standish, N. (1987). Porosity Calculations of Multi-component Mixtures of Spherical Particles, *Powder Technol.*, **52**, 233-241.

18) Formisani, B. (1991). Packing and fluidization properties of binary mixtures of spherical particles, *Powder Technol.,* **66,** 259-264.

19) Goossens, W. R. A., Dumont G.L. and Spaepen, G. L. (1971). Fluidization of binary mixtures in laminar flow region, *Chem. Eng. Prog. Symp. Ser.*, **67**, 38-45.

20) Kumar, A. and Sen Gupta, P. (1974). Prediction of minimum fluidization velocity for multicomponent mixtures, *Ind. J. Technol.*, **12**, 225-227.

21) Rowe, P. N. and Nienow, A. W.(1975). Minimum fluidization velocity of multicomponent particle mixtures, *Chem. Eng. Sci.,* **29**, 1365-1369.

22) Chiba, S. (1977), M. Sc. Thesis, Univ. of Hokkaido, Japan.

23) Thonglimp, V., Hiquily, N. and Laguerie, C. (1984). Vitesse minimale de fluidisation et expansion des couches de mélanges de particules solides fluidisées par un gaz, *Powder Technol.,* **39**, 223-229.

24) Obata, E. H., Watanabe, E. H., Endo, N. (1982). *J. Chem. Eng. Japan*, **46**, 23-28.

25) Uchida, S., Yamada, H. and Tada, I. (1983). Minimum fluidization velocity of binary mixtures. *J. Chem. Eng.,* **14**, 257-264.

26) Noda, K., Uchida, S., Makino, T. and Kamo, H. (1986). Minimum fluidization velocity of binary mixtures of particles with large size ratio *Powder Technol.,* **46**, 149-154.

27) Formisani, B., De Cristofaro, G., Girimonte, R. (2001). A fundamental approach to the phenomenology of fluidization of size segregating binary mixtures of solids, *Chem. Eng. Sci.,* **56**, 1–11.

28) Yu, A. B., Standish, N., McLean, A. (1993). Porosity calculation of binary mixtures of nonspherical particles. *J. Am. Ceram. Soc.*, **76**, 2813–2816.

29) B. Formisani, R. Girimonte, A. Guzzo. Unstable fluidization of size segregated binary mixtures with the coarser component initially on top, Proc. of the 4th World Congress on Particle Technology, 2002, Sydney, Australia.

30) Gelperin, N. I. and Einstein, V. G. : " The analogy between fluidized beds and liquids", in Davidson, J.F., Harrison, D. (Eds.), Fluidization, Cambridge Press, London, 541-568 (1978).

31) Chen, J. L.-P. and Keairns, D. L. (1975), Particle segregation in a fluidized bed, *Can. J. Chem. Eng.*, **53**, 395-402.

32) Yang, W.-C. and Keairns, D. L. (1982), Rate of particle separation in a fluidized bed, *Ind. Eng. Chem. Fundam.*, **21**, 228-235.

33) Vaid, R. P. and Sen Gupta P. (1978). Minimum fluidization velocities in beds of mixed solids, *Can. J. Chem. Eng.,* **56**, 292-296.

34) Carsky, M., Pata, J., Vesely, V. and Hartman, M. (1987), Binary system fluidized bed equilibrium, *Powder Technol.,* **51**, 237-242.

35) Formisani, B., Girimonte, R. and Longo, T. (2009). The fluidization process of binary mixtures of solids: Development of the approach based on the fluidization velocity interval, *Powder Technol.,* **185**, 97-108.

36) Formisani, B., Girimonte, R. and Longo, T. (2008). The fluidization pattern of density-segregating binary mixtures. *Chem. Eng. Res. Des.,* **86**, 344-348.

37) Marzocchella, A., Salatino, P., Di Pastena, V. and Lirer, L. (2000). Transient fluidization and segregation by size difference of binary mixtures of particles *A.I.Ch.E . J.*, 46, 2175-2182.

38) Olivieri, G., Marzocchella, A. and Salatino, P. (2004). Segregation of fluidized binary mixtures of granular solids, *A.I.Ch.E. J.*, **50**, 3095-3106.

39) Geldart, D. (1973). Types of Gas Fluidization, *Powder Technol.*, **7**, 285-292.

40) Formisani B. , Girimonte R. , Vivacqua V. (2010). Fluidization of mixtures of two solids differing in density or size. AIChE J., (in press, DOI: 10.1002/aic.12450).

41) Wallis, G., B., One dimensional two-phase flow. Mc Graw Hill, New York, 1969.

42) Joseph, G. G., Leboreiro, J., Hrenya, C. M. and Stevens, A. R. (2007). Experimental segregation profiles in bubbling gas-fluidized beds, *A.I.Ch.E. J.*, **53**, 2804-2813.

43) Gibilaro, L. G., Di Felice, R., Waldram, S. P. and Foscolo, P. U. (1986). A predictive model for the equilibrium composition and inversion of binary solid-liquid fluidized beds, *Chem. Eng. Sci.*, **41**, 379-387.

44) Hoffmann, A. C., Janssen L. P. B. M. and Prins, J. (1993). Particle segregation in fluidized binary mixtures, *Chem. Eng. Sci.*, **48**, 1583-1592.

PHD ACTIVITY

Journal Papers

Formisani B. , Girimonte R. , Vivacqua V. (2010). Fluidization of mixtures of two solids differing in density or size. AIChE J., (in press, DOI: 10.1002/aic.12450).

International Conference Proceedings

Formisani B. , Girimonte R., Vivacqua V. On the extension of the theory of fluidization to beds of two solids subjected to segregation by density or size. In The Sixth World Congress on Particle Technology (WCPT6), Nuremberg (Germany), April 26-29, 2010.

Formisani B. , Girimonte R., Vivacqua V. Towards a theoretical model of segregating fluidization of two-solid beds. In Fluidization XIII: Eds Kim S. D., Kang Y., Lee J. K., Gyeong-ju (Republic of Korea), May 16-21, 2010, pp 837-844.

Formisani B. , Girimonte R., Bafaro P., Vivacqua V. Bubble-free fluidization of particles in the voids of a packing of coarse spheres. In Fluidization XIII: Eds Kim S. D., Kang Y., Lee J. K.,, Gyeong-ju (Republic of Korea), May 16-21, 2010, pp 33-40.

National Conference Proceedings

Vivacqua V., Girimonte R., Formisani B. Analisi fondamentale delle proprietà di fluidizzazione di letti di due solidi di diversa densità. In Convegno GRICU 2008, Le Castella (KR), Settembre 14-17, 2008, pp. 1237-1242.

Future Papers

Submitted

Formisani B. , Girimonte R., Vivacqua V. The relationship between fluidization velocity and segregation in two-component fluidized beds: a preliminary analysis. In the Tenth Conference in Circulating and Fluidized beds (CFB 10), Sunriver, Or (US), May 1-5, 2011.

Girimonte R., Vivacqua V. The expansion process of particle beds fluidized in the voids of a packing of coarse spheres. Submitted to Powder Tech.

To be Submitted

Formisani B. , Girimonte R., Vivacqua V. Fluidization of mixture of two solids: a unified model for the analysis of the segregation pattern. To be submitted to AIChE J.

Formisani B. , Girimonte R., Vivacqua V. Assessment of the component contributes to the total pressure drop in a bed of two solids: validation of the theoretical model.

Schools

Scuola Nazionale GR.I.C.U. di Dottorato di Ricerca 2008, “Fenomeni di Trasporto / Intensificazione di Processo”, Le Castella (KR), Settembre 17-22, 2008.

Scuola Nazionale GR.I.C.U. di Dottorato di Ricerca 2009, "Termodinamica / Energia", Muravera (CA), Giugno 7-11, 2009.

Teaching

Esercitazioni del Corso di Impianti Chimici 1 (30 h), Laurea in Ingegneria Chimica (Triennale, CFU 5), a.a. 2008/2009.

Esercitazioni del Corso di Impianti Chimici 1 (30 h), Laurea in Ingegneria Chimica (Triennale, CFU 5), a.a. 2009/2010.